Investigating the Nature of the Interaction between the Inner Membrane Quinol Dehydrogenase CymA and the Periplasmic Fumarate Reductase FccA of *Shewanella oneidensis* MR-1

by

Theodoros Laftsoglou

Submitted in accordance with the requirements for the degree of
Doctor of Philosophy

The University of Leeds
Faculty of Biological Sciences
School of Biomedical Sciences

September, 2017

The candidate confirms that the work submitted is his own and that appropriate credit has been given where reference has been made to the work of others.

Acknowledgements

I would like to thank my supervisor Professor Lars Jeuken for his support, and the European Research Council for funding. I am also particular grateful to the following Professors who were very kind in allowing me to use their facilities, without whom, the work presented herein could not have been possible: Professor Peter Henderson, Stephen Baldwin Professor of Biochemistry 1952-2014, Professor Adrian Goldman, and Professor Stephen Evans. Moreover, our collaborators Professor Julea Butt, Dr Colin Lockwood, Dr Antony Blake, Dr Marcus Edwards, and Dr Emma Ainsworth both for allowing me to use their facilities at the University of East Anglia, Norwich, and for insightful discussions.

I would also like to thank the facility managers that have been very helpful with training me on a range of different techniques: Dr Iain Manfield (Biomolecular interaction facility), Dr Chi Trinh (Protein crystallisation facility), Dr James Ault (Mass spectroscopy facility), and Dr Robert Kolodziejczyk & Dr Maren Thomsen (SEC-MALLS facility).

I would also like to extend my many thanks to the following people for sharing their expertise and engaging in insightful discussions: Dr Vincent Postis and Dr Vincent Agboh. Also, to the members of the Jeuken group that have been not only a source of knowledge, but very supportive over those challenging years: Dr Valentin Radu, Dr Ee Taek Hwang, Dr Vlad Vasilca, Dr Khizar Sheikh, Dr George Heath, Dr Hope Adamson, Joseph Oram, soon-to-be Dr Matthias Gantner, Anna Stikane, and Ania Wroblewska-Wolna. Also, the visiting MSc student in 2015, Tomas Sabirovas, for his contributions on this project. I am also extremely grateful to and I would like to acknowledge the excellent technical support I received from Riitta Partanen, Honling Rong, and David Sharples.

Moreover, I would like to thank my family and my close friends, Anastasios Plessas, Eleni Faltaka, and Robert Watson, for their unconditional support throughout. Also, my new friends in Reading, notably Gianni Ryan Smith and Jack Collins, who have been very understanding during a personally difficult period of time.

Last but not least, I would like to extend special thanks to my current colleagues at Immunocore for their support.

To the reader

AND

To my beloved great-grandmother (1912-2017) for her fighting spirit

Abstract

Shewanella oneidensis exhibits a diverse respiratory system, able to use over 20 terminal electron acceptors, including solid metal oxides. CymA is located in the inner membrane, facing the periplasmic space, and it is responsible for the re-oxidation of the quinol/quinone pool. A plethora of proteins re-oxidise CymA, such as the periplasmic fumarate reductase FccA. This thesis investigates the nature of the interaction between CymA and FccA with a variety of biochemical and biophysical techniques.

Chapter 3 describes a new approach in purifying recombinant form of CymA as a pure monodispersed solution that was developed with the reconstruction of the expression vector. The purity was >90% with a yield of 2 mg L^{-1} of culture. The biochemical and electrocatalytic properties of the recombinant CymA remained unaltered.

Chapter 4 presents for the first time the purification of a soluble version of CymA, $CymA_{sol}$ [CymA-Δ(1-31)], at >95% purity, but with a lower yield of 0.3 mg L^{-1} of culture due to limitations from the TEV proteolytic cleavage reaction for tag removal. Nonetheless, the first crystallisation attempt was achieved with $CymA_{sol}$. In total, 2,016 conditions were assayed, from which PEG 3350 seemed to promote atypical protein precipitation, although no crystals were formed.

Chapter 5 presents a systematic investigation of the CymA: FccA interaction, where no strong interaction was observed with cyclic voltammetry using a CymA-containing tethered bilayer lipid membrane system, or with QCM-D using a CymA-containing solid supported bilayer lipid membrane system. Dissolved oxygen alone was the only condition that replicated the previously published electrocatalytic data under the same system. This was further validated with isothermal titration calorimetry with $CymA_{sol}$, while, in a separate experiment, it was shown that CymA is necessary for the FccA-specific fumarate reduction *in vitro* with an initial rate of 3.3 (±0.3, n=3) μM NADH oxidised min^{-1}. Lastly, QCM-D showed that $CymA_{sol}$ binds to a positively charged lipid bilayer, while the MBP-tag of the whole construct binds to a negatively charged lipid bilayer. Thus, the new evidence presented herein points towards a transient nature of weak interaction between CymA and FccA.

The contributions of this work are in advancing the understanding of the anaerobic respiratory system of *S. oneidensis*.

Table of Contents

List of Tables

List of Figures

List of Abbreviations

µBCA	Micro bicinchoninic acid assay
AP	Alkaline phosphatase
ATP	Adenosine triphosphate
BSA	Bovine serum albumin
CL	Cardiolipin
CV	Cyclic voltammogram
CVol	Colume volume
CymA	Gene ID: 1172176; it refers to CymA protein in general terms, or for the full length protein.
CymA†	It refers to the recombinant CymA protein construct (8xHis-HRV3C_site-CymA) that is generated as part of this thesis.
CymA‡	It refers to the recombinant CymA protein construct (CymA-V5 epitope-6xHis) that is generated as part of a previously published study (1).
$CymA_{sol}$	CymA-Δ(1-31)
DDM	n-Dodecyl β-D-maltoside
DMRB	Dissimilaroty metal-reducing microorganisms
DMS	Dimethyl sulfide
DMSO	Dimethyl sulfoxide
DNA	Deoxyribonucleic acid

DOTAP	1,2-dioleoyl-3-trimethylammonium-propane
EDTA	Ethylenediaminetetraacetic acid
FAD	Flavin adenine dinucleotide
FRET	Förster resonance energy transfer
HQNO	2-n-Heptyl-4-hydroxyquinoline N-oxide
HRV3C	Human Rhinovirus 3C protease
IEC	Ion exchange chromatography
IMAC	Immobilised metal affinity chromatography
IPTG	Isopropyl β-D-1-thiogalactopyranoside
ITC	Isothermal titration calorimetry
K_D	Dissociation constant
LB	Luria broth
MBP	Maltose binding protein
methyl-MQ	Methyl-menaquinone
MGD	Molybdopterin guanine dinucleotide
MQ	Menaquinone
NADH	Nicotinamide adenine dinucleotide
NMR	Nuclear magnetic resonance
OD_{600}	Optical density at 600 nm
OG	Octyl-beta-Glucoside
PCR	Polymerase chain reaction

POPC	1-palmitoyl-2-oleoyl-sn-glycero-3-phosphocholine
PTFE	Polytetrafluoroethylene
QCM-D	Quartz crystal microbalance with dissipation
rRNA	Ribosomal ribonucleic acid
SAM	Self-assembled monolayer
SDS-PAGE	Sodium dodecyl sulfate polyacrylamide gel electrophoresis
SERR	Surface-enhanced resonance Raman
SHG	Second-harmonic generation
ssBLM	Solid supported bilayer lipid membrane
TAE	Tris-acetic acid-EDTA buffer
TB	Terrific broth
tBLM	Tethered bilayer lipid membrane
TCA	Tricarboxylic acid cycle
TCEP	Tris(2-carboxyethyl)phosphine
TEA	Terminal electron acceptor
TEV	Tobacco Etch Virus protease
TM	Transmembrane
TMA	Trimethylamine
TMAO	Trimethylamine N-oxide
TMBZ	3,3',5,5'-tetramethylbenzidine
UQ	Ubiquinone

UV-TREF	Ultraviolet two-photon excited fluorescence

Chapter 1 - Introduction

1.1 The family of dissimilatory metal reducing bacteria with an evolutionary perspective

The atmosphere of earth was completely anoxic until 2.4 – 2.3 billions of years (Ga) ago, according to sulphur isotope fractionation studies (2). Laser-Raman spectroscopy of the oldest fossil on geological record (an Apex chert found in north-western Western Australia (3)) has provided conclusive evidence for the presence of microbial life at about 3.5 Ga ago (4). Laser-Raman spectroscopy is able to analyse the chemical composition of fossils, which allows the differentiation between biotic and abiotic features that share the same morphology. Thus, there has been a significant period of anoxic life before the evolution of the first oxygenic photosynthetic organisms. The appearance of photosynthesis led to a period (about 2.5 – 2.3 Ga ago) where the oxygen level was fluctuating before it became stable (5). The phylum of cyanobacteria is believed to have played an important role in the final oxygenation of Earth (2).

During the anoxic period, the atmosphere of earth was reducing with the presence of hydrogen, whose level was later decreased by the evolution of methanogens (by conversion of H_2 and CO_2 to CH_4) and by natural escape to the outer space (6). The earliest forms of microbial respiration may have been based on hydrogen as the electron donor and Fe(III) as the electron acceptor (7, 8). Phylogenetic analysis of 16S ribosomal RNA (rRNA) sequences has been employed to identify all relatives to the last common ancestor (7). Consequently, all identified microbes by the phylogenetic analysis were capable of Fe(III)-reduction in cultures. It was also showed that *Thermotoga maritima,* which was previously thought to be a fermentative organism, was able to conserve energy for growth through Fe(III)-reduction in culture experiments (7). *T. maritima* is one of the most ancient ancestors in existence, although the importance of this observation lies on the fact that anaerobic iron respiration can generate sufficient energy for growth. Thus, all evidence from geochemical and phylogenetic studies point towards an ancient respiratory

system of Fe(III)-reduction whose remnants survive today in a group of bacteria called dissimilatory metal reducing bacteria (DMRB).

Although DMRB have a long history on this planet, they were only identified just over two decades ago with the isolation of *Shewanella oneidensis* MR-1 from the sediment of Lake Oneida in New York (9) and *Geobacter metallireducens* from the sand sediment of Potomac River in Washington D. C. (10). Other DMRB that have been identified to date include those in the genera of *Clostridium* (11), *Aeromonas* (12), *Rhodoferax* (13) and *Desulfobulbus* (14). Today, those microbes are primarily found in aquatic anoxic niches around the world and they are implicated in the geochemical iron cycle of anoxic environments (15).

1.2 Background on *Shewanella oneidensis*

1.2.1 *Shewanella oneidensis* as a dissimilatory metal reducing bacterium with unique characteristics

The genus *Shewanella* has being studied since 1931 (16), while its ability for dissimilatory metal reduction was uncovered in ca. 1988 with the isolation of the MR-1 strain (9). The species of the genus *Shewanella* exhibit diverse physiology and habitants. Thus, the taxonomy of different species within the genus is primarily based on 16S rRNA sequencing. *Shewanella* species often have a symbiotic relationship with fermentative microorganisms in energy-rich niches and/or in environments where the redox conditions can change rapidly. Interestingly, some *Shewanella* isolates from sea-ice niches found in Antarctica are psychro- (tolerant to cold) and piezo-tolerant (tolerant to high pressure). *Shewanella* species have also been described as an opportunistic pathogen of humans (17), or responsible for fish spoilage (18). *Shewanella oneidensis* MR-1 is a strain of this genus based on 16S rRNA sequencing. This species was re-classified three times and re-named once, until it was assigned its current name of *Shewanella oneidensis.* Firstly, it was placed under the genus of *Achromobacter* (16), which was later re-classified as a species of the genus *Pseudomonas* (19), then of *Alteromonas* (20) and lastly of *Shewanella* (21). Much later, in the light of 16S rRNA sequencing data, it was renamed from *Shewanella putrefaciens* to *Shewanella oneidensis* (22).

S. oneidensis is a Gram-negative, motile, facultative anaerobic γ-proteobacterium with bacillus morphology (22). One of the most intriguing aspects of *S. oneidensis*, though, is its metabolic versatility. It is able to respire through a plethora of terminal electron acceptors (TEAs) (23), such as molecular oxygen, fumarate, nitrite, nitrate, DMSO, TMAO, along with a variety of metal oxides and chelates of metals, such as Fe^{3+} (24, 25), Mn^{3+} (24), Mn^{4+} (24), U^{6+} (25, 26), Cr^{6+} (25-27) and Tc^{6+} (25). Consequently, *S. oneidensis* has found great interest from the scientific community.

1.3 The anaerobic respiratory system of *Shewanella oneidensis*

1.3.1 General overview of the pathways that comprise the anaerobic respiratory system

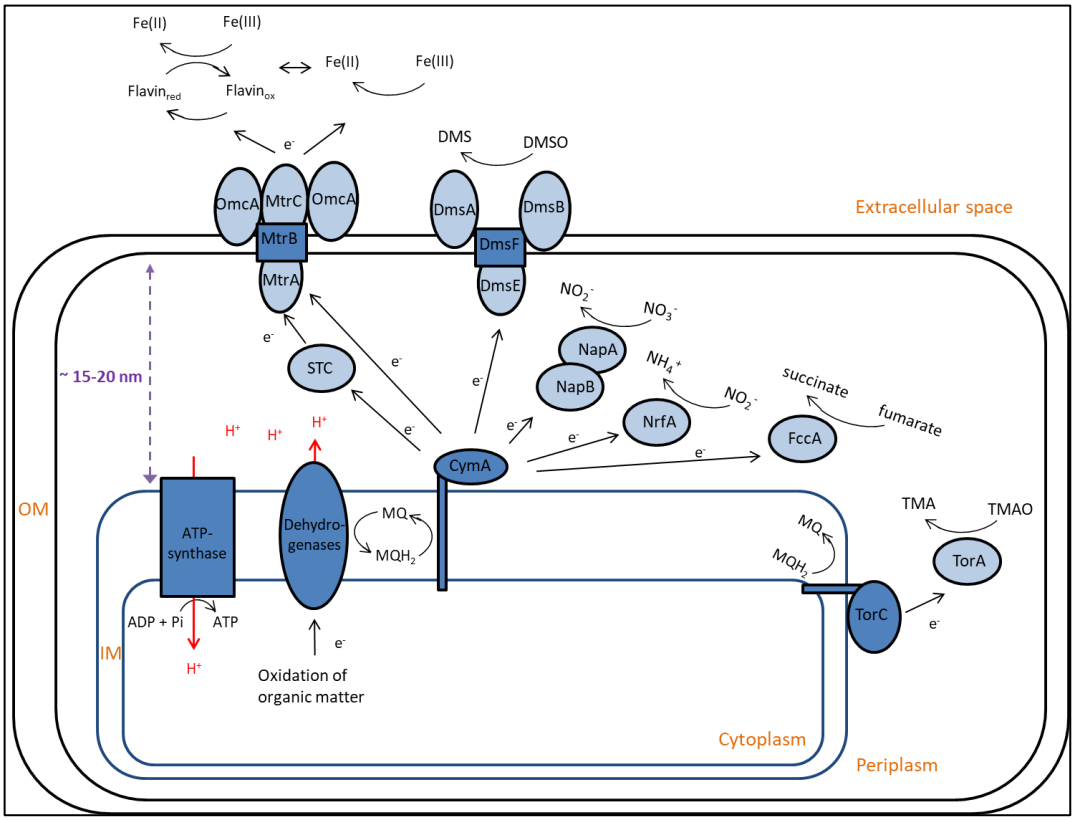

Figure 1: Schematic overview of the anaerobic respiratory system of *Shewanella oneidensis*. Electrons from the oxidation of organic matter in the cytoplasm are directed to the quinone molecules in the inner membrane (IM) via the IM NADH and/ or formate dehydrogenases with the co-current release of protons (H^+) in the periplasm. The generated proton gradient is employed for the synthesis of ATP by ATP-synthase. It is maintained by the re-oxidation of the quinols via the IM CymA or TorC. CymA distributes the electrons either to periplasmic terminal reductases, or towards the outer membrane (OM) complexes for the extracellular reduction of metal oxides or DMSO. TorC is the functional homologue of CymA for the periplasmic reduction of TMAO by TorA. The electron flow is indicated with black arrows, while the H^+ flow is indicated with red arrows.

Scott et al (28) isolated extracts of different *S. oneidensis* strains, which were either aerobically or anaerobically grown, and assayed the activity of enzymes that are linked to different metabolic pathways. It was found that under oxic conditions, the tricarboxylic acid cycle (TCA) is active, while under anoxic conditions formate (or formaldehyde) is the main carbon intermediate and the

bacterium employs a truncated TCA and serine pathway by selecting enzymes from each pathway. As a result, under anoxic conditions, there is a net flow of electrons from the formate dehydrogenase to menaquinone, which is present in the inner membrane. Concurrently, the oxidation of formate produces protons in the periplasmic space. A net flow of electrons can also derive from other anaerobic metabolic pathways in the form of NADH, which is coupled by the inner membrane dehydrogenases. This reduces the menaquinone, while protons are translocated to the periplasm. The proton translocation and the periplasmic proton production generate a proton gradient (the proton motive force) that drives ATP-synthases. The electron flux, hence, is linked to the proton motive force. The proton motive force is maintained by reducing terminal electron acceptors that act as electron sinks. The menaquinol is re-oxidised by primarily CymA, an inner membrane anchored tetrahaem c-type cytochrome. CymA mediates the electrons to other proteins, allowing its own re-oxidation. Thus, the menaquinol and CymA re-oxidation that maintains the electron flux is a crucial component of the respiratory system. The electrons can follow one of three paths: they can be transported directly to (a) periplasmic terminal reductases, to (b) periplasmic electron shuttle proteins, or (c) directly from CymA to the outer membrane complexes. An overview of the pathways involved in the anaerobic respiratory system of *S. oneidensis* is schematically shown in **figure 1**.

1.3.2 CymA as an inner membrane electron-distribution hub

CymA is a quinol dehydrogenase that is localised at the inner membrane and it catalyses the reduction of menaquinol:

$$MQH_2 \xrightarrow{CymA} MQ + 2\ e^- + 2\ H^+$$

where MQH_2 and MQ are the menaquinol and menaquinone respectively.

CymA, the product of *cymA* gene, was successfully cloned and characterised as a tetrahaem c-type cytochrome with an inner membrane anchor domain and an approximate molecular mass of 21 kDa (29). Spectroscopically, the haem groups of the reduced cytochromes show three peaks at the UV-visible region, which are also known as α, β, and γ Soret bands. The wavelength of the α Soret band is often used to establish the type of cytochromes. Generally,

the haem group (iron protoporphyrin IX) of c-type cytochromes is covalently attached to the protein through thioether bonds between the vinyl groups of the haem and the cysteine thiol groups on a CXXCH motif. The sequence of *cymA* revealed that CymA is part of the NapC/ NrfH family of quinol dehydrogenases (29). From gene sequence alignment, *S. oneidensis* CymA is a homologue of *Escherichia coli* NapC, *Desulfovibrio desulfuricans* NrfH, *Wolinella succinogenes* NrfH, *Haemophilus influenza* NapC, *Paracoccus denitrificans* NapC, and *Sulfurospirillum deleyianum* NrfH (29).

Although the crystal structure of CymA remains elusive, the crystal structure of NrfH was solved as an $NrfH_2A_4$ complex to a resolution of 2.3 Å from *Desulfovibrio vulgaris* (30). The entire complex (300 kDa) consists of two NrfA dimers each binding to one NrfH molecule (**figure 2**). NrfH is an α-helical protein with an N-terminal transmembrane (TM) α-helix and a globular domain. Besides the TM α-helix, a second α-helix is also believed to be embedded within the membrane because of its high number of hydrophobic residues. Furthermore, this second membrane-associated helix is implicated in the orientation and membrane attachment of NrfH. Truncated NrfH (31), NapC (32) and CymA (33) constructs, in which the N-terminal TM helix was removed, were all able to interact with the quinol pool in mutant complementation and *in vitro* biochemical studies in line with the suggested role of the second helix in membrane attachment.

NrfH dimerises in such a way that haem I is optimally arranged to interact with the quinol pool (**figure 3**). The globular domain houses the 4 haem groups in a two-pair arrangement (haems 1 and 2 versus 3 and 4), facing the periplasmic space. Rodrigues et al (30) proposed a menaquinone (MQ) binding pocket, which is located between haem I and the second transmembrane α-helix. According to their proposed model, the hydroxyl groups of MQ form hydrogen bonds with the side chains of Asp89 and Lys82, both highly conserved amino acids. Those residues are both located on the second membrane-associated α-helix, which is oriented parallel to the membrane plane, allowing efficient interaction with the quinol pool.

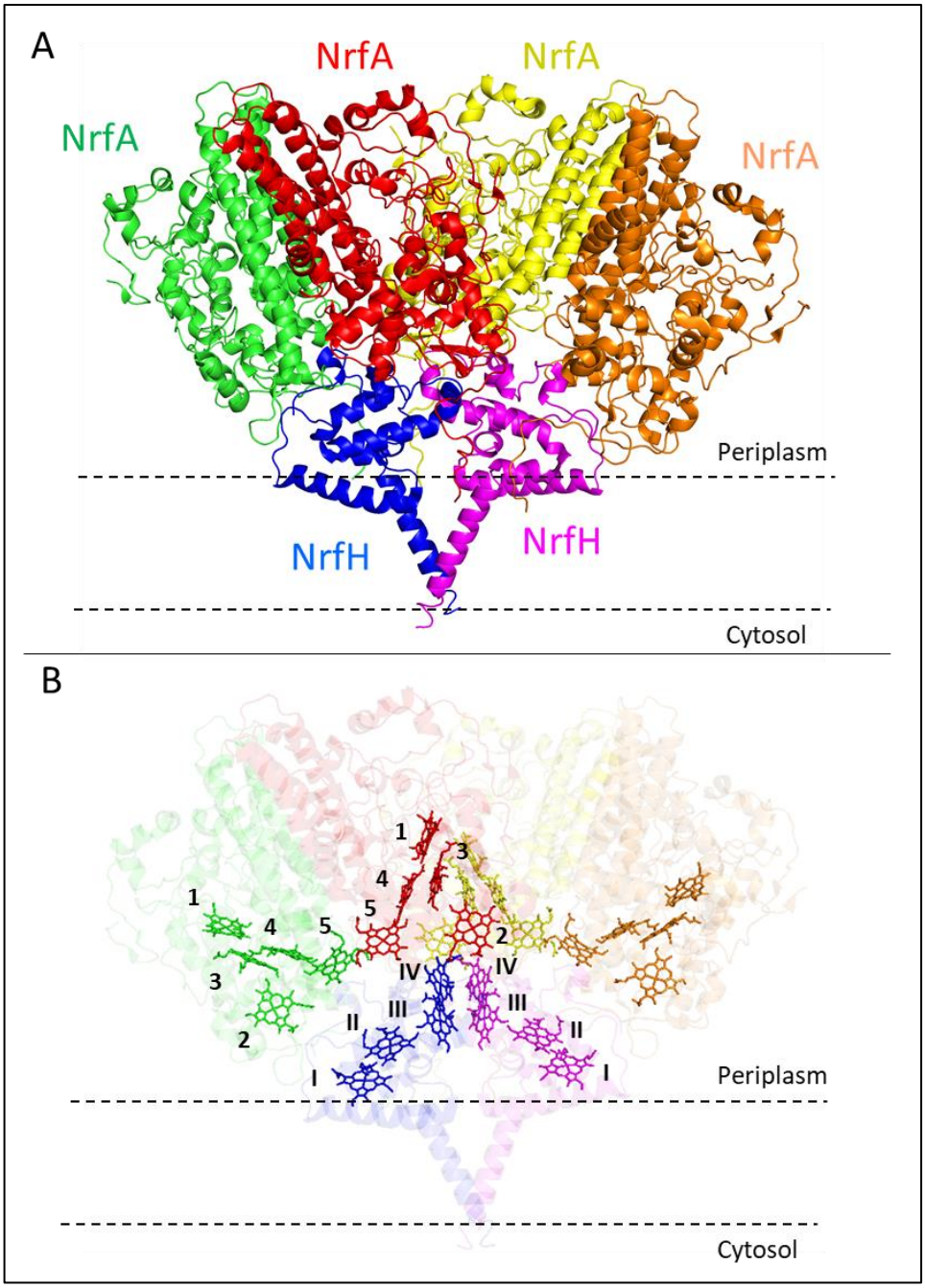

Figure 2: Crystal structure of $NrfH_2A_4$ complex from *Desulfovibrio vulgaris.* A. Crystal structure of the whole complex at 2.3 Å resolution. Dashed lines represent the boundaries of the lipid bilayer membrane. The N-terminal transmembrane α-helices of the two NrfH molecules dimerise through a dimerisation motif, bringing the second membrane-associated N-terminal α-helices perpendicular to the membrane. **B.** The arrangement of the haems is shown for the entire complex. The haem groups of NrfH molecules are labelled with Roman numerals, while the haem groups of two out of the four NrfA molecules are labelled with Arabic numerals. The haem groups are coloured by molecule as shown in panel A. The images were produced with PyMOL (PDB: 2J7A).

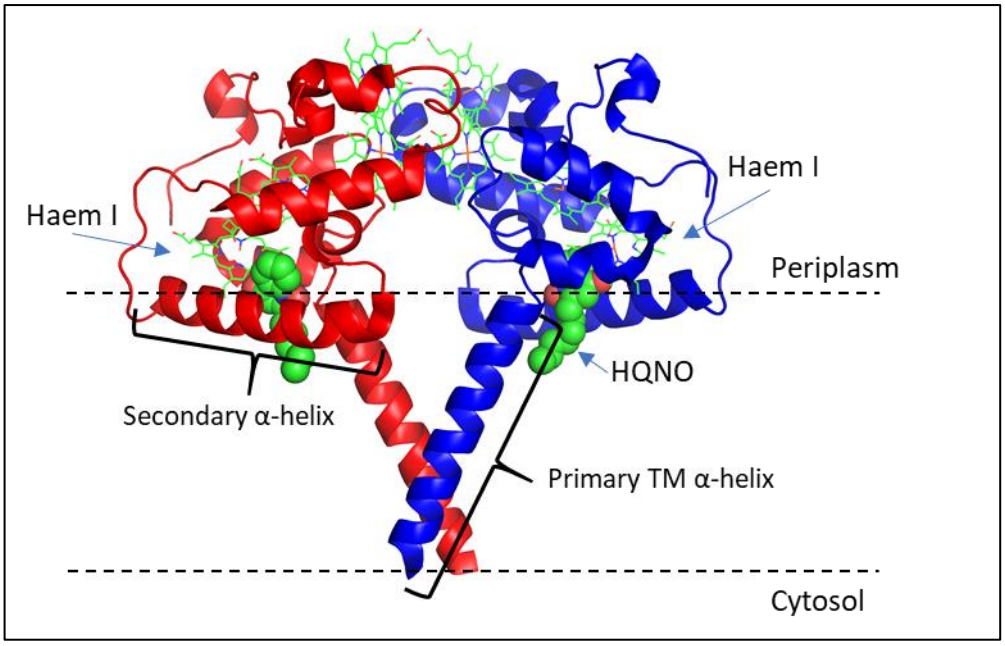

Figure 3: NrfH homodimer crystal structure at 2.8 Å resolution from *Desulfovibrio vulgaris* with bound HQNO. The two NrfH molecules are depicted in red and blue, while the haem groups are presented as sticks. The primary N-terminal α-helix dimerises in such a way so to bring haem I in optimal orientation towards the membrane for quinone interaction through its quinone binding pocket, where HQNO is bound. HQNO (spheres) is an inhibitory quinone analogue. The image was produced with PyMOL (PDB: 2VR0).

A couple of years later, Rodrigues et al (34) presented a crystal structure of the $NrfH_2A_4$ complex bound to a MQ-analogue, 2-heptyl-4-hydroxyquinoline-N-oxide (HQNO), at a resolution of 2.8 Å. There was no structural difference between structures, but the position of HQNO, which confirmed the proposed binding site. Specifically, Asp89 is located at the polar region of the membrane and it is functionally implicated with proton shuttling. Lys82 is likely to act as a direct proton acceptor for quinol oxidation.

Magneto-optical spectroscopic interrogation, along with biophysical characterisation of CymA from *S. frigimarina* and *S. oneidensis* suggests bis-His ligation of the haem groups (1, 35). Dimerisation of CymA is also suggested by the presence of bands of higher molecular weight during CymA purification that contained CymA as confirmed by mass-spectroscopy of tryptic digestion. Dynamic light scattering and size-exclusion chromatography also provided evidence that corroborates the presence of a CymA dimer within the detergent micelles (1).

Although CymA is required for respiration, it was not found to be a terminal reductase (29). Thus, it started becoming clear that CymA must act as an electron mediator between the quinone pool and terminal reductases. Transposon mutagenesis generated a phenotypically deficient mutant in MQ and methyl-MQ, CMTn-1, which was unable to reduce fumarate, nitrate, Fe(III) and a limited ability to reduce Mn(IV), although no difference from the wild-type was observed for TMAO reduction (36). Although CMTn-1 illustrates the importance of the quinone pool, it could not be rescued with MQ and methyl-MQ complementation (37), which suggested a mutation on an upstream element of the pathway. Subsequent genetic investigation of the mutant revealed that the transposon element interrupted the *cymA* gene (37). A *cymA* deletion mutant (Δ*cymA*) exhibited the same phenotype as CMTn-1 mutant (37), which corroborates that CymA is an upstream element that must interact with the quinol pool in order to give a MQ-deficient phenotype.

Regarding *S. oneidensis* respiratory system, three quinones have been identified as the major components of the quinone pool both by thin layer chromatography (36) and high-performance liquid chromatography (38); ubiquinone (UQ), MQ and methylmenaquinone (methyl-MQ). MQ was identified as a co-factor of CymA by co-purification and subsequent electrochemical characterisation that functionally supports the presence of the MQ-binding site on CymA (39). Surface-enhanced Resonance Raman Spectroelectrochemistry (SERR) (40), along with the available crystal structure of NrfH, has provided great insights into the biological importance of the bound MQ. It lowers the redox potential of the entry haem, facilitating the biological electron transfer by an increased overall driving force of a downhill electron transport.

1.3.3 Respiratory pathways involving intracellular electron transfer

1.3.3.1 Nitrate ammonification by the nitrate reductase NapAB and the nitrite reductase NrfA

Bacterial nitrate ammonification occurs anaerobically by a two-step process: First, nitrate is reduced to nitrite by the NAP system (periplasmic nitrate reductase). Second, nitrite is reduced to ammonia by the NRF system (periplasmic nitrite reductase). Generally, the NAP system consists of at least four proteins: NapC, which is a homologue of CymA; the catalytic heterodimer NapAB; and the accessory protein NapD, which is involved in the translocation of NapA to the periplasmic space. Regarding the NRF system, there are two types: the NrfHA system, which is primarily found in δ- and ε-proteobacteria; and the NrfABCD system, which is primarily found in γ-proteobacteria. NrfH is the homologue of CymA and NapC. The NrfBCD is the functional equivalent of NapC and CymA, re-oxidising the inner membrane MQH_2. However, *S. oneidensis* possesses no NrfH or NrfBCD equivalent and no NapC. Instead, NrfH and NapC are functionally replaced by CymA.

The periplasmic heterodimeric nitrate reductase NapAB consists of a large catalytic subunit NapA of an approximate molecular mass of 91 kDa and a small electron-transfer subunit NapB of an approximate molecular mass of 17 kDa. It catalyses the reduction of nitrate to nitrite:

$$NO_3^- + 2\,e^- + 2\,H^+ \xrightarrow{NapAB} NO_2^- + H_2O$$

Although the crystal structure of *S. oneidensis* NapAB has not been solved yet, much information can be obtained by the solved crystal structure of the *Rhodobacter sphaeroides* NapAB at 3.2 Å resolution (41) (**figure 4**). This is the only available crystal structure of the nitrate reductase holoenzyme. The catalytic subunit NapA houses a [4Fe-4S] cluster and a molybdenum cofactor. The overall structure of NapA comprises of four domains. Domain I contains all the cysteines that bind the [4Fe-4S] cluster. Domains II and III have a mixed α/β-fold and bind two molybdopterin guanine dinucleotides (MGD). Domain IV shows a long N-terminal tail that crosses domains II and III, forming a β-barrel structure above both MGD. The catalytic site lies between the two MGD, but

access to it is restricted by domains II and III. The electron transfer subunit NapB contains two c-type haems. NapB interacts with NapA by the C- and N-terminal tails that surround NapA. A monomeric structure of NapB from *H. influenza* shows those tails to be highly disordered when not bound to NapA (42) and a conformational change is implicated to be induced during the association of NapB with NapA (41). Haem II of NapB is brought to close proximity to the [4Fe-4S] cluster, while haem I is solvent-exposed for interacting with NapC. The overall arrangement of the cofactors of NapAB permits electron transfer to the catalytic site from the solvent exposed haem I of NapB (41).

Functionally, NapB is not required for nitrate reduction, but it plays an important regulatory role that provides evolutionary advantage. *S. oneidensis* MR-1 deletion mutants of both subunits were generated by in-frame deletion mutagenesis, namely Δ*napA* and Δ*napB* (43). Δ*napB* grew faster to maximum cell density, compared to the wild type (MR-1), when nitrate was the TEA (43). Furthermore, Δ*napB* generated more colonies (on petri dish) within the first 7 hours, although the final count of colonies was the same as with the wild type. Both mutants, though, grew as the wild type on cultures with nitrite, which indicates that the NAP system has no involvement with the NRF system. Double mutant Δ*napA*Δ*napB* could not grow on nitrate, but it was rescued by gene complementation of the *napA* gene, confirming that NapA is essential for nitrate reduction (43). On a competition assay between Δ*napB* and wild type *S. oneidensis* MR-1, wild type colony count increased by 6.6% after one day, with a further increase of 26.7% after 5 days (43). Thus, the presence of the *napB* gene provides *S. oneidensis* with a fitness gain. In the presence of CymA, electrons flow preferentially to NapB until depletion of nitrate, then the electron flow switches to NrfA.

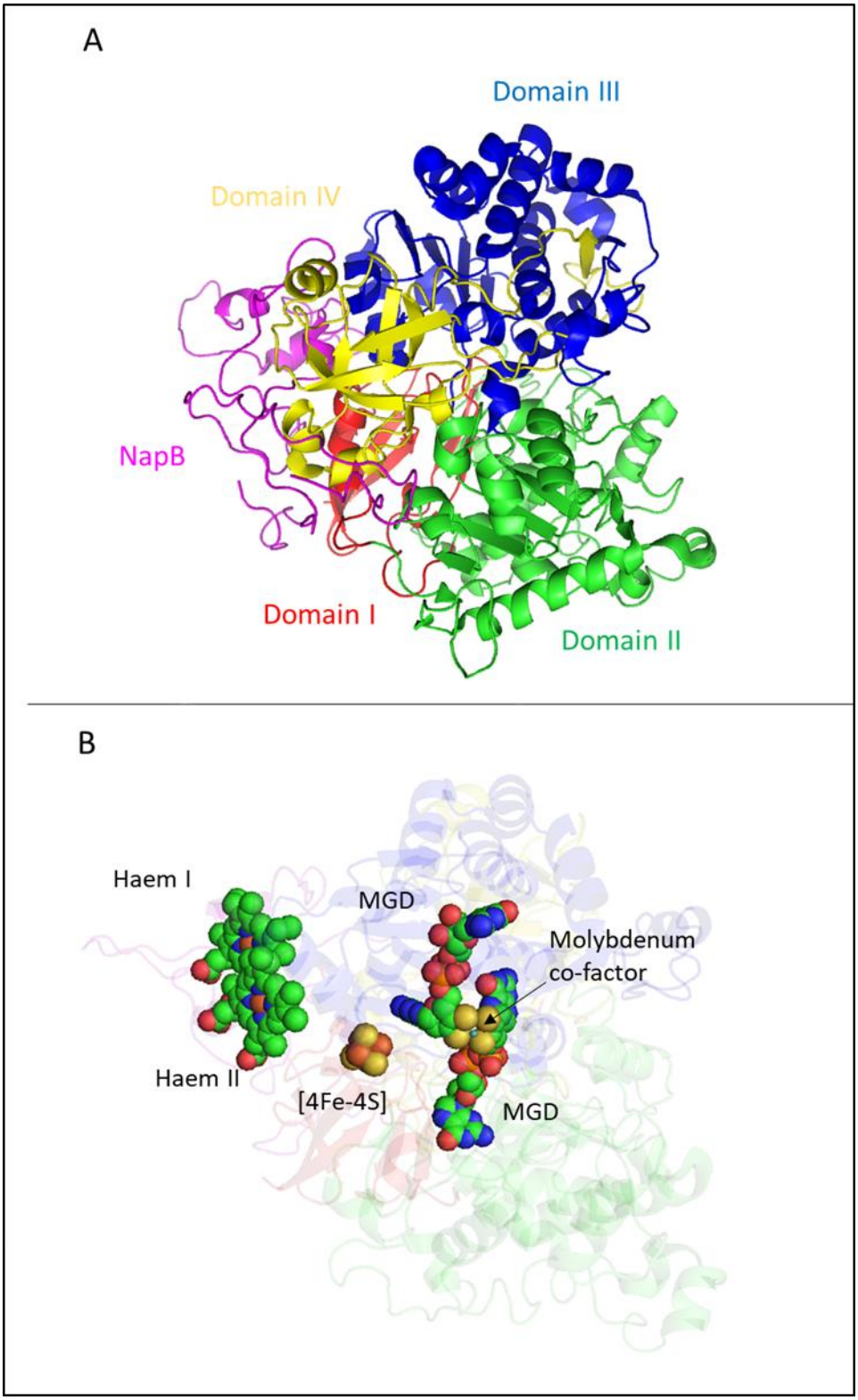

Figure 4: Crystal structure of NapAB complex at 3.2 Å resolution from *Rhodobacter sphaeroides*. A. The much smaller NapB of 17 kDa is coloured in magenta, while the 91 kDa NapA is coloured by its four domains I, II, III, and IV in red, green, blue, and yellow respectively. **B.** The arrangement of the metal co-factors of the NapAB complex is shown, where haem I of NapB is the entry point of electrons. MGD: molybdopterin guanine dinucleotides. The image was produced with PyMOL (PDB: 1OGY).

The periplasmic nitrite reductase NrfA (also referred to as ccNiR), with an approximately molecular mass of 52.6 kDa, catalyses the reduction of nitrite to ammonia:

$$NO_2^- + 6\,e^- + 8\,H^+ \xrightarrow{NrfA} NH_4^+ + 2\,H_2O$$

However, this enzyme can also catalyse the two-electron reduction of hydroxylamine (44) and the five-electron reduction of nitric oxide to ammonia (45). NrfA forms a stable complex with its electron donor partner NrfH and exists in a homodimeric form, as resolved from all crystal structures; most notably, the crystal structures of NrfA from *D. vulgaris* at 2.30 Å resolution (46), *D. desulfuricans* at 2.30 Å resolution (47), *W. succinogenes* at 1.70 Å resolution (48) and *E. coli* at 2.30 Å resolution (49). Nonetheless, NrfA from *S. oneidensis* has been described not to form a stable complex with CymA, but to interact transiently. The crystal structure of NrfA from *S. oneidensis* exists at 2.59 Å resolution (50).

Structurally, NrfA is highly conserved amongst those organisms and the solved structure from *S. oneidensis* is similar to that of *E. coli* except the region where it interacts with its electron donor, CymA (33). NrfA exhibits a bis-His haem arrangement for all haems except the catalytic haem where a lysine is the proximal ligand and a water molecule the distal ligand. A Ca^{2+} binding site is present near haem I at the active site. In contrast with NrfA structures from other organisms, *S. oneidensis* does not have a second Ca^{2+} binding site between haems III and IV. The presence of Ca^{2+} had no profound catalytic effect in solution assays and electrochemical experiments (50, 51). This is in contrast with NrfA from *E. coli* where ≥0.5 mM $CaCl_2$ improved the catalytic cycle of the enzyme (52). The presence of $MgCl_2$ had no effect (52), which confirms that Ca^{2+} ions are necessary, but not essential, for catalysis. Nonetheless, the physiological role of the Ca^{2+} binding sites is not yet completely clear.

The *nrfA* gene was deleted by in-frame deletion mutagenesis, resulting in the Δ*nrfA* mutant of *S. oneidensis* (43). Growth cultures, comparing the optical density at different time points and up to 20 h, showed that the Δ*nrfA* mutant

was not able to grow at all on nitrite and its growth on nitrate was impaired compared to the wild type (43). The impaired growth on nitrate is explained by the fact that nitrite is toxic to cells and it has been shown that it results to a prolonged lag-phase (53). Thus, NrfA is essential for nitrite reduction. Interestingly, it was showed that the onset of nitrite reduction occurs on depletion of nitrate by measuring the amounts of nitrate and nitrite by ion chromatography at different time points of cultures of wild type and mutants, involving both the first step of nitrate reduction (Δ*napA*, Δ*napB* & Δ*napA*Δ*napB*) and the subsequent step of nitrite reduction (Δ*nrfA* & Δ*nrfA*Δ*napB*) (43). This finding suggests that a regulatory mechanism is in place, allowing preferential direction of electrons that depends on the substrate availability.

1.3.3.2 TMAO reduction by TMAO reductase TorA

Shewanella species, being of marine origin, are capable of anaerobic respiration by catalysing the reduction of TMAO:

$$TMAO + 2\,e^- + 2\,H^+ \xrightarrow{TorA} TMA + H_2O$$

TMAO is a chemical found in marine fish and invertebrates, where it acts as an osmoprotector (54). *S. oneidensis* reduces TMAO through a soluble enzyme (TorA) with a molecular mass of about 90 kDa that is localised in the periplasmic space (55). TorA has a single molybdenum co-factor for catalysis, as seen from its crystal structure (2.5 Å resolution) from *Shewanella massilia* (56) (**figure 5**). TorA is encoded by *torECAD* operon, but unlike other periplasmic terminal reductases in *S. oneidensis*, TorA accepts electrons from TorC instead of CymA. TorC was identified as a TMAO-inducible band on Coomassie- and haem-stained SDS-PAGE gels of subcellular membranous fractions from *S. massilia* cells grown with and without TMAO (55). *S. massilia* has 96.8% 16S rRNA sequence similarity with *S. oneidensis* (55). Furthermore, the Δ*cymA* mutant was able to grow in the presence of TMAO (36). A Δ*torC* mutant has not been investigated so far; it would be interesting to assess whether TorA can accept electrons from CymA, despite its specificity to accept electrons from TorC.

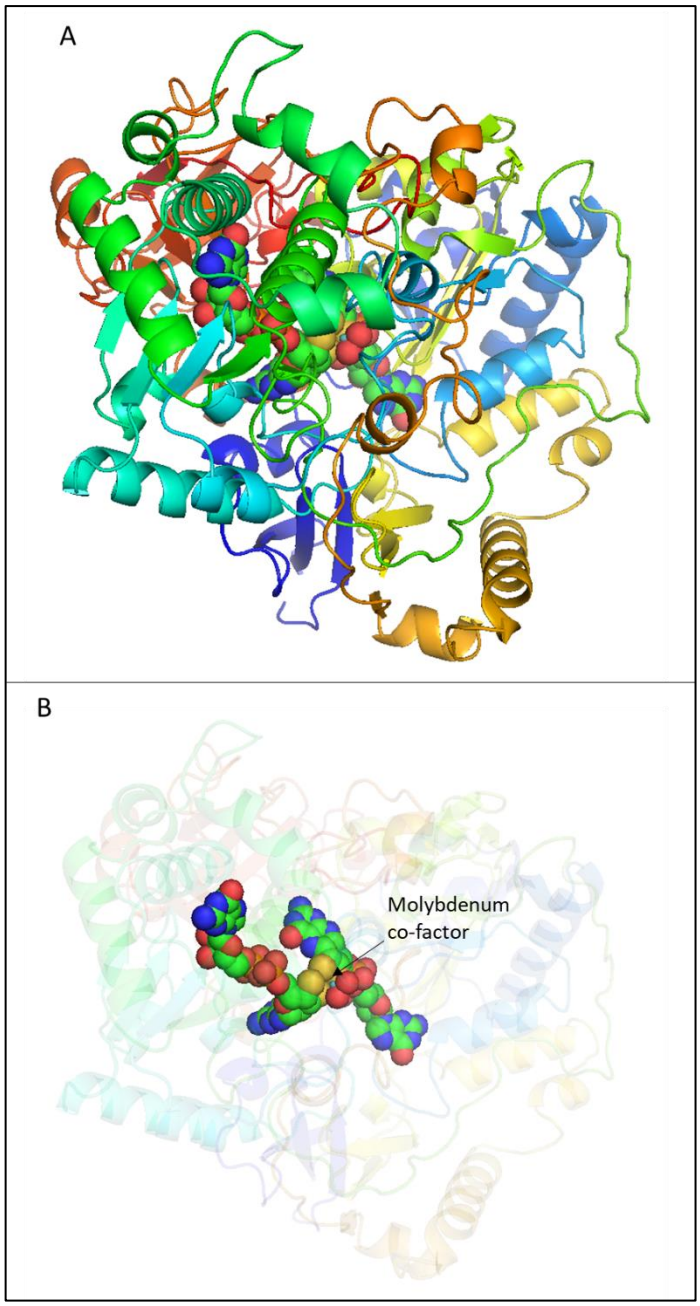

Figure 5: Crystal structure of TorA at 2.5 Å resolution from *Shewanella massilia*. A. The structure is rainbow coloured from N- to C-terminus (blue to red). **B.** The arrangement of the molybdenum co-factor at the catalytic site by two molybdopterin guanine dinucleotides (filled spheres).The image was produced with PyMOL (PDB: 1TMO).

1.3.3.3 Fumarate reduction by fumarate reductase FccA

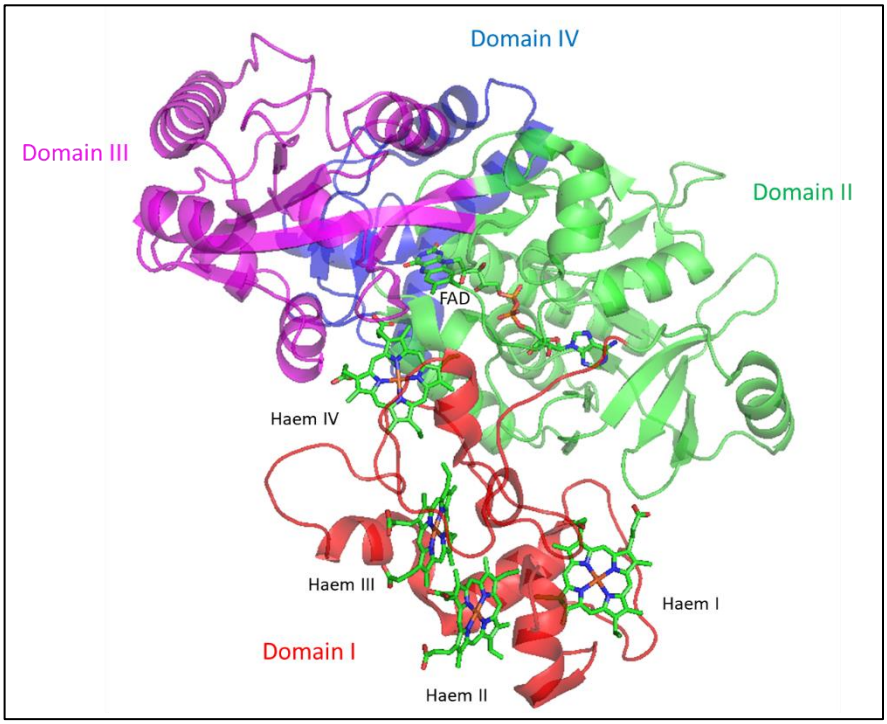

Figure 6: Crystal structure of FccA at 2.9 Å resolution from *Shewanella oneidensis*. The domain I (coloured in red) houses the four haems, which is involved in electron transport to the FAD that is housed in domain II (coloured in green). Domain II along with domains III (coloured in magenta) and IV (coloured in blue) are the catalytic domains of the enzyme. The image was produced with PyMOL (PDB: 1D4C).

The periplasmic fumarate reductase FccA (previously referred to as Fcc_3) is an FAD-containing tetrahaem c-type cytochrome that catalyses the reduction of fumarate to succinate under anaerobic conditions with an approximate molecular mass of 63.8 kDa (57):

$$fumarate + 2\,e^- + FADH_2 \xrightarrow{FccA} succinate + FAD + 2\,H^+$$

In contrast to CymA, there is a plethora of crystal structures of various forms of FccA, including the FccA from *S. oneidensis* MR-1 (58) (**figure 6**). Leys et al (58) presented the solved crystal structures of the free FccA at 2.9 Å resolution, the FccA bound to fumarate at 2.8 Å resolution, and the FccA bound to succinate at 2.5 Å resolution. FccA consists of four domains: three comprising the C-terminal catalytic part of the enzyme and one N-terminal

tetrahaem c-type cytochrome domain. The crystal structure of FccA from *Shewanella frigidimarina* (59% sequence identity) at 1.8 Å resolution is in broad agreement, but it lacks the domain IV (59). Domain I houses four c-type haems, which are covalently bound to the protein. It shows very little secondary structure. Domain I is linked to the FAD pocket via an α-helical linker. Domain II is the FAD domain with a Rossmann fold, which is characteristic of the family of flavoproteins. That is, a 5-stranded parallel β-sheet with 3 α-helices on its one side and a 3-stranded antiparallel β-sheet on the other. Domain III consists of 4-standed antiparallel β-sheet, which is surrounded by a number of α-helices. Lastly, domain IV consists of a small 3-stranded β-sheet and 2 α-helices.

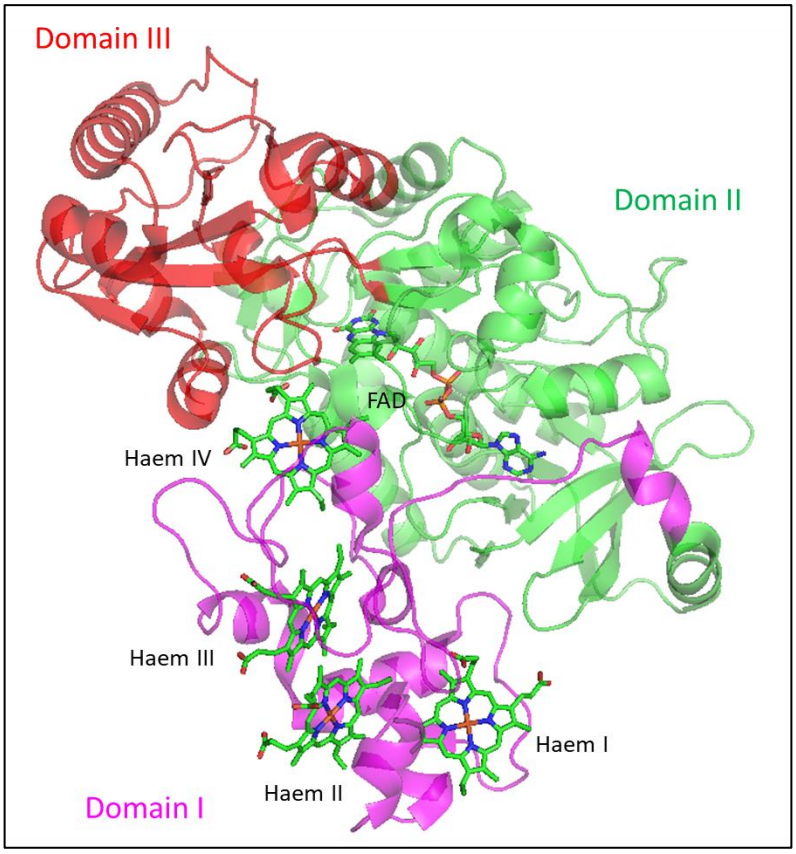

Figure 7: Crystal structure of FccA at 2.9 Å resolution from *Shewanella frigidimarina*. The domain I (coloured in magenta) houses the four haems, which is involved in electron transport to the FAD that is housed in domain II (coloured in green). Domain II along with domain III (coloured in red) are the catalytic domains of the enzyme. The image was produced with PyMOL (PDB: 1QJD).

Domain III (58), which is also referred to as the clamp domain (59), seems flexible and adapts different positions upon substrate binding and subsequent

catalysis, as observed from the three structures mentioned previously. It rotates, forming an enlarged cleft between domains III and IV. The cleft controls access of the substrate to the active site of the protein. This is also in agreement with the FccA structure from *S. frigidimarina* (59) (**figure 7**). It was observed that fumarate and succinate are positioned above and parallel to the isoalloxazine ring of FAD with its two carboxyl groups interacting with residues Arg544, Gly547 and His503 (all of which are highly conserved) (**figure 8**). However, the second carboxyl group of fumarate is shifted compared to that of succinate. Mechanistically, both FccA structures from *S. oneidensis* and *S. fridigimarina* (58, 59) suggest an open conformation of the clamp domain (domain III) in the absence of substrate or product, allowing substrate entry to the active site. Upon binding of fumarate, the clamp domain closes, inducing a twist of the second carboxyl group of fumarate. The central carbon-carbon double bond of fumarate is reduced forming transiently a carbanion intermediate, which is, then, protonated by Arg401.

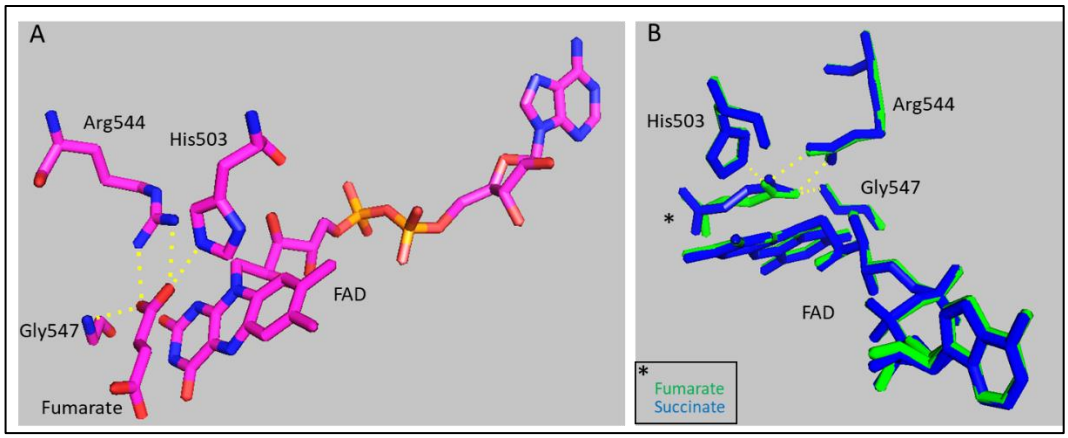

Figure 8: Fumarate and succinate interactions at the catalytic site. A. Fumarate interacts through its two carboxyl groups with the conserved His503, Gly547, and Arg544 residues. **B.** The shifted carboxyl group of succinate in comparison to that of fumarate. The image was produced with PyMOL (PDB: 1D4D and 1D4E).

The N-terminal c-type cytochrome domain (domain I) (58) shows a perpendicular haem arrangement between haem I and II, while haems II and III show a parallel arrangement. Haems III and IV show an edge-to-edge arrangement with the iron atoms to be maximally separated. All four haems, though, are in van der Waals contact that stabilises them and allows fast

electron transfer. This haem arrangement is also observed for FccA from *S. fridigimarina* (59).

FccA was of the first periplasmic proteins to be studied in connection with CymA (33, 60, 61). A cloned CymA lacking its N-terminal trans-membrane domain, $CymA_{sol}$, was constructed and was shown to interact directly with FccA *in vitro* (33). Such interaction is supported by a genomic analysis that specifically links a 3- to 8-fold increase of the transcription levels of *cymA* under fumarate reducing conditions (62). However, another study using formaldehyde cross-linking failed to cross-link the CymA: FccA complex (63). Although four potential CymA complexes with a molecular mass of 34, 54, 95 and 116 kDa were observed, using an antibody against CymA, the binding protein(s) could not be identified (63). An independent nuclear magnetic resonance (NMR) study supports the formation of CymA: FccA complex with a K_D = 398 µM, which is indicative of transient interactions between the two proteins (64). Thus, there is a controversy surrounding the nature of CymA: FccA interactions.

1.3.3.4 Small tetrahaem c-type cytochrome STC

The small Tetrahaem cytochrome, STC, was first isolated from *S. frigidimarina* and later from *S. oneidensis* MR-1 with a molecular mass of 11.8 kDa and 12.2 kDa, respectively, derived from mass-spectroscopy, which is in agreement with the theoretical values (63, 65). STC, previously known as CctA, is encoded by the *cctA* gene (65). It must be noted that the STC protein from *S. oneidensis* MR-1 is 64% similar to that from *S. frigidimarina.* Deletion mutants lacking the *cctA* gene were not able to reduce iron in *S. frigidimarina*, implicating the STC in the iron reduction pathway (65). Consistent with this observation, *in vivo* formaldehyde cross-linking of *S. oneidensis* MR-1 cells that were grown with ferric citrate revealed a complex of STC with CymA by monoclonal antibodies against both CymA and STC (63). Nonetheless, in more recent genetic studies, STC was implicated to have a role in the DMSO reduction pathway and a minor role in the iron citrate reduction pathway, most likely acting as an electron carrier (66). STC was also shown by NMR to interact transiently with MtrA with a K_D of 572 µM (64).

The crystal structures of STC from *S. oneidensis* MR-1 both at its oxidised and reduced form have been solved to a very high resolution of 0.97 Å (**figure 9**) and 1.02 Å respectively (67). It has a protein fold of a series of α-helices that are connected with extended loops. Its four haems are bis-His ligated and are packed in pairs. The arrangement of the haems is highly conserved with the transport of electrons over long distances as the common function. The haems are closely aligned with the haems of the FccA.

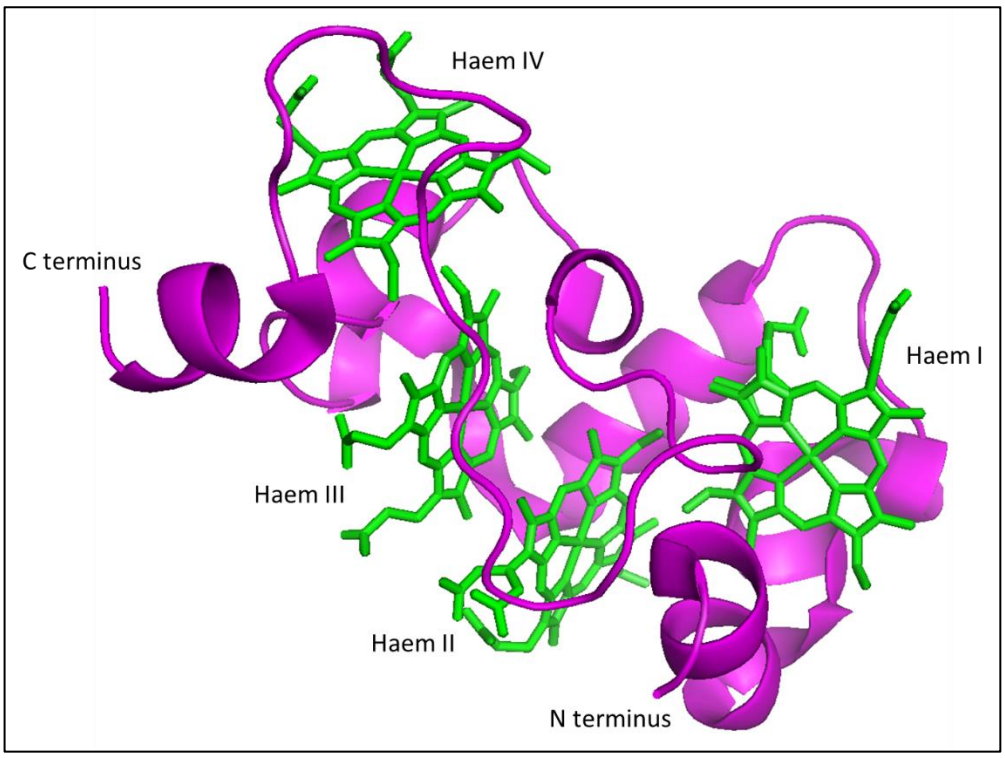

Figure 9: Crystal structure of STC at 0.97 Å resolution from *Shewanella oneidensis*. The polypeptide is shown in magenta, while the four haem groups are presented as green sticks. The image was produced with PyMOL (PDB: 1M1Q).

1.3.4 Respiratory pathways involving extracellular electron transfer

1.3.4.1 Reduction of metal oxides by the MtrCAB/OmcA complex

One of the remarkable abilities of *S. oneidensis*, which is ubiquitous to the *Shewanella* genus, is the use of solid metals for growth. *S. oneidensis* reduces solid metals through extracellular electron transfer, which reaction is catalysed by the MtrCAB/OmcA complex *in vivo*. It must be noted that the minimal machinery for extracellular reduction of solid metals is the MtrCAB complex, which system has also been reconstituted in *E. coli* (68, 69). The proteins forming this outer-membrane complex are found at the gene cluster *mtrDEF-omcA-mtrCAB* (70). MtrF, MtrD and MtrE are homologues of MtrC, MtrA and MtrB respectively and both complexes populate the outer-membrane. OmcA is a homologue of MtrC, which is a decahaem c-type cytochrome that forms the catalytic subunit of the complex. MtrB is a β-barrel integral outer-membrane protein that is responsible for the localisation and stabilisation of the complex proteins at the outer-membrane. MtrA is a periplasmic globular protein and is believed to be involved in electron relay from the inner-membrane to the outer-membrane.

The periplasmic globular protein MtrA is a decahaem c-type cytochrome of an approximate molecular mass of 40 kDa. Homology modelling suggests that it consists of two domains that are homologous to NrfB from *E. coli* (71). Such homology corroborates that MtrA is involved in electron relay, rather than it acts as a terminal reductase. Small-angle X-ray scattering was employed to provide structural insights of MtrA (72). It has been verified by analytical ultracentrifugation that MtrA exists in a monomeric state between 0.5 mg /ml and 4 mg /ml (72). The modelling of data derived from this study suggests a prolate ellipsoid shape of 10.4 nm in length and 5 nm in the widest cross-sectional dimension (72). CymA spans about 4 nm from the inner membrane and the MtrA has a length of about 10 nm, which makes it possible to directly interact with CymA upon its association with the integral MtrB. Further evidence to support this hypothesis arrives from biochemical studies, where MtrA was shown to form a tight complex with MtrB (71). The periplasmic space is about 13 to 25 nm across (73, 74). However, there is not sufficient evidence

to conclusive describe this pathway. It is unclear how MtrA associates with MtrB and how deep inside the porin this association takes place. Thus, if MtrA does not act as a molecular wire spanning across the periplasmic space, it is more likely that STC may act as a molecular shuttle, or be part of the molecular wire. This hypothesis explains the implication of STC to iron reduction.

Analysis of the predicted amino acid sequence revealed that MtrB (approximate molecular mass of 85 kDa) is similar to outer-membrane proteins such as OmpC (27% identical, 41% similar) from *Salmonella typhimurium* and AltE (21% identical, 53% similar) from *Staphylococcus epidermidis* (75). Briefly, OmpC is a non-specific general porin in *E. coli* and the crystal structure was solved with 2.0 Å resolution (76). It exists in a heterotrimeric form with a 16-standed hollow β-barrel fold. It has short connections at the periplasmic side and irregular loops at the extracellular side.

Thus, MtrB is predicted to have a β-barrel structure embedded in the outer membrane, forming a pore of about 4 nm in diameter (71). Early studies analysing membrane fractions from wild-type and Δ*mtrB* mutant showed that MtrB is localised in the outer-membrane, where it is transported by the type-II sretion system (no MtrB was detected in mutants defective in type-II secretion system) (75, 77). This is further supported by a signal peptide found in the *mtrB* gene (75). Furthermore, MtrB does not contain any co-factors related to electron relay. MtrAB co-purified and showed a strong association, while the separation of the two proteins was not possible under non-denaturing conditions (71). Sedimentation equilibrium showed a stoichiometry of 1:1 (MtrA: MtrB) and when MtrC was introduced it showed a stoichiometry of 1:1 (MtrAB: MtrC) (71). The possible role of MtrB (i.e to stabilise the MtrCAB complex in the outer membrane), comes from analysis of the sedimentation equilibrium data: MtrC and MtrA associate with an equilibrium K_D of 11 ± 4 μM, where in the presence of MtrB (MtrAB + MtrC ↔ MtrCAB) the association was much stronger with a $K_D \leq 0.1$ μM (71).

The decahaem c-type outer membrane-anchored cytochrome, MtrC, has an approximate molecular mass of 90 kDa. Structural information derives from the solved crystal structure of its homologue MtrF from *S. oneidensis* at 3.2 Å

resolution (78) (**figure 10**). MtrF is organised into four domains: domains II and IV house the haems, while domains I and III each consists of 7 anti-parallel β-strands with an extended Greek-key topology. The overall fold of the protein is of a split β-barrel. The haems are arranged into a staggered cross structure, suggesting three pathways of electron relay, which explains the association and interaction of MtrC with the outer-membrane anchoring OmcA.

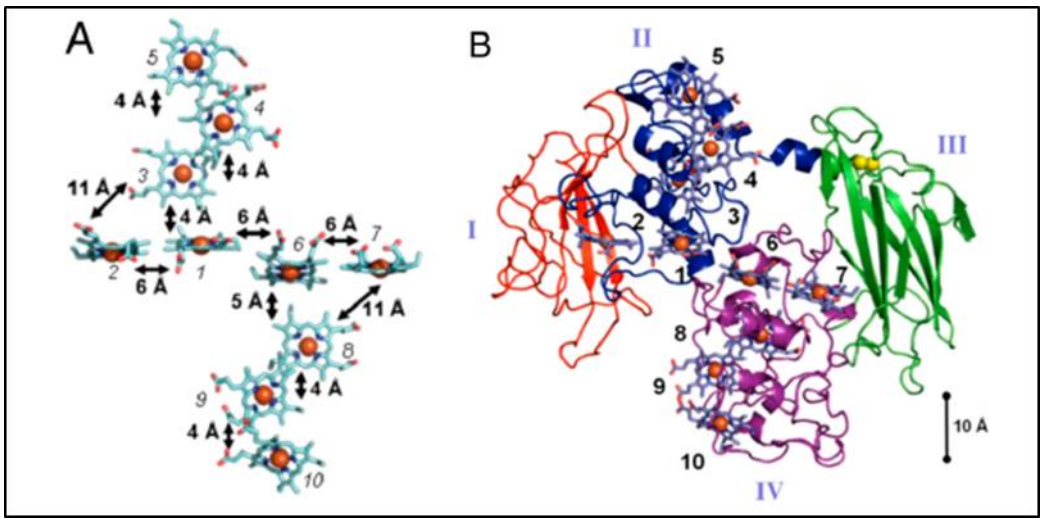

Figure 10: Crystal structure of MtrF at 3.2 Å resolution from *Shewanella oneidensis*. A. The staggered cross arrangement of the haems, which suggests three possible pathways of electron relay: electron entry occurs at haem X, while the possible electron exit could occur through either haems II, VII, or V. B. The structure of MtrF is coloured by domain corresponding to the Latin numerals shown. The images were reproduced from (78).

Based on the crystal structure of MtrF, a homology model of MtrC was generated and analysed (79) (**figure 11**). The MtrC homology model showed a highly similar structure of MtrC to that of MtrF. Co-immunoprecipitation and co-purification studies showed that two molecules of OmcA associate with one molecule of MtrC (80). OmcA is implicated in reducing solid minerals directly, as well as indirectly via the redox cycling of secreted riboflavins (80).

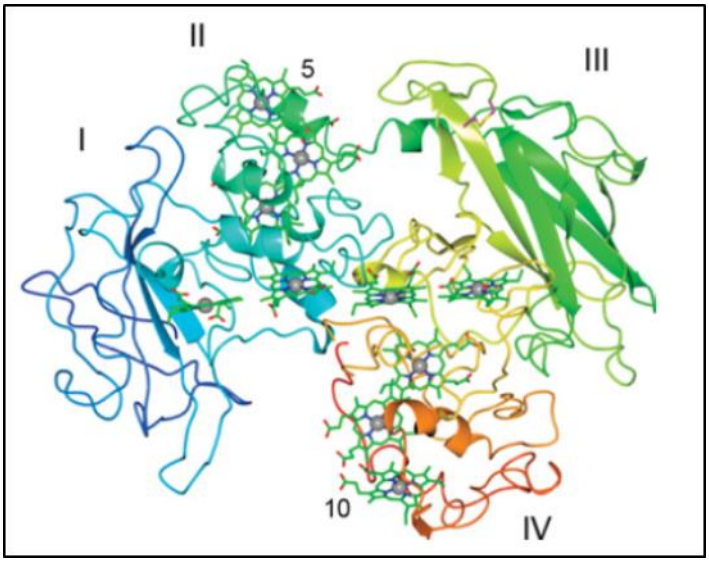

Figure 11: A homology model of MtrC of *Shewanella oneidensis* based on the structure of MtrF. The modelled structure of MtrC is coloured by domain corresponding to the Latin numerals shown. The figure is reproduced from (79).

Further validation of the direct reduction of solid minerals comes from investigation of the cytochrome-hematite interface (using both whole cells and purified proteins) with atomic force microscopy, where it was shown that both OmcA and MtrC form a specific bond with hematite (81). The crystal structure of OmcA from *S. oneidensis* at 2.7 Å resolution has very recently been solved (82). By further investigation of the oligomeric state of OmcA with small-angle X-ray reflection, it was confirmed that OmcA exists as a dimer (82) (**figure 12**), which explains the 2:1 OmcA: MtrCAB interaction and suggests that a dimer (rather than two individual molecules) binds the MtrCAB complex, through interactions with MtrC. The resolved OmcA structure (82) reveals that OmcA is organised into four domains: domains I and III form a Greek-key split β-barrel structure, domains II and IV houses 5 haems each. Domains I and III also have a disulphide bond. All haems exhibit bis-His axial ligation and, like MtrC, they are arranged as a staggered cross. The structure of the OmcA dimers in the crystal (82) suggests that the solvent-exposed haem 10 acts as the exit haem of electrons for the reduction of extracellular metals or small molecules. Interestingly, insertions and deletions of polypeptides were found when OmcA was aligned with MtrF and are responsible for changing the overall surface potential (82). Thus, it is proposed that interactions between

the partner proteins may be achieved by the neutralisation of the negatively charged propionate groups of the c-type haems (82).

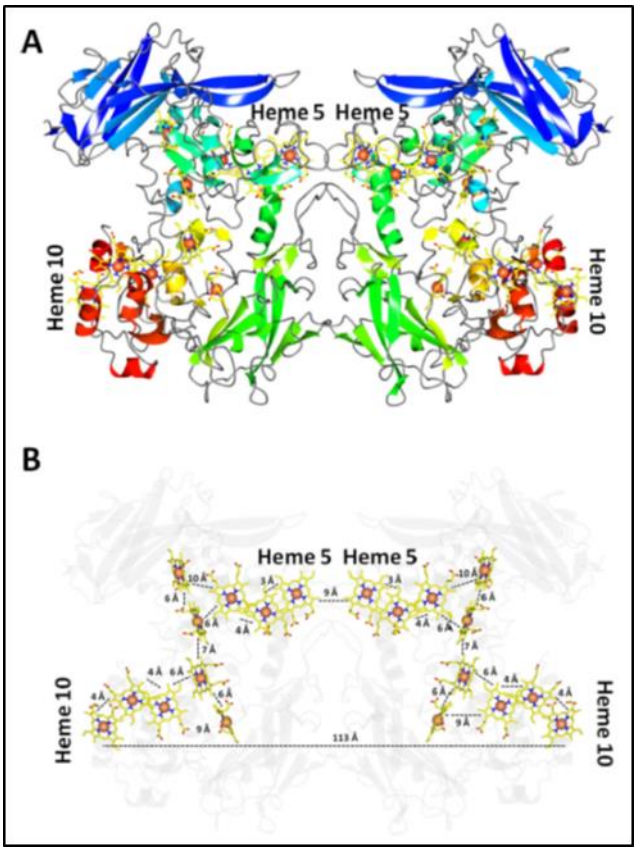

Figure 12: Crystal structure of OmcA homodimer at 2.7 Å resolution from *Shewanella oneidensis*. A. The OmcA homodimer structure coloured by domains: I in green, II in yellow, III in blue, and IV in red. B. The staggered cross haem arrangement. The figure is reproduced from (82).

1.3.4.2 DMSO reduction by the DMSO reductase DmsAB

S. oneidensis reduces DMSO through extracellular electron transfer, which reaction is catalysed by the outer-membrane DMSO reductase DmsAB:

$$DMSO + 2\,e^- + 2\,H^+ \xrightarrow{DmsAB} DMS + H_2O$$

This is in contrast with *E. coli* and *Rhodobacter spp.* DMSO reductase system, which is located at the periplasm (83, 84). DmsAB consists of two subunits, a molybdenum containing DmsA and an iron-sulfur containing DmsB. DmsAB is encoded as part of the operon *dmsEFABGH* (85). DmsB was observed to be localised on the outer-membrane through the construction

of a DmsB construct bearing an epitope tag from human influenza type A virus, which was immunodetected and visualised on whole cells (85). The outer-membrane localisation was further verified by Western blot of cell fractions. Interestingly, similar levels of DmsB were observed in cells grown both anaerobically and aerobically. Δ*dmsE* mutant showed a decreased ability to grow on DMSO, while Δ*dmsB* abolished its ability to grow on DMSO (85). Thus, DmsE is proposed to act as a periplasmic electron shuttle, most probably from shuttling electrons from CymA to the outer-membrane complex. DmsF is an integral membrane protein, localising the outer-membrane that is responsible for anchoring DmsAB. Further analysis of the sequence of the genes, along with electrochemical interrogation of DmsE has shown that DmsE and MtrA share most properties. Thus, Bewley et al (86) suggest a functional relationship between DmsEFAB and MtrCAB.

1.4 Aim of this thesis

This thesis and the work herein is focused on the study of CymA and the nature of its interaction with the periplasmic fumarate reductase FccA of *S. oneidensis*. The underlining basis of those studies is two-fold: firstly, to generate new approaches for the overexpression and purification of CymA in providing new tools in advancing the research field, and, secondly, to investigate the nature of FccA: CymA interaction. Currently, a controversy exists around this interaction. On the one hand, NMR data showed a transient nature of interaction between CymA and FccA with a K_D of 0.4 mM (87), while, on the other hand, biophysical and electrochemical data led the authors to argue for the formation of stable long-lived FccA: CymA complex (88). This thesis directly addresses this controversy. Chapter 3 presents a re-constructive vector and a new recombinant gene for the homologous overexpression for the production of CymA. Chapter 4 presents the heterologous expression for the production of $CymA_{sol}$ [Δ(1-31)-CymA (89): a recombinant form that lacks most of the transmembrane α-helix] and the first reported crystallisation attempt of $CymA_{sol}$, which is instructive for the determination of its crystal structure in the future. Lastly, chapter 5 presents new evidence surrounding the FccA: CymA interaction, which they also address directly previously published observations as a contribution in resolving the controversy on whether they interact transiently or form a stable long-lived complex. Thus, this thesis central aim is to present evidence in arguing that the nature of FccA: CymA interaction is probably of a transient nature under our current knowledge of the system.

Chapter 2 – Materials & Methods

2.1 Materials and Reagents

All materials were used as purchased; a list of vendors for common chemicals that were used in this work is provided in appendix A. Milli-Q grade water with a resistance of 18 MΩ·cm at 21 °C was used in the preparation of all solutions unless otherwise stated. Room temperature: 18 ± 3 °C. A PHM63 digital pH meter was used for measuring the pH of solutions, which was calibrated according to the manufacturer's instructions immediately prior to any measurements.

2.2 Bacterial strains, and plasmids

The bacterial strains that were used in this work were as follows:

- *Shewanella oneidensis* MR-1
  Genotype: Wild type.
  Source: kindly donated by Professor Julea Butt.
- *Escherichia coli* OmniMAX2
  Genotype: F′ {proAB+ lacIq lacZΔM15 Tn10(TetR) Δ(ccdAB)} mcrA Δ(mrr-hsdRMS-mcrBC) φ80(lacZ)ΔM15 Δ(lacZYA-argF) U169 endA1 recA1 supE44 thi-1 gyrA96 relA1 tonA panD.
  Source: kindly provided by Professor Lars Jeuken, but also commercially available by a variety of vendors, such as ThermoFisher Scientific (Cat. no.: C854003).
- *Escherichia coli* BL21 (DE3)
  Genotype: *E. coli* str. B F– ompT gal dcm lon hsdSB(rB–mB–) λ(DE3 [lacI lacUV5-T7p07 ind1 sam7 nin5]) [malB+]K-12(λS).
  Source: kindly provided by Professor Lars Jeuken, but also commercially available by a variety of vendors, such as New England Biolabs (Cat. no.: C2527I).
- *Escherichia coli* BL21 STAR™ (DE3)
  Genotype: F-ompT hsdSB (rB-, mB-) galdcmrne131 (DE3).
  Source: kindly donated by Dr Vincent Postis, but also commercially

available by a variety of vendors, such as ThermoFisher Scientific (Cat. no.: C601003).

The plasmids that were used in this work were as follows:

- pLS167
  A modified pBAD202/D-TOPO, by Invitrogen, vector encoding for CymA with C-terminal fusion of V5-epitope and a His_6 tag.
  Source: kindly donated by Professor Julea Butt with permission from Dr Liang Shi.
- pTH24-TEV-SH
  An expression vector encoding for TEV protease with C-terminal fusion of a V5-epitope and a His_6 tag.
  Source: kindly donated by Dr Vincent Postis.
- pRARE2
  A vector from Novagen that supplies tRNAs for seven rare codons (AUA, AGG, AGA, CUA, CCC, GGA, and CGG) for overcoming *E. coli* codon selection bias during heterologous protein expression.
  Source: kindly donated by Dr Vincent Postis.
- pEC86
  A vector derived from pACYC184 encoding the *ccmA-H* gene cassette that expresses the System I c-type cytochrome assembly complex required for c-type haem maturation of co-expressed c-type cytochromes.
  Source: kindly donated by Professor Julea Butt.
- pMKL1
  An expression vector for the heterologous expression of cytochromes encoding $CymA_{sol}$ with N-terminal fusion of His_6 tag followed by maltose binding protein (MBP). A recognition site for TEV-specific proteolytic cleavage between the tags and the $CymA_{sol}$ is also present.
  Source: kindly donated by Professor Julea Butt with permission from Dr Liang Shi.

2.3 Growth media, and growth & expression conditions

2.3.1 Growth media recipes

- Lysogeny broth (LB) per 1 L: 10 g tryptone, 10 g NaCl, 5 g yeast extract.
- Terrific broth (TB) per 0.9 L: 12 g tryptone, 24 g yeast extract, 4 ml glycerol. The medium was supplemented with 0.1 L of 0.17 M KH_2PO_4, 0.72 M K_2HPO_4 phosphate buffer.
- 2xYT broth per 1 L: 16 g tryptone, 10 g yeast extract, 5 g NaCl.
- Solid-phase medium: LB supplemented with 1.5% w/v agar.

Stocks of kanamycin (in water), carbenicillin (in water), and chloramphenicol (in ethanol) were prepared at 50 mg/ml, 100 mg/ml, and 30 mg/ml respectively. The antibiotics, where indicated, were added to final concentrations of 50 µg/ml kanamycin, 100 µg/ml carbenicillin, and 30 µg/ml chloramphenicol unless otherwise stated. Antibiotic stocks were filter-sterilized and stored at 4 °C for a maximum of 6 months.

2.3.2 Growth media sterilisation

Growth media were sterilised by autoclaving them at 121 °C for 20 min. Chemicals prone to degradation under autoclaving conditions (antibiotics, phosphate buffer, lactate, and fumarate) were sterilised by filtration with filter pore size of 0.22 µm prior to adding them to cooled sterile media using standard aseptic technique.

2.3.3 Standard growth conditions

The standard growth conditions that were used for growing bacteria for general purposes, such us for use in mini-preps, booster cultures, or for producing glycerol stocks were:

For *Shewanella oneidensis* MR-1

Liquid cultures: 30 °C with orbital shaking at 200 rpm for 16 h.

Solid-phase cultures: 30 °C for 24 h.

For *Escherichia coli* strains

Liquid cultures: 37 °C with orbital shaking at 250 rpm for 16 h.

Solid-phase cultures: 37 °C for 16 h.

2.3.4 Expression conditions of CymA† in *Shewanella oneidensis* MR-1/ pTL01

The expression conditions for overexpressing CymA† were based on previously published work (1, 35).

S. oneidensis MR-1/pTL01 was grown on solid-phase medium supplemented with kanamycin under standard growth conditions. A single colony was then used to inoculate 10 ml of LB medium containing kanamycin for small-scale growth under standard conditions. Subsequently, 3% v/v inoculum from the LB culture was used to inoculate 100 ml of 2xYT medium containing kanamycin for medium-scale growth under standard conditions. For expression, the TB cultures (1 L of medium per 2.5 L Erlenmeyer flask) containing kanamycin were inoculated with 3% v/v inoculum from the 2xYT cultures and were incubated under standard conditions until they reached mid-exponential phase (cell density OD_{600} ~ 0.7 AU). Subsequently, the cells were induced with L-arabinose at final concentration of 1 mM and the orbital shaking speed was reduced to 180 rpm in order to further promote microaerobic conditions. The expression of CymA† was allowed to proceed for 18 h before harvesting the cells by centrifugation.

2.3.5 Expression conditions of FccA in *Shewanella oneidensis* MR-1

The expression conditions for overexpressing native FccA were based on previously published work (90).

S. oneidensis MR-1 (wild type) was grown on solid-phase medium under standard growth conditions. A single colony was then used to inoculate 50 ml of LB medium, which was incubated under standard growth conditions. Subsequently, 5 L Duran bottle containing LB supplemented with 25 mM neutralized fumarate and 50 mM DL-lactate, which was pre-equilibrated at 30 °C for 24 h, was inoculated with 0.5% v/v inoculum from the LB cultures. The cells were grown with no agitation (nearly anaerobically in order to induce the expression of FccA) at 30 °C for 24 h before they were harvested by centrifugation.

2.3.6 Expression conditions of {His_6-Maltose Binding Protein (MBP)-TEV cleavage site-$CymA_{sol}$} in *Escherichia coli* BL21(DE3)/ pEC86/ pMKL1

The expression conditions for overexpressing {His_6-MBP-TEV cleavage site-$CymA_{sol}$} were modelled on previously published work (89).

E. coli BL21(DE3)/pEC86/pMKL1 was grown on solid-phase medium that was supplemented with carbenicillin and chloramphenicol under standard growth conditions. A single colony was then used to inoculate 10 ml of LB medium supplemented with carbenicillin and chloramphenicol for small-scale growth under standard conditions. Subsequently, 3% v/v inoculum from the LB culture was used to inoculate 100 ml of 2xYT medium containing carbenicillin and chloramphenicol for medium-scale growth at 30 °C with orbital shaking at 200 rpm for 16 h. The expression TB cultures (1 L of medium per 2.5 L Erlenmeyer flask) containing carbenicillin and chloramphenicol were inoculated with 3% v/v inoculum from the 2xYT cultures and were incubated at 30 °C with orbital shaking at 200 rpm until they reached the mid-exponential phase (cell density OD_{600} ~ 0.7 AU). Subsequently, the cells were induced with isopropyl β-D-1-

thiogalactopyranoside (IPTG) at final concentration of 50 µM. The expression was allowed to proceed for 16 h before harvesting the cells by centrifugation.

2.3.7 Expression conditions of recombinant TEV in *Escherichia coli* BL21 STAR™ (DE3)/ pRARE2/ pTH24-TEV-SH

The expression conditions for overexpressing recombinant TEV were in accordance to a kindly provided protocol by Dr Vincent Postis.

E. coli BL21 STAR™ (DE3)/pRARE2/pTH24-TEV-SH cells were grown on solid-phase medium supplemented with carbenicillin and chloramphenicol under standard conditions. A single colony was used to provide the inoculum for the expression culture in LB supplemented with carbenicillin and chloramphenicol, which was grown under standard conditions. A 30 L fermenter with TB medium containing carbenicillin and chloramphenicol was inoculated with 1% v/v inoculum. The OD_{600} was ~ 0.05 AU at the time of inoculation. The culture was incubated at 20 °C with agitation until the OD_{600} reached ~ 0.6 AU, before expression was induced with IPTG at final concentration of 0.1 mM. The expression was allowed to proceed for 20 h before the cells were harvested by centrifugation. The 30 L fermenter culture was prepared by David Sharples operating a Fermenter Bioflow3000 by Newbrunswick.

2.4 Molecular Biology Methods

2.4.1 Plasmid purification (mini-prep)

Routinely, bacterial cells harbouring the target plasmid(s) for purification were grown in LB cultures supplemented with the necessary antibiotics under standard conditions. Plasmid purification was conducted using the ChargeSwitch® Pro Filter Plasmid Miniprep Kit (Invitrogen), following the provided protocol, from 4 ml of bacterial culture. Purified plasmids were stored at 4 °C for use within a week, or at -20 °C for long-term storage.

2.4.2 DNA quantification

DNA quantification was performed spectrophotometrically using a Shimadzu UV-2450 UV-VIS spectrophotometer and a quartz-crystal cuvette with 0.1 cm path-length. The DNA sample was diluted 50-fold with water before absorbance values were measured at 260 nm and 280 nm. The value that was used for quantification was 50 µg/ml of dsDNA = 1.0 AU absorbance at 260 nm for a cuvette with 0.1 cm path-length. The ratio A_{260}/A_{280} was used as a measure of sample purity and samples that exhibited purity ratio between 1.6 and 2.0 were used in subsequent experiments.

Quantification of DNA fragments purified from agarose gels was performed using the ND-1000 Nanodrop™ micro-spectrophotometer (ThermoFisher Scientific).

2.4.3 Digestion of plasmids with NcoI and HindIII restriction enzymes

Digestion of pUC57 or pLS167 plasmids was performed in thin-wall PCR tubes with high-fidelity restriction enzymes NcoI-HF® (20,000 units/ml by New England Biolabs) and HindIII-HF® (20,000 units/ml by New England Biolabs). The buffer that was used was NEBuffer 4 (cat. No.: B7004S) from New England Biolabs. Approximately 2 µg of plasmid DNA and 40 units of each restriction enzyme were used in a 50 µl total reaction volume.

The tubes were incubated at 37 °C for 3 h in a DNA Engine Dyad® peltier thermal cycler (Bio-Rad).

2.4.4 Separation of DNA fragments by agarose gel electrophoresis

Agarose gel was prepared in tris acetic acid EDTA (TAE) buffer, which consisted, at final concentration, of 40 mM Tris pH 8.3, 20 mM acetic acid, and 1 mM EDTA.

Agarose was added to 1-2 % w/v and the suspension was heated in a microwave until all of the agarose was fully dissolved (approximately 1.5 min at maximum power in a 900W microwave). Subsequently, the solution was cooled under running tap water before 2 µl of SYBR® safe DNA gel stain was added (per 30 ml of solution) and mixed by gentle swirling. The solution was poured into a gel cassette with an attached comb of an Embi Tec RunOne™ electrophoresis cell and was left to set at room temperature for approximately 20 min.

Concentrated (6-fold) MassRuler™ DNA loading dye was added to all DNA samples prior to loading them onto the agarose gel. Fermentas MassRuler™ DNA ladder mix (5 µl) was loaded alongside the DNA samples onto the agarose gel. The agarose gel was run at constant voltage of 100 V until the DNA loading dye line had migrated approximately ¾ of the way down the gel.

2.4.5 Purification of DNA fragments from agarose gels

DNA fragments were separated by agarose gel electrophoresis and the bands of interest were carefully excised from the gel using a scalpel-blade while visualising the DNA bands with Invitrogen Safe Imager™. The DNA fragments were purified using Wizard® SV Gel and PCR clean-up System (Promega) by following the supplied protocol.

2.4.6 Ligation of DNA fragments

Ligation reactions that contained 50 ng of linearized vector and sufficient insert to give a molar ratio of 3:1, 5:1, and 6:1 (insert to vector) were performed in thin-wall PCR tubes. 2,000 units of T4 DNA ligase (2,000,000 units/ml from New England Biolabs) and the supplied 10xT4 DNA ligase reaction buffer (New England Biolabs) was used in a total reaction volume of 25 µl.

The tubes were incubated at 21 °C for 16 h in a DNA Engine Dyad® peltier thermal cycler (Bio-Rad). The temperature was then lowered to 4 °C and the samples were used to transform *E. coli* OmniMAX2 cells within 1hr.

2.4.7 Preparation of competent bacterial cells for transformation

2.4.7.1 Electro-competent *Shewanella oneidensis* MR-1

S. oneidensis MR-1 was grown on solid-phase LB medium under standard conditions, from which a single colony was used to inoculate 10 ml LB medium that was grown under standard conditions. Subsequently, 100 ml LB medium (in 250 ml Erlenmeyer flask) was inoculated with 2% v/v inoculum from the 10 ml LB culture and was grown at 30 °C with orbital shaking at 200 rpm until the cell density reached OD_{600} ~ 0.4 AU. The cells were pelleted by centrifugation at 3,220 g for 15 min at 4 °C. The supernatant was discarded and the cells were resuspended in 16.5 ml of ice-cold filter-sterilized 1 M sorbitol (per cell pellet from 50 ml of culture). The cells were pelleted by centrifugation as before. The supernatant was discarded and the cells were resuspended in 2 ml of ice-cold filter-sterilized 1 M sorbitol (per cell pellet from 50 ml of culture). The resulting electro-competent cells were used within 15 min, as they do not remain viable any longer. The cells were kept on ice at all times.

2.4.7.2 Chemically competent *Escherichia coli* strains

E. coli strains were grown on solid-phase LB medium under standard conditions, from which a single colony was used to inoculate 10 ml LB medium that was grown under standard conditions. Subsequently, 100 ml LB medium (in 250 ml Erlenmeyer flask) was inoculated with 2% v/v inoculum from the 10

ml LB culture and was grown at 30 °C with orbital shaking at 200 rpm until the cell density reached OD_{600} ~ 0.5 AU. The cell culture was then incubated on ice for 10 min before the cells were pelleted by centrifugation at 3,220 g for 15 min at 4 °C. The supernatant was discarded and the cells were resuspended in 10 ml of ice-cold filter-sterilized 50 mM Ca_2Cl (per cell pellet from 50 ml of culture). The suspension was incubated on ice for 15 min before the cells were pelleted by centrifugation as before. The supernatant was discarded and the cells were resuspended in 1 ml of ice-cold filter-sterilized 100 mM Ca_2Cl, 15% v/v glycerol (per cell pellet from 50 ml of culture). The cells were aliquoted into 50 µl aliquots (working on ice), flash-frozen in liquid nitrogen, and stored at -80 °C.

2.4.8 Transformation of competent bacterial cells

2.4.8.1 Transformation of *Shewanella oneidensis* MR-1 by electroporation

The transformation of *S. oneidensis* MR-1 by electroporation was based on previously described work (91). Electro-competent *S. oneidensis* MR-1 cells were placed on pre-cooled electroporation Bio-Rad Gene Pulser® cuvettes (390 µl cells for 0.2 cm gap cuvettes, or 50 µl cells for 0.1 cm gap cuvettes). Plasmid DNA in the range of 0.1 µg to 0.5 µg was also added to the cuvettes. It must be noted that no equilibration is necessary for electroporation. The cuvettes were then transferred from ice to Micropulser™ Electroporation Apparatus (Bio-Rad) and a single pulse of 1.10 kV or 0.55 kV was delivered for 0.2 cm or 0.1 cm gap cuvettes respectively. Care was taken to remove water condensation from the cuvettes by gently wiping the exterior of the electrodes with tissue-paper before pulse-delivery. Subsequently, the cells were transferred to a sterile Eppendorf tube and 800 µl or 300 µl of pre-warmed at 30 °C LB medium was added for 0.2 cm or 0.1 cm gap cuvettes respectively. The cells were allowed to recover by incubation at 30 °C for 1.5 h to 2 h with intermittent mixing by inversion. The cells were, lastly, plated on selective solid-phase LB medium supplemented with 30 µg/ml kanamycin and were incubated at 30 °C for 48 h.

Cell colonies from the selective plates were used to inoculate solid-phase LB medium supplemented with kanamycin (50 µg/ml) and were further incubated at 30 °C for 48 h. Cell colonies were used to inoculate 10 ml LB medium supplemented with kanamycin (50 µg/ml) and were grown under standard conditions. Cultures that exhibited good growth were used for mini-prep for plasmid analysis by Sanger sequencing, as well as for making glycerol stocks.

2.4.8.2 Transformation of *Escherichia coli* strains by heat shock

Chemically competent *E. coli* strains pre-aliquoted into 50 µl aliquots were thawed on ice. Sufficient DNA was added and the suspension was incubated on ice for 30 min. Subsequently, a heat-shock was delivered by incubation at 42 °C for 60 – 120 s, before incubation on ice for 5 min. Then, 300 µl of pre-warmed at 37 °C LB medium was added in each tube. The cells were allowed to recover by incubation at 37 °C for 45 min to 1 hr with intermittent mixing by inversion. The cells were lastly plated on selective solid-phase LB medium supplemented with the appropriate antibiotic(s) and were incubated at 37 °C for 16 h in order to allow selection of the transformed bacterial cells.

2.4.9 Sanger sequencing of plasmids

DNA sequencing of pBAD202/D-TOPO type of plasmids (pLS167 and pTL01-pTL04) was performed with the Sanger method using PBAD forward (5'-ATG CCA TAG CAT TTT TAT CC-3'), or PBAD reverse primers (5'-GAT TTA ATC TGT ATC AGG-3') by ©Source BioScience. The DNA concentration for samples submitted for Sanger sequencing was 100 ng/µl.

Bases were called by ABI Basecaller by © Source BioScience and no further processing of the chromatograms was conducted. The Phred quality score for all sequencing results was 30. That is, 1 in 1,000 probability of incorrect base calling, or 99.9% base call accuracy.

2.4.10 Preparation of glycerol stocks of bacterial cultures

Bacterial cultures that had been grown under standard conditions were used for preparing glycerol stocks. Cryovials (2.5 ml) containing 500 µl of 50% v/v glycerol were sterilized by autoclaving them at 121 °C for 20 min. A volume of 500 µl of bacterial cell culture was added in a sterile cryovial (containing 50% v/v glycerol) using standard aseptic technique. The suspension was mixed by inversion, flash-frozen with liquid nitrogen, and stored at -80 °C.

2.5 Biochemical Methods

2.5.1 UV-visible absorbance spectroscopy

Spectroscopic experiments were performed at ambient conditions using a Shimadzu UV-2450 UV-VIS spectrophotometer and a quartz-crystal cuvette with 0.1 cm path-length unless otherwise stated. Spectra of reduced protein samples were obtained by addition of excess of sodium dithionite to the quartz-crystal cuvette and mixing by inversion immediately before measurements. Sodium dithionite powder was dissolved in degassed buffer and used immediately.

2.5.2 Sodium-dodecyl sulphate polyacrylamide gel electrophoresis (SDS-PAGE)

SDS-PAGE was performed on hand-casted mini gels with 1.0 mm thickness using a Bio-Rad Mini-PROTEAN® cell casting apparatus.

The recipe for resolving and stacking gel solutions is shown in **table 1**.

Table 1: Recipe of resolving and stacking solutions for the preparation of two mini-gels.

Components	12.5% Resolving	15% Resolving	6% Stacking
10% w/v SDS	0.1 ml	0.1 ml	50 µl
40% w/v Acrylamide	3.475 ml	4.22 ml	0.77 ml
2% w/v bis-acrylamide	0.45 ml	0.49 ml	0.39 ml
0.5 M Tris-HCl, pH 6.8	-	-	0.75 ml
1.5 M Tris-HCl, pH 8.8	2.81 ml	2.81 ml	-
water	4.267 ml	3.48 ml	3.2 ml
10% w/v Ammonium persulphate	37 µl	37 µl	30 µl
TEMED	24 µl	24 µl	9 µl

Tetramethylethylenediamine (TEMED) was added last and immediately prior to pouring each gel. The resolving gel was poured first. A layer of isopropanol was carefully poured on top of it and it was allowed to set for approximately 20 min at room temperature. Once the gel was set, the isopropanol layer was removed before the stacking gel was poured on top of the resolving gel. A Bio-Rad Mini-PROTEAN® 10-well 1.0 thickness comb was placed and the gel was allowed to set for approximately 20 min at room temperature.

The mini-gels were run in a Bio-Rad Mini-PROTEAN® Tetra Vertical Electrophoresis Cell at room temperature in running buffer. Typically, two or four mini-gels were run until the dye reached the end of the mini gel at constant current of 40 mA or 60 mA respectively using a Bio-Rad PowerPac™ Basic Power Supply. The running buffer consisted, at final concentration, of 25 mM Tris-HCl pH 8.6, 192 mM glycine, and 0.1% w/v SDS.

2.5.3 Treatment of samples for SDS-PAGE analysis

Samples for SDS-PAGE analysis were mixed with denaturing loading buffer, briefly vortexed, and incubated at either (a) 90 °C for ~ 15 min, or (b) 37 °C for between 1 to 2 h. Usually, condition *a* was used for globular proteins, while condition *b* was used for membrane proteins. Samples containing whole cells were treated using condition *a* and briefly centrifuged at 13,000 g.

The loading buffer consisted, at final concentration, of 50 mM Tris-HCl pH 6.8, 20% w/v glycerol, 2% w/v SDS, 2% v/v β-mercaptoethanol, and 0.01% w/v bromophenol blue.

The loading buffer of samples for mini-gels that were to be subjected to the haem staining procedure consisted, at final concentration, of 6 M urea, 5% w/v SDS, 0.1 % w/v glycerol, and 0.05% w/v bromophenol blue. This allows the elimination of the reducing agent β-mercaptoethanol that prohibits the oxidation of the chromogenic reagent tetramethylbenzidine (TMBZ) during the haem staining procedure (described in section ***2.5.5 SDS-PAGE mini-gel staining with Haem staining***).

2.5.4 SDS-PAGE mini-gel staining with Coomassie stain

Visualisation of proteins resolved by SDS-PAGE on a mini-gel was performed by Coomassie stain (92). The mini-gel was incubated in Coomassie stain for 16 h with gentle orbital shaking at room temperature. Subsequently, the mini-gel was de-stained until background staining was removed by several (usually three) 30 min washes in de-staining solution with gentle orbital shaking at room temperature.

The Coomassie staining solution consisted, at final concentration, of 1.21 mM Coomassie brilliant blue R-250, 50% v/v methanol, and 10% v/v acetic acid. For preparing the Coomassie staining solution, the components were mixed and were stirred at room temperature for 4 h before being filtered with standard coffee filter paper. The de-staining solution consisted, at final concentration, of 40% v/v methanol, and 10% v/v acetic acid. Both the Coomassie staining and de-staining solutions were stored at room temperature.

Alternatively, the mini-gels were stained by incubation in Expedeon InstantBlue™ protein stain for 15 min with gentle orbital shaking at room temperature (a de-staining step was not required).

2.5.5 SDS-PAGE mini-gel staining with Haem staining

Visualisation of c-type cytochromes was performed by haem staining of SDS-PAGE mini-gel that utilizes the haem-associated peroxidase activity to the oxidation of the chromogenic reagent TMBZ that turns blue when it is oxidised. This haem staining procedure of electrophoretically resolved cytochromes are particular specific for c-type cytochromes since c-type haems are covalently bound to the polypeptide. In contrast, b-type haems are not covalently bound to the polypeptide and may dissociate from the protein under denaturing conditions, allowing them to migrate out of the gel during electrophoresis.

This procedure was based on previously described work (93). The mini-gel was incubated in 80 ml of 0.25 M sodium acetate pH 5.0 for at least 20 min at room temperature with gentle orbital shaking in a container that was covered with aluminium foil in order to prevent light degradation of the light sensitive

TMBZ. Subsequently, a TMBZ solution was prepared by dissolving 40 mg of TMBZ in 40 ml methanol and was added to the sodium acetate solution containing the pre-equilibrated mini-gel. The mini-gel was further incubated for 14 min at room temperature with gentle orbital shaking. Lastly, 400 µl of ≥ 30% hydrogen peroxide was added to the main solution and was incubated for 16 h at room temperature with gentle orbital shaking.

2.5.6 Western blot

Samples for immunodetection analysis were prepared as described in section ***2.5.3 treatment of samples for SDS-PAGE analysis*** and the proteins were electrophoretically resolved as described in section ***2.5.2 sodium-dodecyl sulphate polyacrylamide gel electrophoresis***.

Subsequently, the mini-gel was incubated in transfer buffer (47.8 mM Tris-HCl pH 8.3, 38.6 mM glycine, 20% v/v methanol) for 15 min at room temperature with gentle orbital shaking. The gel was then subjected to semi-dry electro-transfer of proteins from the mini-gel onto a Bio-Rad nitrocellulose membrane with 0.45 µm pore size using a Millipore MilliBlot Graphite Electroblotter II. The electrode assembly for protein electro-transfer was from bottom (positive electrode) to top (negative electrode): 2x Whatman® gel blotting paper, nitrocellulose membrane, mini-gel, 2x Whatman® gel blotting paper. All of the components were soaked in transfer buffer immediately before being assembled. Electro-transfer was conducted at room temperature under constant current at 150 mA for 42 min (for one mini-gel) or for 61 min (for two mini-gels) using a Bio-Rad PowerPac™ Basic Power Supply.

Alternatively, electro-transfer of resolved proteins from a mini-gel onto a nitrocellulose membrane was performed with the Bio-Rad Trans-Blot® Turbo™ RTA Mini Nitrocellulose Transfer kit, following the provided protocol, and operating a Bio-Rad Trans-Blot® Turbo™ Transfer System, according to the manufacturer's instructions.

The nitrocellulose membrane was then blocked with blocking buffer, 3% w/v bovine serum albumin (BSA) in TBST, for 16 h at room temperature with roller-mixing. TBST buffer consisted, at final concentration, of 25 mM Tris-HCl pH

7.5, 150 mM NaCl, and 1% v/v Tween®20. Subsequently, the membrane was incubated with the primary antibody for 1.5 h at room temperature with roller-mixing before being washed with TBST buffer 4x 20 min under the same conditions. The membrane was then further incubated with the secondary antibody (when necessary) for a further of 1.5 h before being washed with TBST buffer 4x 20 min under the same conditions.

The membrane was developed with the application of Pierce™ 1-Step NBT-BCIP chromogenic reagent for alkaline phosphatase (AP) probes using the manufacturer's instructions that were provided with the product.

The antibodies that were used for Western blotting were as follows:

1. Anti-6X His tag® antibody [HIS-1] (alkaline phosphatase) ab49746 purchased from abcam®. This is a monoclonal antibody with clone number HIS-1 and IgG2a isotype, provided at 1.8 mg ml^{-1}. This antibody was used at 1:5,000 in TBST buffer containing 3% w/v BSA.
2. Goat Anti-Rabbit IgG H&L (alkaline phosphatase) ab97048 purchased from abcam®. This is a polyclonal antibody with IgG isotype, provided at 1.0 mg ml^{-1}. This antibody was used at 3:20,000 in TBST buffer containing 3% w/v BSA.
3. Rabbit Anti-CymA2 kindly donated by Professor Julea Butt. This is a monoclonal antibody against a CymA epitope (NEVLASAHGGGKAGC), provided at 1.88 mg ml^{-1}. This antibody was used at final concentration of 0.6 µg/ml in TBST buffer containing 3% w/v BSA.

2.5.7 Protein quantification

The quantification of total protein of solutions was performed with the micro bicinchoninic acid (µBCA) assay in a 96-well plate. BSA was used for producing a calibration curve in triplicate with a range from 0 to 1 µg $µl^{-1}$. A calibration curve was derived from BSA standards for each 96-well plate; a typical calibration curve is shown in **figure 13**. The sample volume was 10 µl, while the total reaction volume was 210 µl. The samples of unknown

concentration were diluted 2- and 10-fold in order to avoid extrapolation. Each unknown sample was performed in triplicate.

Pierce™ BCA Protein Assay Reagent A was mixed with 4% w/v Copper sulphate at 50:1 ratio respectively to yield the final reagent solution. A volume of 200 µl of the final reagent solution was added to each well containing 10 µl of sample. Subsequently, the plate was incubated at 37 °C for 30 min. The plate was then transferred to room temperature and was left to cool down for 5 min before absorbance readings at 551 nm were taken with Multiskan™ FC Microplate Photometer (ThermoFisher Scientific).

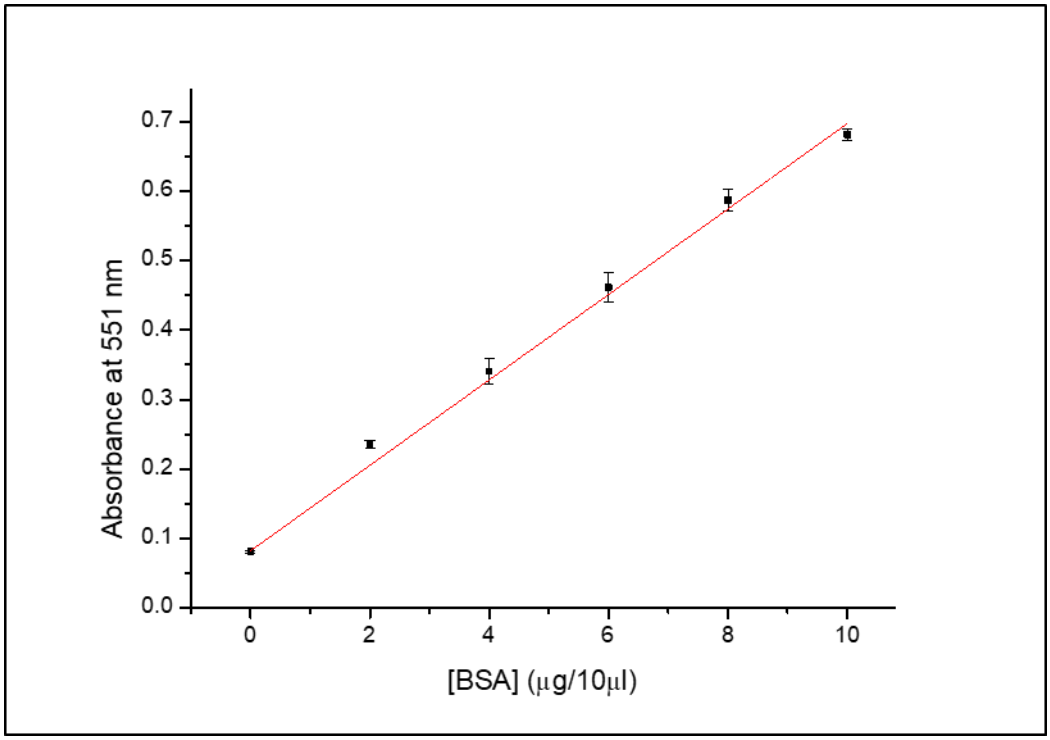

Figure 13: A typical BCA calibration curve using BSA standards. Triplicate samples of known BSA concentration plotted against their measured 551 nm absorbance values. The line of best fit (in red) was computed by linear fitting of the points and was used for the interpolation of the values of the samples of unknown protein concentration.

Purified recombinant forms of CymA and purified native form of FccA protein samples were quantified spectrophotometrically from their obtained spectra using the Beer-Lambert law:

$$Abs_{\lambda_1} = \varepsilon_{\lambda_1} \cdot C \cdot l \qquad (1)$$

where Abs_{λ_1} and ε_{λ_1} are the absorbance and extinction coefficient respectively at wavelength λ_1, C is the concentration, and l is the cuvette path length .The extinction coefficient values that were used for CymA and FccA were $\varepsilon_{407\,nm}^{CymA} = 380 \pm 38\, mM^{-1}\, cm^{-1}$ (1) and $\varepsilon_{410\,nm}^{FccA} = 728.4\, mM^{-1}\, cm^{-1}$ (57) respectively.

2.5.8 Protein crystallisation screens

Protein crystallisation screens were performed in 96-well 3-drop plates with 30 µl reservoir crystallisation solution and with purified $CymA_{sol}$ at 1 mg ml^{-1}. Crystallisation solutions were added manually to reservoir of each well. Drops 1, 2, and 3 contained 1:1, 1:2, and 2:1 ratios of protein to crystallisation solution respectively, and were mixed and dispensed automatically by Formulatrix NT8 automated nanolitre volume liquid handler operated by Formulatrix 2.0 Rock Maker software. The plates were sealed with clear polystyrene standard lid and were deposited in the Formulatrix Rock Imager 1000, where the plates were incubated at room temperature and automatically imaged according to a user-defined imaging schedule. Optical imaging of the individual drops were performed at: time of plate deposition (0 d 0 hr), 0 d 12 h, 1 d 12 h, 2 d 12 h, 3 d 12 h, 5 d 12 h, 8 d 12 h, 13 d 12 h, 21 d 12 h, and 34 d 12 h. Ultraviolet two-photon excited fluorescence (UV-TPEF) and second-harmonic generation (SHG) imaging of the individual drops were performed at: 5 d 12 h, 13 d 12 h, 21 d 12 h, and 34 d 12 h.

The commercially available screens that were performed (seven in total) are as follows:

1. JCSG Core I, II, III, and IV Suites (Qiagen)
2. PACT Suite (Qiagen)
3. MemGold2™ (Molecular Dimensions)
4. Morpheus® (Molecular Dimensions)

This allowed the screening of 672 different solution compositions for crystallizing $CymA_{sol}$ at room temperature and at three different protein to solution ratios for each. Thus, the total number of different conditions that were assayed was 2,016.

2.5.9 Handling of lipids and preparation of lipid mixtures

Lipids were purchased from Avanti® Polar Lipids Limited as chloroform solutions in glass ampoules. The provided lipid concentration, which was typically within 10% error, was used for calculations. The glass ampoules were stored at -20 °C for long-term storage. Working aliquots of 5 mg lipids were prepared in glass vials; the chloroform was evaporated under a current stream of nitrogen gas and the vials were placed in a vacuum desiccator for at least 4 h to ensure complete removal of residual chloroform. The vials, containing 5 mg of dry lipids, were stored under nitrogen gas in a sealed glass round flask at -20 °C.

Lipid mixtures were prepared by dissolving the lipids in 1:1 methanol: chloroform solution. Quinones were dissolved in chloroform and working stock solutions were stored in glass vials at -20 °C. Appropriate volumes of each required lipid and/or quinones were mixed into a glass vial. Subsequently, the organic solvents were evaporated under a current stream of nitrogen gas and then the vials were placed in a vacuum desiccator for at least 4 h to remove residual organic solvents. The vials, containing dry lipid mixtures with/without quinones, were stored under nitrogen gas in a sealed glass round flask at -20 °C.

2.5.10 Preparation of homogeneous solutions of liposomes

Aliquots of lipids or lipid mixtures (5 mg) were used in the preparation of homogenous solutions of liposomes. The dry lipids were hydrated with the addition of buffer (typically: 20 mM MOPS pH 7.4, 30 mM Na_2SO_4) and vortex-mixed to ensure complete suspension of the dry lipids. At this stage, the solution of liposomes is highly heterogeneous. In order to homogenise the formed liposomes, the solution was extruded 11 times through a 200 nm pore size (unless otherwise stated) Whatman® Nuclepore™ track-etched membrane using an Avanti® mini extruder. The resulted solutions of liposomes was considered to be homogenous and was used on the day of preparation.

2.5.11 Reconstitution of CymA† into liposomes

CymA† proteoliposomes were prepared by the octyl-glycoside (OG) rapid dilution method, as described previously (88, 94). An aliquot of the desired lipids or lipid mixtures (5 mg) was hydrated and resuspended in 20 mM MOPS pH 7.4, 30 mM Na_2SO_4 buffer to a concentration of 9 mg ml^{-1} by vortex-mixing. Subsequently, 250 mM OG stock solution (prepared in the same buffer) was added to the liposome solution, which was pipette mixed in order to dissolve the liposomes. The concentration of OG at this step was 55 mM. CymA† was then added at 1%, 1.5%, or 2% w/w (protein: lipid). The concentration of OG at this step was around 51 mM. The mixture was then incubated for 15 min on ice. Subsequently, ice-cold buffer was rapidly added to the mixture providing rapid dilution of approximately 140-fold. The formed proteoliposomes were pelleted by ultra-centrifugation at 131,000 g for 60 min at 4 °C. The pellet was resuspended in buffer at concentration of 5 mg ml^{-1} (assuming no lipid loses). The resuspended proteoliposomes were homogenised by extruding the solution 11 times through a 200 nm pore size Whatman® Nuclepore™ track-etched membrane using an Avanti® mini extruder. At this stage, each CymA† reconstitution was spectrophotometrically assayed for the incorporation of CymA†. UV-visible absorbance spectra were taken where, in a successful protein reconstitution, the Soret γ-band (at wavelengths 407 nm → 419 nm, which corresponds to CymA) can be observed; a representative example is shown in **figure 14**. The proteoliposome solution was used on the day of preparation.

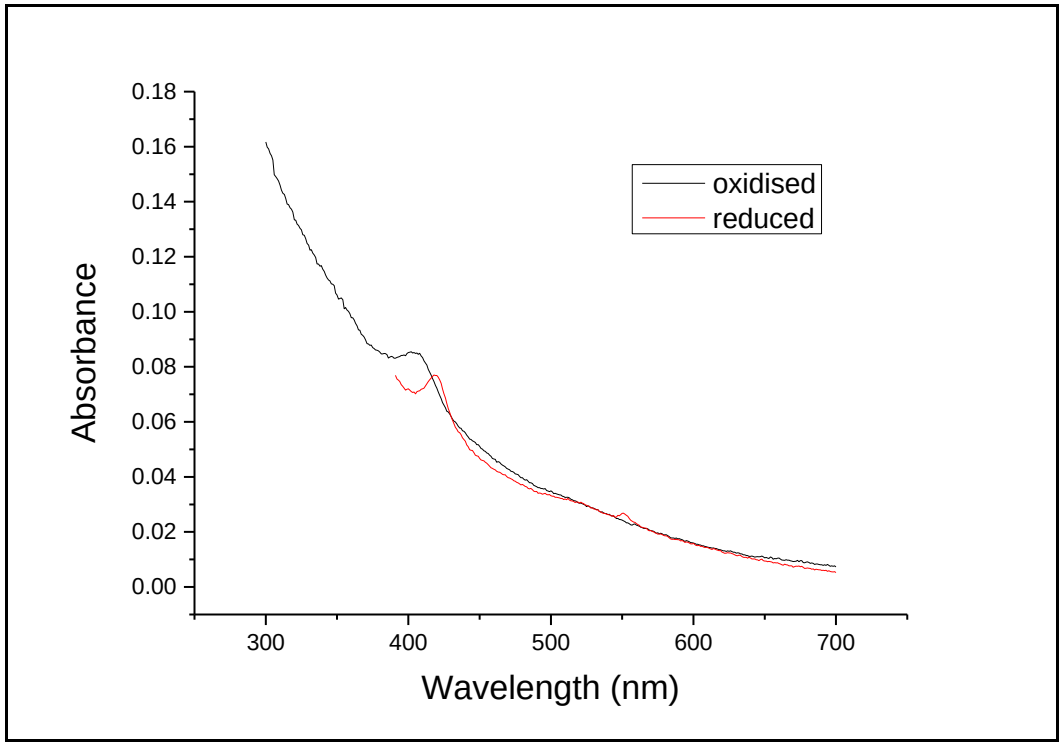

Figure 14: Representative UV-visible absorbance spectra of oxidized and reduced CymA†-proteoliposomes. The presence of the Soret γ-band at CymA-specific wavelengths of 407 nm and 419 nm for oxidized and reduced CymA respectively as an indication for the incorporation of CymA† into liposomes. The slope is due to light scattering by the proteoliposomes.

2.5.12 Methyl-viologen spectrophotometric assay for fumarate reductase activity

Fumarate reductase activity was assayed in various samples during the FccA purification by coupling the reduction of fumarate by FccA to the oxidation of reduced methyl-viologen. The protocol that was followed was according to the published literature with modifications (90).

Final concentration of 0.5 mM methyl-viologen in buffer (20 mM HEPES pH 7.0, 100 mM NaCl) containing 1 mM fumarate was first reduced *in situ* to an absorbance at 600 nm of approximately between 1.5 and 2.0 AU by the addition of 1 M sodium dithionite. Methyl-viologen exhibits strong absorbance at 600 nm at its reduced form, while no significant absorbance occurs at its oxidised form. The absorbance at 600 nm was then measured over time at 4 °C while the sample was introduced.

All solutions that were used for this assay were degassed by adequate purging with nitrogen gas and all experiments were conducted under anoxic conditions. It must be noted that this assay was performed qualitatively during only the first purification preparation (for optimisation reasons) in order to monitor the presence of FccA during the various purifications steps. Representative traces are shown in **figure 15** detailing what was assigned as positive or negative result for FccA-specific fumarate reduction, while ***table 2*** lists the results of the samples that were assayed.

Table 2: Fumarate reductase activity was qualitatively determined for various samples from the initial FccA purification. ***Figure 3*** illustrates representative traces of a positive and a negative result. *some FccA loses during this step.

Sample	Activity result
Isolated periplasmic fraction	**Positive**
Flow-through (IEC)	Negative
Wash (IEC)	Negative
High-salt fractionation (supernatant)	**Positive**
High-salt fractionation (pellet)	**Positive***
Flow-through (ultrafiltration)	Negative
Wash 1 (ultrafiltration)	Negative
Wash 2 (ultrafiltration)	Negative
Wash 3 (ultrafiltration)	Negative
Wash 4 (ultrafiltration)	Negative
Purified FccA	**Positive**

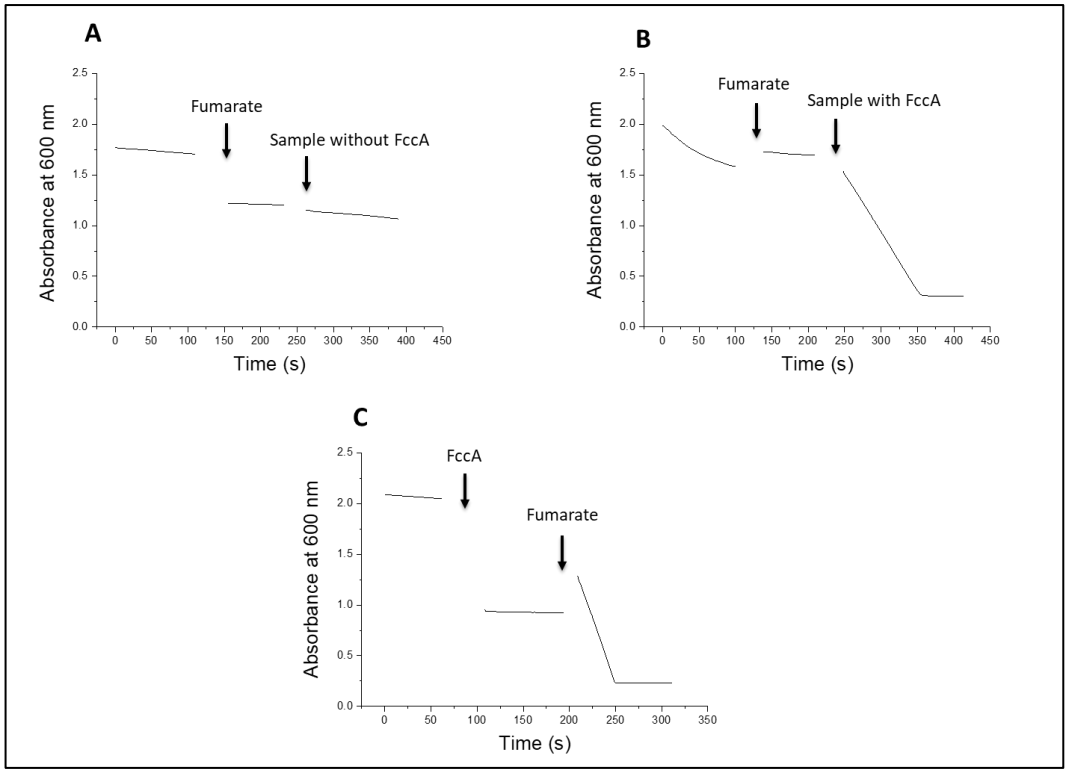

Figure 15: Representative traces of methyl-viologen fumarate reductase activity assay as a qualitative test for the presence of FccA. Gaps in the recordings are due to the removal of the cuvette for the addition of solutions. Changes in the background absorbance values were attributed to displacing the cuvette and/or due to dilution effect. **A:** Representative trace of a sample with negligent fumarate reductase activity. Samples that exhibited similar activity traces were classed as a negative result for activity. **B:** Representative trace of a sample with clear fumarate reductase activity. Samples that exhibited similar activity traces were classed as a positive result for activity. **C:** This is a control trace, where FccA was added without the presence of its substrate, fumarate, in order to assay for background reactions.

2.5.13 Diaphorase spectrophotometric activity assay

The diaphorase spectrophotometric activity assay (detailed in section ***5.2.2 CymA† is able to interact with FccA in vitro***) was based on previously published work (1).

All stock solutions were prepared under a nitrogen atmosphere (inside the glovebox) with degassed buffer by purging extensively with nitrogen gas. The components of the assay were mixed in buffer (20 mM HEPES pH 7.0, 0.5 mM EDTA, 0.05% w/v n-Dodecyl-beta-Maltoside (DDM)) inside the glovebox at final concentrations of 100 µM NADH, 10 µM menadione, 1 mM fumarate, 1 µM CymA†, and 1 µM FccA. The solution was then incubated inside the

glovebox for approximately 15 min with mild stirring, before it was placed in a plastic disposable spectrophotometric cuvette with 1.0 cm path-length. The cuvette was sealed and was transferred outside the glovebox for spectrophotometric measurements (measuring absorbance of NADH at 340 nm over time), which were conducted under anoxic conditions at room temperature. Diaphorase from *Clostridium kluyveri* (purchased from Sigma) was added using a Hamilton's syringe at final concentration of 3 μM to the sealed cuvette in order to initiate the reaction.

The initial rate of the reaction was calculated according to the following formula:

$$rate = -\frac{\Delta[NADH]}{\Delta t} \qquad (2)$$

The concentration of NADH was calculated using the Beer-Lambert law with $\varepsilon_{340\,nm}^{NADH} = 6{,}220\ M^{-1}\ cm^{-1}$.

2.6 Protein Purification Procedures

2.6.1 Manual nickel affinity chromatography

Manual nickel affinity chromatography was performed at room temperature using a GE Healthcare Life Sciences HisTrap™ HP 5ml column operated manually with the use of syringes.

2.6.2 ÄKTA chromatography

Automated chromatography was performed at 4 °C with a GE Healthcare Life Sciences ÄKTA pure 25 L chromatographic system with a GE Healthcare Life Sciences Fraction collector F9-R operated by GE Healthcare Life Sciences Unicorn 7 software. Chromatograms shown in this thesis were produced by plotting the exported raw data with OriginPro 8.6 software.

2.6.3 Isolation of bacterial membranes

The harvested bacterial cell pellet was resuspended in resuspension buffer at 4.36 ml per 1 g of wet cell mass. The suspension was kept on ice and fully homogenized by an IKA® Ultra-Turrax® homogenizer. The homogenized suspension was passed twice through a Constant Systems TS5/40/AB/GA cell disruptor operated at 30 Kpsi pressure and 5 °C temperature in order to lyse the bacterial cells. The lysate was collected in a pre-chilled Duran bottle resting on ice.

The lysate was centrifuged at 12,000 g for 50 min at 4 °C in order to pellet cell debris. The supernatant was collected and centrifuged at 131,000 g for 60 min at 4 °C in order to pellet the membranes. The supernatant was discarded and the membranes were resuspended in the resuspension buffer and the solution was homogenised using a hand-held glass homogeniser while working on ice. The membranes were collected by centrifugation at 131,000 g for 60 min at 4 °C; this washing step was repeated two more times. The washed and homogenised membranes in resuspension buffer can be flash-frozen in liquid nitrogen and stored at -80 °C.

The resuspension buffer consisted of 100 mM Hepes pH 7.5, 100 mM NaCl, and Roche cOmplete™ EDTA-free protease inhibitor cocktail (according to the manufacturer's instructions) or Roche cOmplete™ protease inhibitor cocktail (according to the manufacturer's instructions).

2.6.4 Purification of CymA†

The isolated and washed bacterial cell membranes were resuspended in solubilisation buffer (20 mM Tris-HCl pH 8.0, 0.5 M NaCl, 5 mM imidazole, 1% w/v DDM) at 12.5 ml per membranes derived from ~ 39 g wet cell mass of bacterial pellet and the solution was homogenised using a hand-held glass homogeniser while working on ice. The solution was incubated for 4 h at 4 °C with roller-mixing. Any remaining insoluble material was removed by ultra-centrifugation at 131,000 g for 60 min at 4 °C. The supernatant was filtered manually through a 0.45 µm pore size filter. This constituted the column load.

The load was loaded onto a pre-equilibrated GE Healthcare Life Science HisTrap™ HP 5 ml column with binding buffer (20 mM Tris-HCl pH 8.0, 0.5 M NaCl, 5 mM imidazole, 0.1% w/v DDM) slowly (during manual nickel affinity chromatography) or at 0.5 ml min^{-1} (during ÄKTA chromatography). Subsequently, the column was washed with 5-10 column volumes (CVol) of binding buffer followed by 8-10 CVol of binding buffer containing 30-50 mM imidazole slowly (during manual chromatography) or at 1.0 ml min^{-1} (during ÄKTA chromatography). Step-elution was performed slowly during manual chromatography with binding buffer containing 130 mM and 300 mM imidazole. For ÄKTA chromatography, a gradient of increasing imidazole concentration was applied from 50 mM to 500 mM imidazole over 10 Cvol and from 500 mM to 1 M imidazole over 5 CVol at 1.0 ml min^{-1}.

The desired fractions, after SDS-PAGE analysis, were pooled and dialysed with two buffer exchanges (2 h incubation and 16 h incubation at 4 °C) against 20 mM Hepes pH 7.5 150 mM NaCl using ThermoFisher Scientific SnakeSkin™ dialysis tubing with 10 kDa molecular weight cut-off.

The dialysed protein sample was concentrated using a Vivaspin® spin-concentrator with 10 kDa molecular weight cut-off filter by centrifugation at 3,220 g and at 4 °C until the desired volume was reached.

The concentrated protein sample was quantified, aliquoted, flash-frozen in liquid nitrogen, and stored at -80 °C.

2.6.5 Purification of recombinant TEV protease

The purification of TEV protease was based on a kindly supplied protocol by Dr Vincent Postis.

The harvested bacterial cell pellet was resuspended in resuspension buffer (50 mM Tris-HCl pH 8.0, 400 mM NaCl, 0.5 mM EDTA) at 2 ml per 1 g of wet cell mass. The suspension was kept on ice and fully homogenized by an IKA® Ultra-Turrax® homogenizer. The homogenized suspension was passed twice through a Constant Systems TS5/40/AB/GA cell disruptor operated at 30 Kpsi pressure and 5 °C temperature in order to lyse the bacterial cells. The lysate was collected in a pre-chilled Duran bottle resting on ice.

The lysate was centrifuged at 131,000 g for 60 min at 4 °C in order to pellet insoluble material. The supernatant was collected and DNase I was added to an approximate final concentration of 10 µg ml^{-1} in order to digest DNA resulting in a less viscous solution. The solution was stirred at 4 °C before it was supplemented with imidazole to final concentration of 35 mM, and filtered manually through a 0.45 µm pore size filter. This constituted the column load.

The column load was loaded onto a pre-equilibrated GE Healthcare HisTrap™ HP 5 ml column with binding buffer (50 mM Tris-HCl pH 8.0, 400 mM NaCl, 35 mM imidazole, 0.32 mM tris(2-carboxyethyl)phosphine (TCEP)) at 2 ml min^{-1} at 4 °C. The column was washed with binding buffer until the UV signal was stable (maximum of 20 CVol). Subsequently, elution was performed by applying a gradient of imidazole from 35 mM to 500 mM imidazole over 30 Cvol and from 500 mM to 1 M imidazole over 5 Cvol at 2 ml min^{-1} and at 4 °C.

The desired fractions, after SDS-PAGE analysis, were pooled and dialysed with two buffer exchanges (2 h incubation and 16 h incubation at 4 °C) against 50 mM Tris-HCl pH 8.0, 200 mM NaCl, 2 mM EDTA, 125 µM TCEP using

ThermoFisher Scientific SnakeSkin™ dialysis tubing with 10 kDa molecular weight cut-off.

The dialysed protein sample was quantified with µBCA assay, aliquoted, flash-frozen in liquid nitrogen, and stored at -80 °C. It must be noted that TEV protease aggregates at concentrations approximately ≥ 5 mg ml^{-1}, which is why the purified sample was not concentrated.

2.6.6 Purification of native FccA

The purification of native FccA was based on previously published work (90). The initial purification attempt was conducted together with Dr Colin Lockwood at the University of East Anglia. This section describes the purification approach that was developed from the work that was conducted at the University of East Anglia, but with reference to the instrumentation that was used for further purification preparations at the University of Leeds.

The harvested cell pellet was subjected to a crude periplasmic extraction since the periplasm is the cellular location at which FccA is found. Furthermore, periplasmic extraction allows the elimination of most of the globular cytosolic proteins aiding the isolation of pure FccA. The cell pellet was resuspended in ‘lysis’ buffer (100 mM Tris-HCl pH 8.0, 500 mM sucrose, 3 mM EDTA, 2 mg ml^{-1} lysozyme from chicken egg white, Roche cOmplete™ EDTA-free protease inhibitor cocktail) at 10 ml per 1.7 g of wet cell mass. The suspension was incubated for 40 min at 37 °C with gentle orbital shaking. Subsequently, the suspension was centrifuged at 15,000 g for 45 min at 4 °C. The supernatant, which constituted the periplasmic fraction, was diluted 1-fold with 20 mM Tris-HCl pH 8.0, and filtered manually through a 0.45 µm pore size filter. This constituted the column load.

A GE Healthcare Life Sciences HiTrap™ DEAE (sepharose) FF 5 ml column was pre-equilibrated with 5 CVol of 20 mM Tris-HCl pH 8.0, 1 M NaCl buffer, followed by 10 CVol of 20 mM Tris-HCl pH 8.0 buffer. The column load was loaded on the pre-equilibrated column at 1 ml min^{-1} at 4 °C. The column was then washed with 5 CVol of 20 mM Tris-HCl pH 8.0, 5 mM NaCl. Elution was

performed by applying a salt gradient from 5 mM to 600 mM NaCl over 60 CVol and from 600 mM to 1 M NaCl over 5 CVol at 1 ml min^{-1} at 4 °C.

The desired fractions, after SDS-PAGE analysis, were pooled and were subjected to 50% ammonium sulphate fractionation cut in order to precipitate contaminating proteins. The high salt fractionation was performed in a cold-room (4 °C), and the salt was added very slowly into the solution under constant stirring. Once all of the salt was added and dissolved, the solution was stirred for another 15 min before it was centrifuged at 15,000 g for 20 min at 4 °C. The supernatant, containing FccA, was carefully collected and filtered through a 0.22 µm pore size filter. Subsequently, the filtered supernatant was dialysed with two buffer exchanges (2 h incubation and 16 h incubation at 4 °C) against 20 mM HEPES pH 7.4, 150 mM NaCl using ThermoFisher Scientific SnakeSkin™ dialysis tubing with 10 kDa molecular weight cut-off.

The dialysed protein sample was concentrated using a Vivaspin® spin-concentrator with 50 kDa molecular weight cut-off filter by centrifugation at 3,220 g and at 4 °C until the desired volume was reached.

The concentrated protein sample was further purified by size exclusion chromatography in 20 mM HEPES pH 7.4, 150 mM NaCl. The protein sample was injected onto a pre-equilibrated GE Healthcare Life Sciences HiLoad™ 16/600 Superdex 200 pg preparatory grade column at approximately 10 mg ml^{-1} FccA. The size exclusion chromatography was performed at 0.5 ml min-1 at 4 °C.

The desired peak fractions, after SDS-PAGE analysis, were pooled and were concentrated using a Vivaspin® spin-concentrator with 50 kDa molecular weight cut-off filter by centrifugation at 3,220 g and at 4 °C until the desired volume was reached.

The concentrated final protein sample was quantified, aliquoted, flash-frozen with liquid nitrogen, and stored at -80 °C.

2.6.7 Purification of $CymA_{sol}$

The purification of $CymA_{sol}$ was modelled on previously published work (89).

Firstly, the {His_6-MBP-TEV cleavage site-$CymA_{sol}$} protein construct was purified by ÄKTA nickel affinity chromatography. The harvested cell pellet was subjected to a crude periplasmic extraction since the protein construct was engineered to localise in the periplasm. Furthermore, periplasmic extraction allows the elimination of most of the globular cytosolic proteins aiding the elimination of contaminating proteins. The cell pellet was resuspended in TSE buffer (20% w/v sucrose, 30 mM Tris-HCl pH 8.3, 1 mM EDTA, 0.5 mg ml^{-1} lysozyme from chicken egg white, Roche cOmplete™ EDTA-free protease inhibitor cocktail) at 30 ml per approximately 16 g of wet cell mass. The suspension was incubated for 20 min at room temperature with roller-mixing. Subsequently, an equal volume to the TSE buffer volume of ice-cold 1 M NaCl was added and the suspension was incubated for another 15 min at 4 °C with roller-mixing. The suspension was then centrifuged at 25,000 g for 30 min at 4 °C. The supernatant, which constituted the periplasmic fraction, was carefully collected, supplemented with 5 mM imidazole and 3 mM $MgCl_2$ at final concentration, and filtered through a 0.45 µm pore size filter. This constituted the column load.

The column load was loaded onto a pre-equilibrated GE Healthcare HisTrap™ HP 5 ml column with binding buffer (20 mM Tris-HCl pH 8.0, 0.5 mM NaCl, 5 mM imidazole) at 0.5 ml min^{-1} at 4 °C. The column was washed with 5-10 CVol of binding buffer, followed by 5-10 CVol of buffer containing 50 mM imidazole at 1 ml min^{-1} and at 4 °C. Subsequently, elution was performed by applying a gradient of imidazole from 50 mM to 400 mM imidazole over 25 Cvol and from 400 mM to 1 M imidazole over 3 Cvol at 1 ml min^{-1} and at 4 °C.

The desired fractions, after SDS-PAGE analysis, were pooled and quantified with µBCA assay and TEV protease was added to 2:1 (TEV protease: protein) protein amount ratio. The TEV-specific proteolytic cleavage reaction was performed during dialysis; the solution was dialysed for 20 h at 4 °C against 20 mM Tris-HCl pH 8.0, 0.5 M NaCl using ThermoFisher Scientific SnakeSkin™ dialysis tubing with 10 kDa molecular weight cut-off in order to remove excess of imidazole.

The dialysed solution was subjected to a manual reverse nickel affinity chromatography in order to bind all proteins. The $CymA_{sol}$ (without tags),

unable to bind to the nickel column, was run through the column and collected in the flow-through fraction. A pre-equilibrated GE Healthcare Life Sciences HisTrap™ HP 5 ml column with 20 mM Tris-HCl pH 8.0, 0.5 M NaCl was used for reverse affinity purification.

The flow-through was concentrated using a Vivaspin® spin-concentrator with 10 kDa molecular weight cut-off filter by centrifugation at 3,220 g and at 4 °C until the desired volume was reached. Subsequently, the protein sample, containing $CymA_{sol}$, was loaded onto a pre-equilibrated GE Healthcare Life Sciences HiLoad™ 16/600 Superdex 75 pg preparatory grade column with 20 mM HEPES pH 7.5, 150 mM NaCl for size exclusion chromatography with flow rate 1 ml min^{-1} at 4 °C. The sample was injected onto the column at an approximate concentration of 3 mg ml^{-1}.

The desired peak fractions, after SDS-PAGE analysis, were pooled and were concentrated using a Vivaspin® spin-concentrator with 10 kDa molecular weight cut-off filter by centrifugation at 3,220 g and at 4 °C until the desired volume was reached.

The concentrated final protein sample was quantified, aliquoted, flash-frozen with liquid nitrogen, and stored at -80 °C.

2.7 Electrochemical Methods

2.7.1 Cyclic voltammetry & Electrochemical cell set-up

Cyclic voltammetry (CV) is a surface sensitive electrochemical method, where electron transfer occurs at the interfacial region between redox active molecules and the surface of the electrode. Proteins with metal co-factors, which are usually involved in electron relay either to an active site within the same protein or to another partner protein, are able to electrically interact with the electrode and they are studied via a variety of electrochemical methods including cyclic voltammetry.

In CV, the potential are cycled through a defined potential window linearly over time at a defined scan rate. Once the potential reaches the defined end, it swipes back in the opposite direction until it reaches back to the starting potential. During the potential cycling the output current is measured and plotted against the potential. Normally, reductive current is shown as negative current, while oxidative current is shown as positive.

An electrochemical cell (schematically depicted in **figure 16**), which was able to hold a volume of 2 ml, was assembled with a three-electrode standard set-up: an ultra-flat modified gold working electrode (described in sections ***2.7.2 Preparation of gold electrodes*** and ***2.7.3 Modification of gold electrodes***); a platinum wire as a counter electrode in order to close the electrical circuit; and a Radiometer Analytical Hg/Hg_2SO_4 reference electrode (+0.651 V vs SHE at 20 °C). The working ultra-flat modified gold electrode was embedded in a poly-tetrafluroethylene (PTFE) electrode holder that was sealed with a rubber O-ring. Another rubber O-ring was used to seal the PTFE electrode holder and the glass cell. The assembled electrochemical cell was housed in a Faraday's cage in order to minimise electrical noise during the electrochemical measurements.

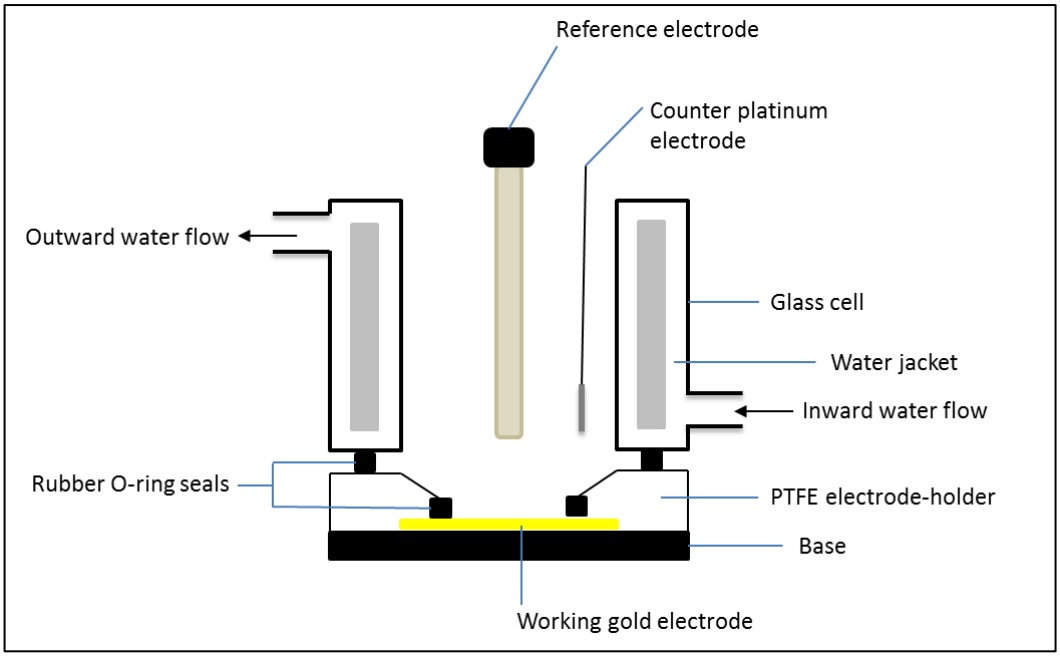

Figure 16: Schematic representation of the electrochemical cell setup in cross-sectional view.

2.7.2 Preparation of gold electrodes

The preparation of ultra-flat template-stripped gold electrodes was performed as described previously (95).

Silicon wafers (N<100>, 100 mm diameter, 1-10 Ohm cm, 525 µm thickness, SSP grade polish) were cleaned by three discreet steps of ≥ 5 min sonication per step. The silicon wafer was submersed in dichloromethane (step 1), ethanol (step 2), and 10% v/v Decon® 90 (step 3). The silicon wafer was dried under a stream of nitrogen gas after each sonication step. A layer of 150 nm of gold was deposited onto the cleaned silicon wafers by evaporation using an Edwards 306 evaporator (according to the manufacturer's instructions). The cleaning and gold evaporation procedures were performed by Dr Mengqiu Li, Dr Ee Taek Hwang, or Dr George Heath.

Fisherbrand™ plain glass microslides were manually cut with a diamond pen cutter in order to produce 13 mm x 13 mm glass squares. The glass squares were cleaned by three discreet steps of 10 min sonication per step. The glass squares were submersed individually in isopropanol (step 1), 10% v/v Decon® 90 (step 2), and water (step 3). Between steps 2 and 3, the glass squares

were rinsed with copious amounts of water to ensure complete removal of residual Decon® 90.

The two components of EPOXY Technology EPO-TEK® 377 glue were mixed at 1:1 ratio and any trapped air was removed using a vacuum desiccator for 1-2 h. Subsequently, the glue was used to glue the cleaned glass squares onto the gold layer of the provided silicon wafer. The glue was cured for 2 h at 120 °C using a hot plate. The resulting silicon wafer with the glued glass squares on its gold layer was stored at room temperature.

A glued glass square onto the gold layer of the silicon wafer was stripped carefully using a surgical scalpel blade immediately before use, yielding an ultra-flat template-stripped gold electrode.

2.7.3 Modification of gold electrodes

The ultra-flat template-stripped gold electrodes were modified with a self-assembled monolayer (SAM) of organic thiol compounds with varying length exploiting the strong interaction between sulphur and gold. The organic thiol compounds had terminating functional chemical groups or chemical moieties with which the surface of the gold electrode was modified. As part of the work presented in this thesis the following organic thiol compounds were used either on their own or as part of a thiol mixture:

- 8-mercapto-1-octanol (Sigma; 98% purity)
- 6-mercapto-1-hexanol (Sigma or Fluka; 97% purity)
- 8-amino-1-octanethiol (Dojindo; 97.6% purity)
- EO_3-cholesteryl (96) (kindly provided by Dr Lars Jeuken)

The formation of SAMs was achieved by incubating the electrodes for 16 h at room temperature submerged in a solution of total thiol concentration of 1 mM in isopropanol. The electrode was rinsed with isopropanol and dried under a stream of nitrogen gas immediately prior to use in the assembly of the electrochemical cell (described in section ***2.7.1 Electrochemical cell set-up***).

2.7.4 Electrochemical measurements

All electrochemical measurements were performed under a nitrogen atmosphere (≤ 0.1 ppm O_2) in an MBRAUN LABmaster glovebox workstation at room temperature and in 20 mM MOPS pH 7.4, 30 mM Na_2SO_4 buffer unless otherwise stated. The buffer solutions and water used for rinsing the reference electrode were degassed with nitrogen gas and equilibrated under a nitrogen atmosphere (inside the glovebox) for at least four weeks before they were used in experiments.

Electrochemical measurements were conducted with an Autolab (Eco-chemie) electrochemical analyser that carries a PGSTAT30 potentiostat, a SCANGEN module, and a FRA2 frequency analyser, which was operated with Nova 1.8 or Nova 1.10 software. Cyclic voltammetry experiments were routinely carried out by holding the potential at 0.5 V for 5 s before cycling at various scan rates.

Peaks were integrated using the Nova software with manually determination of the baseline. Cyclic voltammograms shown in this thesis were produced by plotting the exported analysed data with OriginPro 8.6 software. The data were typically smoothed with a 10-point adjacent averaging method and they were visibly inspected for conformity with the raw data (an example is given in **figure 17**). In cases where the smoothed data showed deviations from the raw data, a 5- or 8-point adjacent-averaging was performed instead.

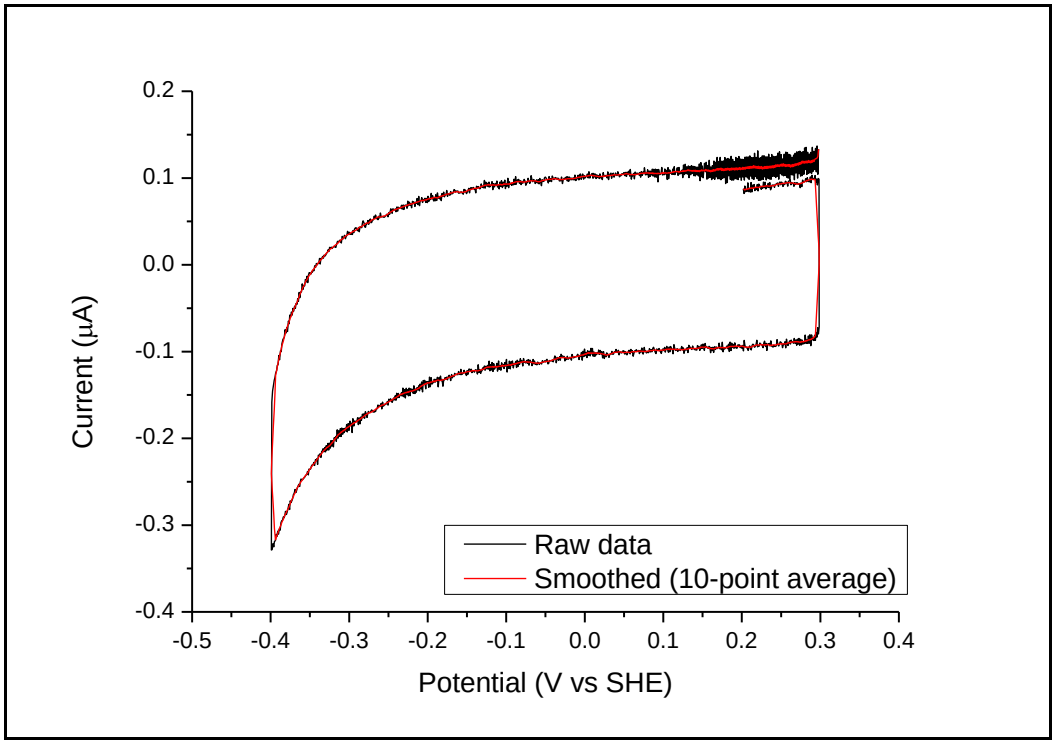

Figure 17: Comparison between raw and smoothed data by the 10-point adjacent averaging method for cyclic voltammograms. An overlay of cyclic voltammetric data before (raw data; black line) and after (10-point adjacent averaging method) smoothing. This visible inspection was conducted for all voltammograms presented in this thesis.

2.7.5 Formation of a protein film on modified gold electrodes

The formation of a protein film on the surface of the modified gold electrodes (described in section ***2.7.3 Modification of gold electrodes***) was performed in an assembled electrochemical cell (described in section ***2.7.1 Electrochemical cell set-up***). The modified electrode was incubated with the target protein at ≥ 0.1 μM in buffer (20 mM MOPS pH 7.4, 30 mM Na_2SO_4) for 20 min at room temperature inside the glovebox. Subsequently, the electrode was washed with 2 ml of buffer three times in order to remove excess protein.

The amount of electro-active adsorbed protein (Γ) was estimated according to the following formula:

$$\Gamma = \frac{\text{peak area}}{n \cdot F \cdot A \cdot \upsilon} \qquad (2)$$

where n is the number of electrons for a protein molecule, F is the Faraday's constant (96,485.332 C mol^{-1}), A is the area of the electrode (0.2 cm^2), υ is

the scan rate (V s^{-1}), and peak area for the area of the reductive or oxidative non turn-over signal (V·A).

2.7.6 Formation of a tethered lipid bilayer membrane (tBLM) on modified gold electrodes

For tBLM experiments, an electrode was modified with SAM containing a mixture of EO_3-cholesteryl and 6-mercapto-1-hexanol (as described in section ***2.7.3 Modification of gold electrodes***). EO_3-cholesteryl carries a cholesterol moiety that provides tethering points for the lipid bilayer membrane. The modified electrodes were analysed by electrochemical impedance spectroscopy that allows the coverage of EO_3-cholesteryl to be estimated under the assumption of a linear additive correlation as fractions of complete coverage of the individual thiols (97). Thus:

$$C_{total} = \chi_1 C'_1 + \chi_2 C'_2 \qquad (3)$$

where C_{total} is the capacitance of the SAM experimentally determined by electrochemical impedance spectroscopy, χ is the surface fraction, and C' is the capacitance of a pure thiol SAM. The notations '1' and '2' denote the fractional components of a mixed SAM, in this case, EO_3-cholesteryl and 6-mercapto-1-hexanol respectively. The capacitance values that were used in equation (3) for EO_3-cholesteryl and 6-mercapto-1-hexanol were 0.78 µF cm^{-2} and 4.3 µF cm^{-2} respectively (experimentally determined).

The modified electrode was incubated *in situ* with liposomes or proteoliposomes at final concentration of 0.5 mg ml^{-1} and 10 mM $CaCl_2$ (in order to screen the charges and therefore enable the aggregation of liposomes or proteoliposomes, aiding to their spontaneous rupture) for approximately 1 h at room temperature. Subsequently, the electrodes were washed *in situ* with 2 ml of buffer twice in order to remove excess of liposomes or proteoliposomes, followed by a wash with 1 mM EDTA (in water) in order to chelate any Ca^{+2} ions, followed by two further buffer washes in order to remove any residual EDTA. It must be noted that care was taken not to disrupt the formed tBLM by maintaining the meniscus of the solutions above the tBLM. The formation of the tBLM was monitored with electrochemical

impedance spectroscopy, where a drop in the capacitance value is indicative of a formed tBLM, normally below 1.2 µF cm^{-2} as previously established for this system (97). A representative example of the formation of tBLM monitored with electrochemical impedance spectroscopy is shown in **figure 18** in the form of a Cole-Cole plot. Formed tBLMs that exhibited a drop in the capacitance value ≤ 2.3 µF cm^{-2} were deemed acceptable for electrochemical experiments for the work presented in this thesis.

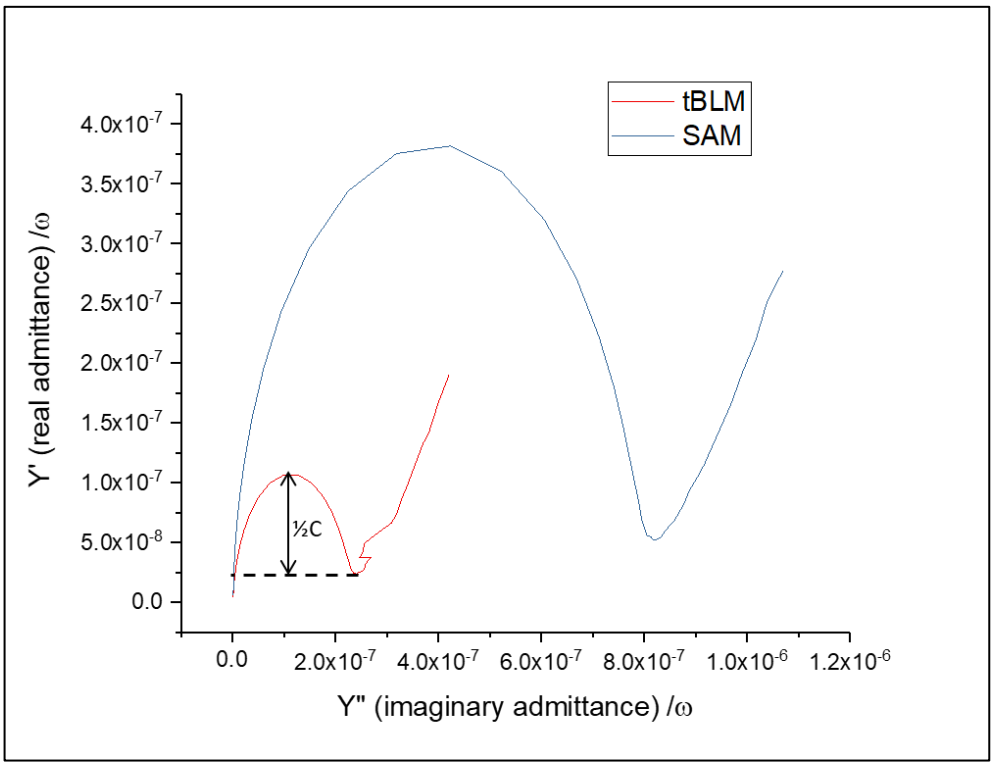

Figure 18: Overlay of electrochemical impedance spectroscopy Cole-Cole plots before (SAM; blue line) and after (tBLM; red line) the formation of tBLM on a SAM modified gold electrode. A representative example for monitoring the formation of tBLM that was conducted for all tBLM electrochemical experiments in order to verify the formation of tBLM. Y" and Y' denote the imaginary and real components of admittance (Y) respectively, while ω denotes the angular frequency. The depicted Y/ω (s Ω^{-1}) is equivalent to the capacitance, C (units: F where C V^{-1} is equivalent to s Ω^{-1}). Thus, the radius of the semi-circle is half of the capacitance (F). For comparative reasons, the capacitance is divided by the surface area of the electrode (cm^2) and, therefore, the capacitance is reported in F cm^{-2}.

2.8 Biophysical Methods

2.8.1 Quartz-crystal microbalance with dissipation (QCM-D)

2.8.1.1 Experimental details

QCM-D experiments were performed with a Biolin Scientific 4-channel Q-sense Analyzer at 21 °C and SiO_2-coated crystals (QSX 303; 14095_A). Fluidic flow was controlled with a Biolin Scientific Ismatec IPC-N 4 peristaltic pump operated at 70 µl min^{-1}, unless otherwise stated. All solutions were degassed prior to use. The crystals were cleaned in four consecutive steps immediately prior to use: (a) 20 min sonication in 0.4% w/v SDS, (b) 20 min in Milli-Q grade water, (c) 20 min UV/ozone treatment with a Spectrum UVOCS 10x10/ OES UV-ozone cleaning system, and (d) 10 min sonication in milli-Q grade water. The crystals were dried under a stream of nitrogen gas. Subsequently, the crystals were mounted on the cells, as per the manufacturer's instructions, and calibrated in air first and then in water before being equilibrated first in water and then in buffer. Each equilibration step was performed under constant flow until the baseline signal became stable (normally between 3 h and 5 h, depending on the crystal quality).

Liposomes (as described in section ***2.5.10 Preparation of homogeneous solutions of liposomes***) or proteoliposomes (as described in section ***2.5.11 Reconstitution of CymA† into liposomes***) were introduced to an equilibrated crystal at 0.5 mg ml^{-1} in 20 mM MOPS pH 7.4, 30 mM Na_2SO_4 buffer containing 10 mM $CaCl_2$. The Ca^{2+} ions screen the surface charge promoting aggregation, which along with their exposure to the SiO_2 surface cause their spontaneous rupture and formation of a solid-supported lipid bilayer membrane. Excess of liposomes or proteoliposomes was removed by a water step. Then, buffer containing 1 mM EDTA was used to chelate Ca^{2+} ions, followed by a buffer step to remove residual EDTA and to establish the baseline signal of the formed bilayer. Representative traces of this process for the formation of a solid-supported lipid bilayer membrane is shown in **figure 19**.

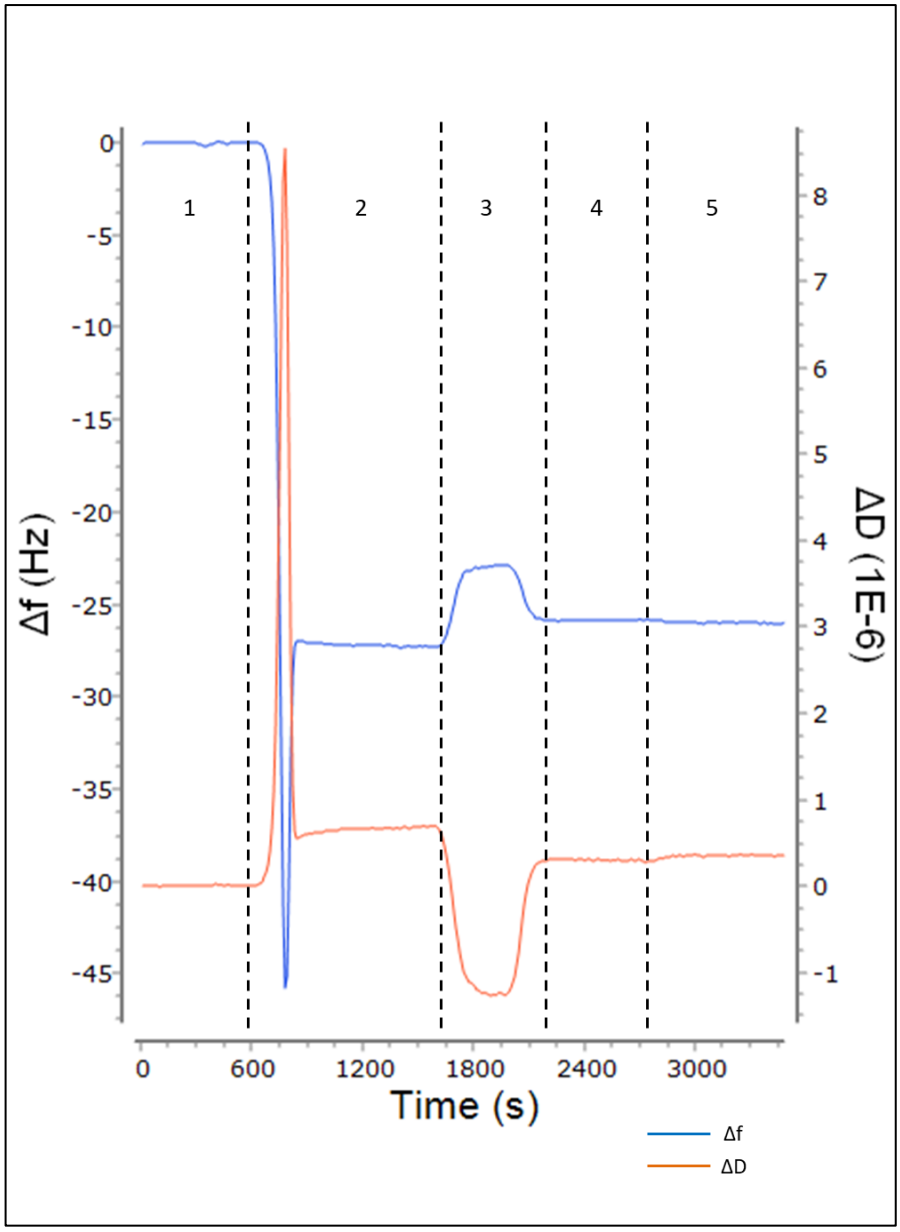

Figure 19: A representative trace of a solid supported lipid bilayer membrane formation from the spontaneous rupture of 10% w/w CL/POPC liposomes monitored with QCM-D. 1: buffer equilibration to ensure that there is no drift. 2: introduction of liposomes at 0.5 mg ml^{-1} and 10 mM $CaCl_2$. Initially the liposomes are adsorbed on the surface which is mediated by the screening of their surface charge by $CaCl_2$ and observed as a drop in Δf. The liposomes are then spontaneously rupture, realising the trapped buffer, which is observed as an increase in and stabilization of Δf. 3: Milli-Q water wash in order to remove intact liposomes and CaCl2. 4: Buffer wash with 1 mM EDTA in order to chelate residual Ca^{2+} ions. 5: buffer wash in order to remove EDTA and establish the baseline of the experiment. Δf = 25 Hz is the ideal value of a good quality uniform POPC bilayer membrane (98).

2.8.2 Isothermal Titration Calorimetry

2.8.2.1 Experimental details

Protein samples were co-dialysed in the same buffer, which consisted of 20 mM MOPS pH 7.4, 150 mM NaCl in two consecutive steps: (a) 2 h at 4 °C, and (b) 16 h at 4 °C. A sample of the final buffer was kept for control experiments. All solutions (including protein samples) were degassed prior to use. The ITC cell contained $CymA_{sol}$ at 10 µM. FccA of various concentrations comprised the titrant, which was loaded in the syringe. ITC experiments were conducted with a MicroCal™ iTC_{200} (Malvern) at the following settings: reference power of 5 µcal s^{-1}, 60 s initial delay, 750 rpm stirring, 25 °C temperature, initial sacrificial injection of 0.5 µl with 1 s duration, 19 injections of 2 µl with 4 s duration each, and 120 s spacing between each injection.

Chapter 3 – An improved Approach for the production of Homologously Expressed Recombinant CymA† from *Shewanella oneidensis* MR-1

3.1 Introduction

The dissimilatory metal-reducing *Shewanella oneidensis* MR-1 has become an important organism for microbial electrochemistry due to its metabolic versatility for a range of applications in the areas of microbial fuel cell technology, biosensor technology, bioremediation, and electrosynthesis. At the centre of the anaerobic respiration lies CymA – a transmembrane tetrahaem c-type cytochrome that is responsible for the re-oxidation of the menaquinone pool of the inner membrane.

The purification of CymA for the elucidation of its structural and mechanistic details has seen several attempts, but with limited success. Field et al. were the first to report the purification of CymA from *Shewanella frigidimarina* NCIMB400 in native form, but with a low yield of 5 mg of purified CymA from 20 L of culture (250 µg L^{-1} of culture) (35). More than a decade later, Marritt et al. reported the overexpression and purification of a recombinant CymA from *S. oneidensis* LS447 (1). The LS447 strain is the transformed *S. oneidensis* MR-1 with the pLS167 plasmid. The pLS167 plasmid is the expression vector with the cloned *cymA* gene. The expression vector is a modified pBAD202/D-TOPO based system for homologous and heterologous overexpression of multihaem-cytochromes in *S. oneidensis* MR-1 (99). The pBAD202/D-TOPO plasmid from Invitrogen incorporates a His-patch thioredoxin on the N-terminus as well as a V5 epitope and a His_6 tag on the C-terminus of recombinant proteins. The modified system for multihaem-cytochromes contains a stop codon at the end of the His-patch thioredoxin encoding region, resulting in the incorporation of only the C-terminal modifications on the recombinant protein. Thus, in this case, the purified recombinant CymA carried a V5 epitope followed by a His_6 tag on the C-terminus (referred to as CymA‡). However, this protein construct did not bind to immobilised metal ion affinity columns, which resulted in a laborious purification procedure that comprised of various ion-exchange and size

exclusion chromatographic steps (1). As a result, the yield was considered low for an overexpression approach, though higher than purifying CymA in native form. Moreover, the purified fractions of the CymA‡ were not consistent in that recombinant CymA co-purified with varying amounts of quinone molecules. Such co-purification of quinone-containing contaminants, or bound quinone molecules to purified CymA‡ was not previously reported, when native CymA was purified (35). This was addressed to some extent by the addition of washing steps that reduced the amount of quinone molecules (1). Hence, this construct exhibits inherent issues that may promote incorrect folding and, by extension, alter the properties of the protein. Furthermore, the presence of tags on the C-terminus may interfere with protein-protein interactions, rendering this protein construct unsuitable for such studies.

This chapter presents an improved approach for the production of pure recombinant CymA (referred to as CymA†) that is suitable for, but not limited to, protein-protein interaction studies. It begins with the presentation of an approach for designing new genes that address tag interference issues, as well as for re-constructing the expression vector for the easy sub-cloning of those recombinant genes. Subsequently, it presents the results of expression in *S. oneidensis* MR-1 and purification of CymA†. Finally, the biochemical, biophysical, and electrochemical characterization of the purified CymA† is presented.

3.2 Results

3.2.1 Gene design and vector re-construction

The working CymA model is based on the crystal structure of NrfH, a homologue of CymA, which is solved as an $NrfH_2A_4$ complex to a resolution of 2.3 Å from *Desulfovibrio vulgaris*. NrfH and, by extension, our CymA model has a single N-terminal transmembrane α-helix and a periplasmic-facing globular domain that houses the four haems. Thus, the design of the new genes focuses on adding N-terminal tags for affinity purification purposes and abandoning any C-terminal modifications.

The *cymA* gene (PubMed Gene ID: 1172176) was designed to allow fusion of a His_8 tag followed by a human rhinovirus 3 C (HRV3C) proteolytic site to the N-terminus of CymA (*cymA01*). The His_8 tag was used for affinity purification purposes, while the HRV3C site was incorporated to allow for the removal of the His_8 tag, should it be deemed necessary. In order to allow for directional cloning, two unique restriction sites were also incorporated into the design: NcoI at the start of *cymA01*, which included the start codon in its sequence, and HindIII immediately after an incorporated stop codon at the end of the gene in order to abolish the addition of any C-terminal modifications. The DNA sequence was, lastly, subjected to codon optimisation for optimal fusion of the N-terminal modifications during overexpression in *S. oneidensis* MR-1 using JCat Codon Adaptation Tool (**Apendix B**). The *cymA01* gene is schematically depicted in **figure 20**, while the complete and annotated DNA sequence is presented in **appendix B**. The gene synthesis of *cymA01* was outsourced to GenScript, which provided the *cymA01* gene cloned in a pUC57 vector.

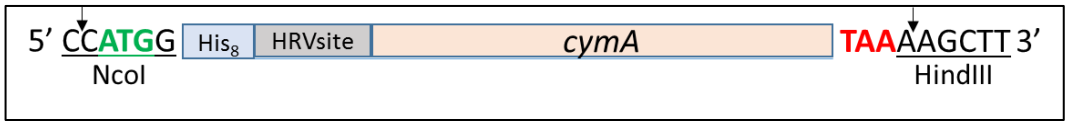

Figure 20: Schematic representation of *cymA01* gene that encode for His_8-HRV3Csite-CymA. The start and stop codons are shown in green and red respectively. The NcoI and HindIII restrictions sites are underlined, while the nucleotide position of restriction is indicated with arrows.

The pLS167 plasmid was kindly donated by Professor Julea Butt and with permission from Dr. Liang Shi, who is the original creator of pLS167. The restriction sites NcoI and HindIII were chosen for providing directional cloning. The region between NcoI and HindIII allows the removal of the N-terminal modifications that the pBAD202/D-TOPO provides (vector map shown in **figure 21**), along with any cloned gene up to where the region that provides the C-terminal modifications is.

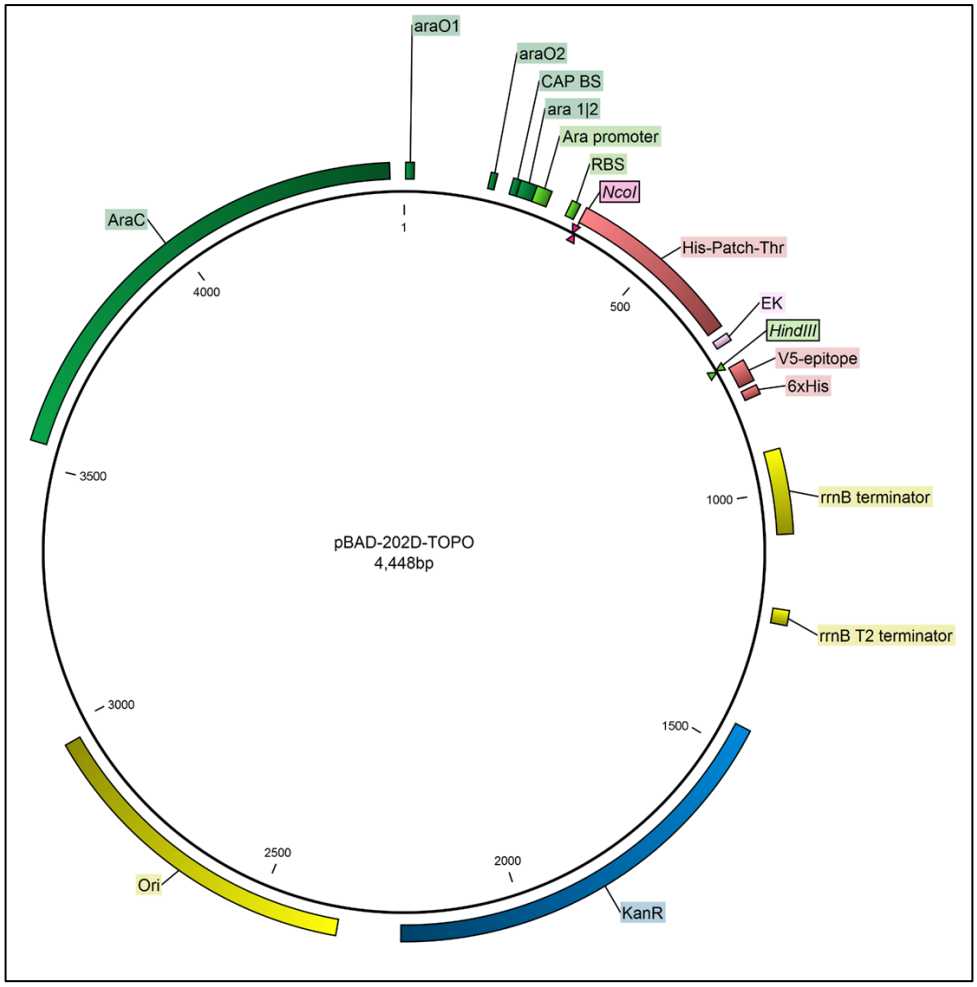

Figure 21: pBAD202/D-TOPO (Invitrogen) vector map. The map is annotated to show the key features of the vector: **KanR**: region encoding gene that confers kanamycin resistance, **Ori**: origin of replication, **AraC**: encoding gene that confers tight regulation of the promoter, **Ara promoter**: promoter region, **RBS**: ribosomal binding site, **NcoI**: position of the restriction site, **HindIII**: position of the restriction site, **araO1/ araO2**: operator regions, **ara 1|2**: binding sites of araC for the activation of transcription, **CAP BS**: binding site of the cAMP binding protein for the activation of the transcription, **His-Patch-Thr**: region encoding His-Patch thioredoxin, **EK**: region encoding enterokinase recognition site, **V5-epitope**: C-terminal V5-epitope, **6xHis**: C-terminal His_6 tag, **rrnB terminator** and **rrnB T2 terminator**: strong transcription termination regions. The vector map was produced using CLC Genomics Workbench 9.5.1 software.

The *cymA01* gene was restricted from the pUC57 vector with the use of NcoI and HindIII restriction enzymes, isolated by agarose gel electrophoresis, and purified from the agarose gel. The pLS167 was also restricted with the same restriction enzymes and the linearized vector was isolated by agarose gel electrophoresis, and purified from the agarose gel. Subsequently, the *cymA01* gene and the restricted linear vector were ligated, yielding the pTL01 vector.

A general version of pTL01 vector map is shown in **figure 22**, where the desired gene is presented as 'insert'.

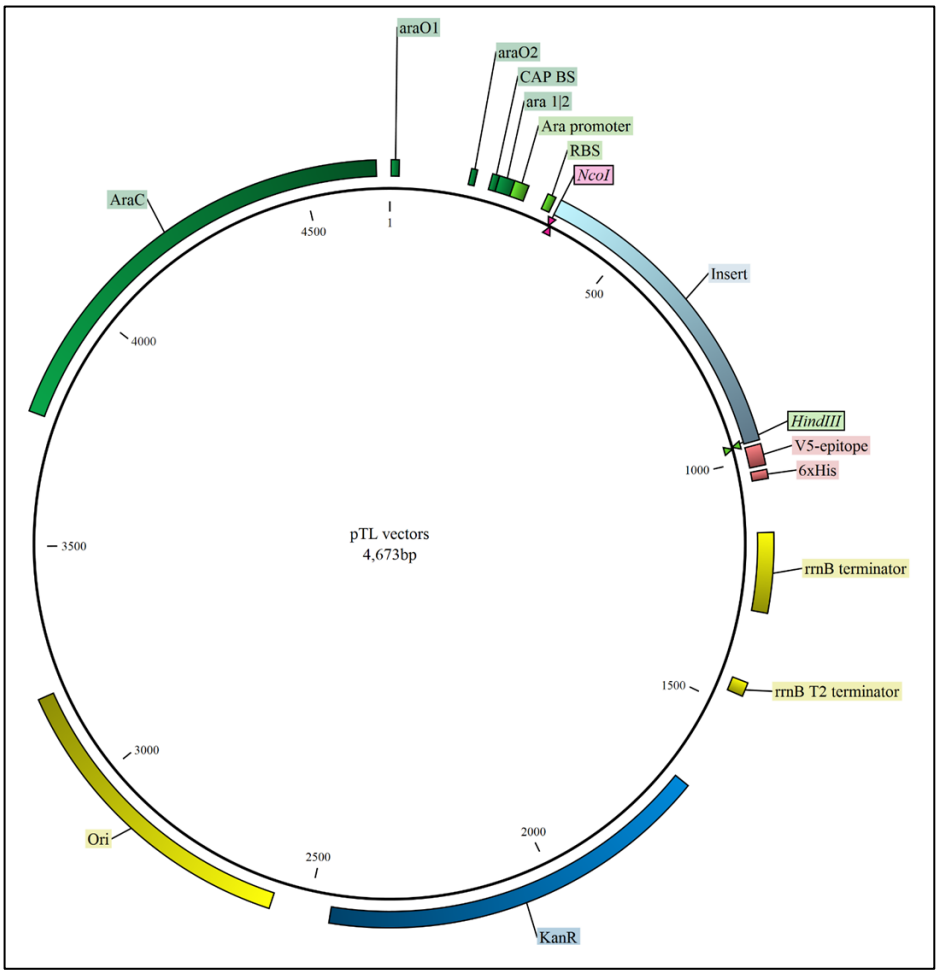

Figure 22: pTL vector map. The map is annotated to show the key features of the vector: **KanR**: region encoding gene that confers kanamycin resistance, **Ori**: origin of replication, **AraC**: encoding gene that confers tight regulation of the promoter, **Ara promoter**: promoter region, **RBS**: ribosomal binding site, **NcoI**: position of the restriction site, **HindIII**: position of the restriction site, **araO1/ araO2**: operator regions, **ara 1|2**: binding sites of araC for the activation of transcription, **CAP BS**: binding site of the cAMP binding protein for the activation of the transcription, **Insert**: *cymA01* gene, **V5-epitope**: C-terminal V5-epitope, **6xHis**: C-terminal His_6 tag, **rrnB terminator** and **rrnB T2 terminator**: strong transcription termination regions. The vector map was produced using CLC Genomics Workbench 9.5.1 software.

The correct ligation of the *cymA01* gene to the re-constructed expression vector was assayed by Sanger sequencing of pTL01 vector. Subsequently, *S. oneidensis* MR-1 was transformed with pTL01 by electroporation. Competent *Escherichia coli* BL21 (DE3), already carrying pEC86 that encodes the *ccm* haem maturation cassette, was also transformed with pTL01 by heat shock.

3.2.2 Small-scale gene overexpression trials

The overexpression of the His_8-HRV3Csite-CymA protein construct was assayed in small-scale liquid cultures of both *S. oneidensis* MR-1 and *E. coli* BL21 (DE3)/pEC86. The expression conditions were optimised for pLS167 by Marritt et al (2012 (1); as well as unpublished data), and thus temperature and medium screens were not performed. The bacterial cells were grown in LB under microaerobic conditions at 30 °C and shaking at 200 rpm. Protein expression was induced when the cultures reached mid-exponential phase (OD_{600} ~ 0.7) with 1 mM L-arabinose. The expression was allowed for 18 h before the cells were harvested by centrifugation and subjected to ultrasonic lysis in buffer containing 100 mM HEPES pH 7.4, 100 mM NaCl. The suspension was centrifuged at 15,000 g for 30 min at 4 °C to pellet insoluble material. The resuspended pellet in the same buffer (100 mM HEPES pH 7.4, 100 mM NaCl), constituted the insoluble fraction.

Samples of the insoluble fractions of non-induced and induced cells were analysed by SDS-PAGE (**figure 23**). Although Coomassie-stained SDS-PAGE did not show any prominent bands appearing in the samples of the induced cells of either expression system (**panel A figure 23**), haem-stained SDS-PAGE provided an indication of some protein overexpression (**panel B figure 23**). The sample of the insoluble fraction of induced *S. oneidensis* MR-1/pTL01 on haem-stained SDS-PAGE showed a band with increased intensity that run at about 20 kDa, when compared to the sample of the insoluble fraction of non-induced *S. oneidensis* MR-1/pTL01 (red box in **panel B figure 23**). For the *E. coli* BL21 (DE3)/pEC86 expression system, some leaky-expression of a c-type cytochrome was observed that run at about 15 kDa (arrow in **panel B figure 23**) while no bands were observed in the induced sample on haem-stained SDS-PAGE. This small-scale expression trial was replicated with consistent results. Thus, *S. oneidensis* MR-1/pTL01 was selected as a potential candidate for the overexpression of recombinant CymA and was used for large-scale expression and purification.

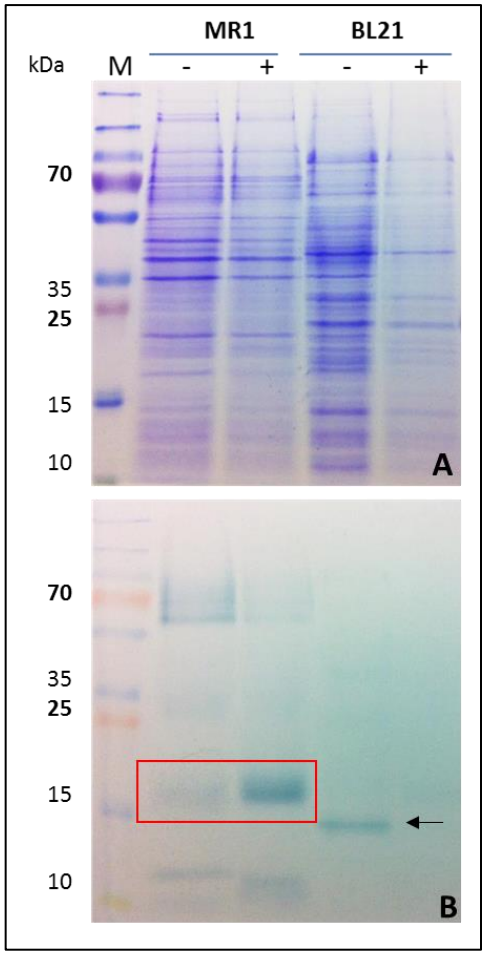

Figure 23: Electrophoretic profiles of protein expression from insoluble fractions of non-induced (-) and after 16 h of induced with 1 mM L-arabinose (+) lysed *S. oneidensis* MR-1/pTL01 (MR1) and *E. coli* BL21 (DE3)/pEC86/pTL01 (BL21) cells. A: 15% SDS-PAGE stained with Coomassie stain. B: 15% SDS-PAGE stained with c-type cytochrome-specific haem-stain. Lane M: molecular mass protein markers.

3.2.3 Expression and purification of CymA† from *Shewanella oneidensis* MR-1

S. oneidensis MR-1/pTL01 was grown in TB medium in order to support higher cell mass during large-scale expression cultures. The cells were grown to mid-exponential phase (OD_{600} ~ 0.7) under microaerobic conditions at 30 °C with orbital shaking at 200 rpm, before they were induced with 1 mM L-arabinose. To further support overexpression of the CymA protein construct for a period of 16 h the agitation speed of the orbital shaking was reduced to 180 rpm.

The purification of recombinant CymA from DDM-solubilised membranes was achieved by immobilised-Ni^{2+} affinity chromatography. During manual chromatography, a two-step-elution was performed at 130 mM and 300 mM imidazole. The electrophoretic purification profile is shown in **figure 24**, which shows a prominent band at approximately 20 kDa with the majority of it eluting at 300 mM imidazole, although smaller amounts also eluted at 130 mM imidazole (red box). There is also indication that binding of the target protein may have been incomplete since the disappearance of a protein band cannot be distinctly observed when the load and flow-through samples are compared (red box in **figure 24**).

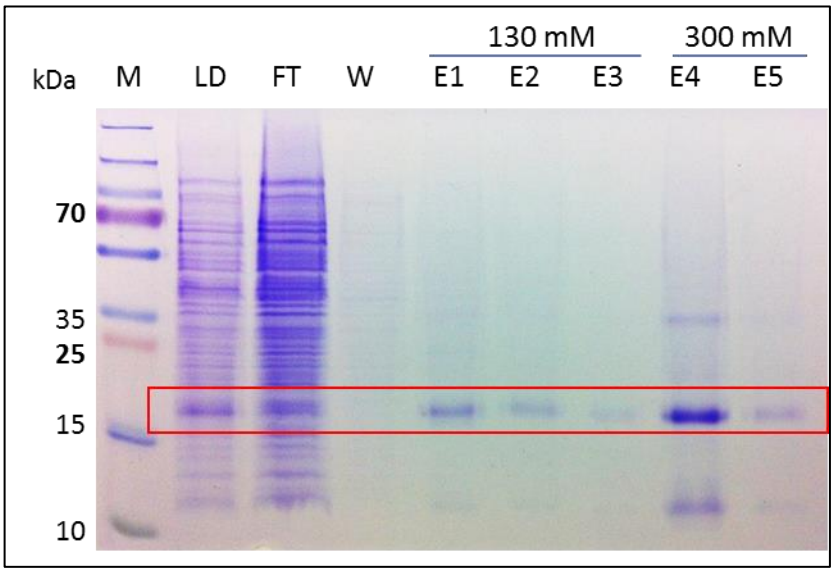

Figure 24: Immobilised-Ni^{2+} affinity electrophoretic purification profile from DDM-solubilized *S. oneidensis* MR-1/pTL01 membranes that shows elution of a prominent band at approximately 20 kDa at 300 mM imidazole. 15% SDS-PAGE stained with Coomassie stain. M: molecular mass protein markers; LD: column load; FT: flow-through during binding; W: 5 mM binding buffer wash; E1-E3: 130 mM imidazole eluates; E4-E5: 300 mM imidazole eluates.

The purification was replicated with the use of an ÄKTA pure 25 chromatographic system at 4 °C with a flow rate of 0.5 ml min^{-1}. Elution was performed by employing a gradient with increasing imidazole concentration at a flow rate of 1 ml min^{-1}. The chromatogram (**figure 25**) resolved two peaks at 220 mM and 280 mM imidazole. The target protein eluted at 280 mM

imidazole, while the peak at 220 mM imidazole eluted a high number of contaminating proteins as observed on SDS-PAGE (**figure 26**).

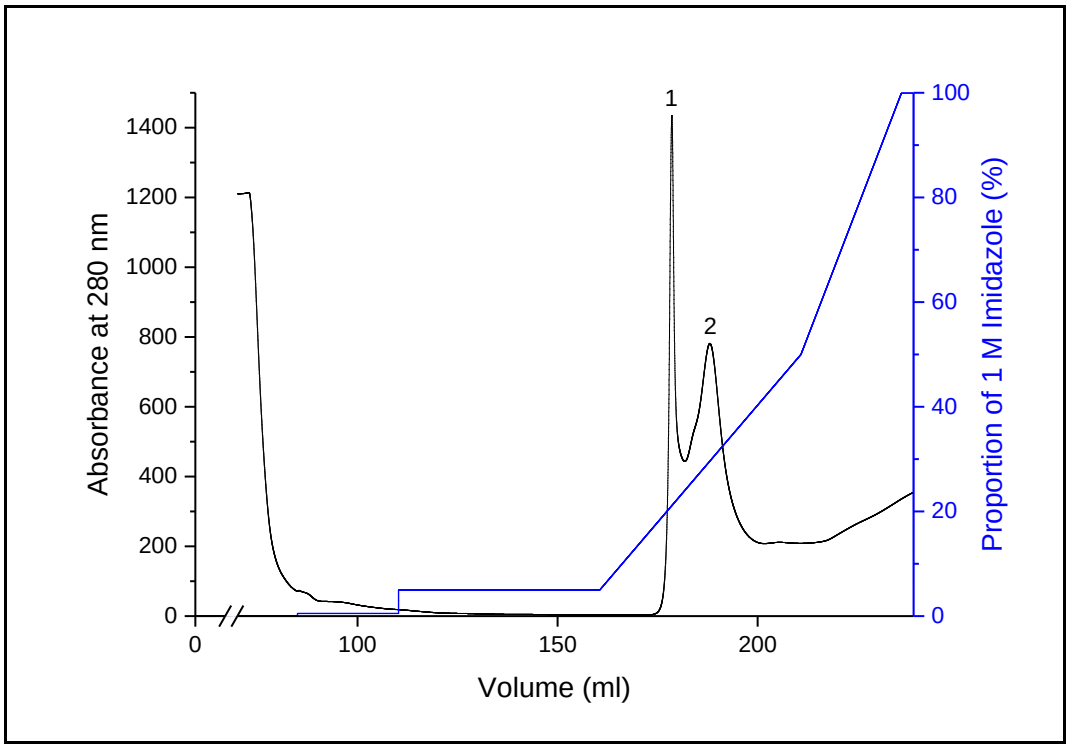

Figure 25: Immobilised-Ni^{2+} affinity chromatographic elution profile with the application of a gradient of imidazole concentration on HisTRAP-HP column. The column equilibration and subsequent protein loading onto the column are truncated. Chromatography was performed at 4 °C with a flow rate of 0.5 ml min^{-1} during binding and of 1 ml min^{-1} for all subsequent steps. The buffer composition was 20 mM Tris-HCl pH 8.0, 0.5 M NaCl, 0.1% w/v DDM and varying imidazole concentration.

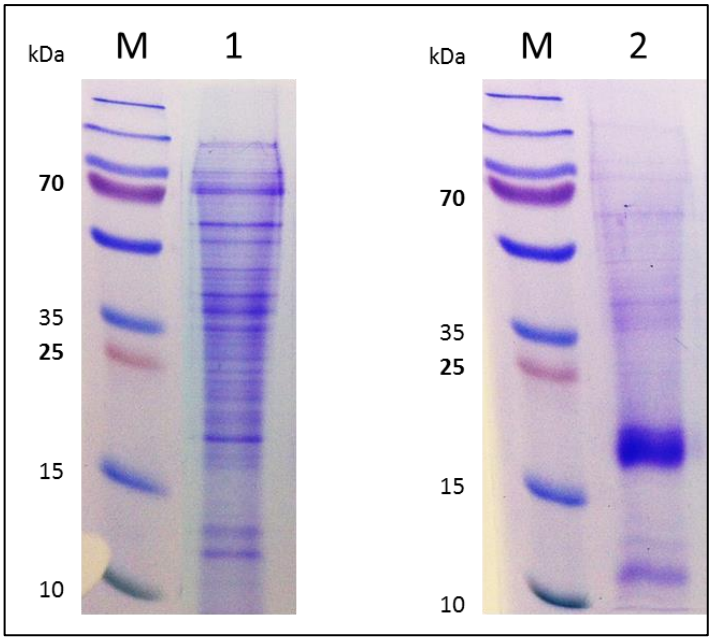

Figure 26: Electrophoretic analysis of elution peak fractions from immobilized-Ni^{2+} affinity chromatography. 15% SDS-PAGE stained with Coomassie stain of chromatographic peak fractions 1 and 2 as shown in figure 6. M: molecular mass protein markers.

The concentrated purified protein sample electrophoretically resolved three prominent protein bands, running at approximately 35 kDa, 20 kDa, and 11 kDa on SDS-PAGE (**figure 27**), all of which stain for c-type cytochromes (**panel B figure 27**).

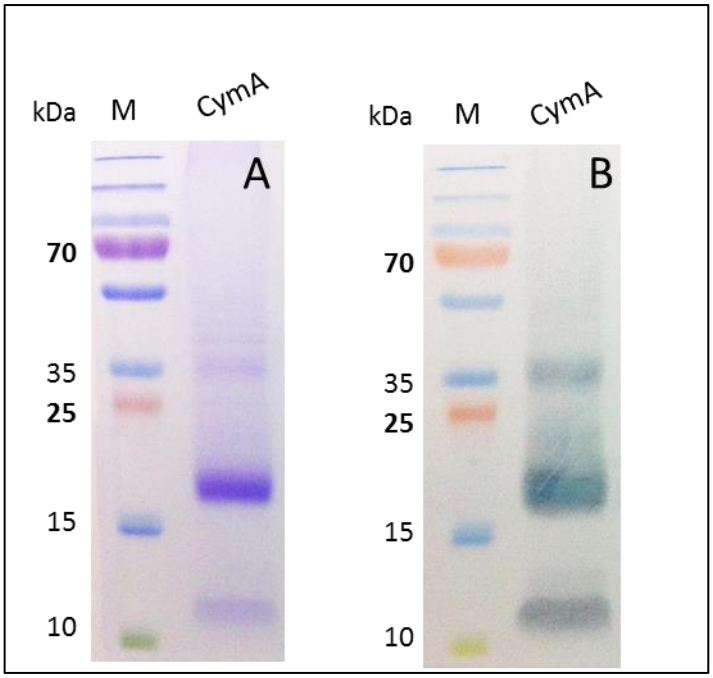

Figure 27: Electrophoretic profile of purified recombinant CymA by single step immobilised-Ni^{2+} affinity chromatography performed manually. 15% SDS-PAGE stained with Coomassie stain (A), and haem-stain (B). M: molecular mass protein markers.

The 20 kDa band was excised and analysed by liquid chromatography coupled to mass spectroscopy upon trypsin digestion that identified two unique peptides (R.IYENQPETMKPMAVR.M: residues 161-175; and F.NTQAWLDENR.K: residues 126-135), giving 12% protein coverage, for CymA from *S. oneidensis* MR-1. Although the theoretical molecular mass of the holoprotein construct is 25,468 Da (taken into account the incorporation of four haems with an approximate molecular mass of 616.5 Da per haem), the 20 kDa band is judged to be recombinant CymA that has been partially denatured and, therefore, run lower than expected. This is supported by the fact that c-type haems are covalently bound to the polypeptide, often providing extra stability.

The protein sample was further analysed by size exclusion chromatography with a subsequent immunodetection approach in order to determine whether the 35 kDa and 11 kDa bands are the product of an SDS-PAGE artefact, as well as identify them. Size exclusion chromatography performed at 4 °C partially separated those bands and, hence, excluded the possibility of an SDS-PAGE induced artefact (**figure 28**). Subsequent immunodetection of the peak fractions detected the three protein bands with monoclonal antibodies

against both CymA-specific and poly-His epitopes (**figure 29**). Thus, it is concluded that the 20 kDa band is partially denatured recombinant CymA in monomeric form carrying a His-tag, while the 35 kDa band may be CymA in oligomeric form. This electrophoretic profile has been previously described for CymA. The 11 kDa band is thought to may have been derived as a product of a C-terminal truncation since it carries a His-tag that is located on the N-terminus of this CymA construct. The purity is estimated to be > 90 % and the final typical yield from this purification approach is 2 mg CymA L^{-1} of culture.

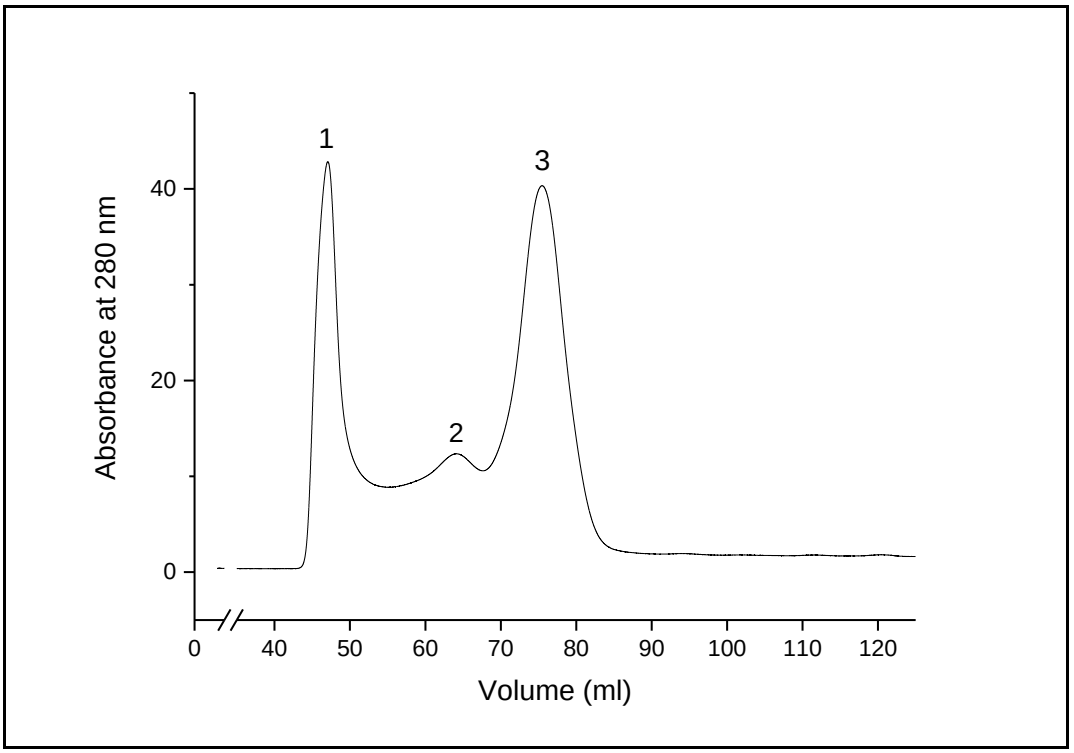

Figure 28: Size exclusion chromatographic profile of purified CymA with HiLoad 16/600 Superdex 200 prep-grade column. The void volume (V_o) is 45 ml. The chromatography was performed with ÄKTA pure 25 at 4 °C with a flow rate of 0.5 ml min^{-1}. The buffer composition was 20 mM HEPES pH 7.5, 150 mM NaCl, and 0.05% w/v DDM. The concentration of purified CymA that was injected onto the column was 1.7 mg ml^{-1}.

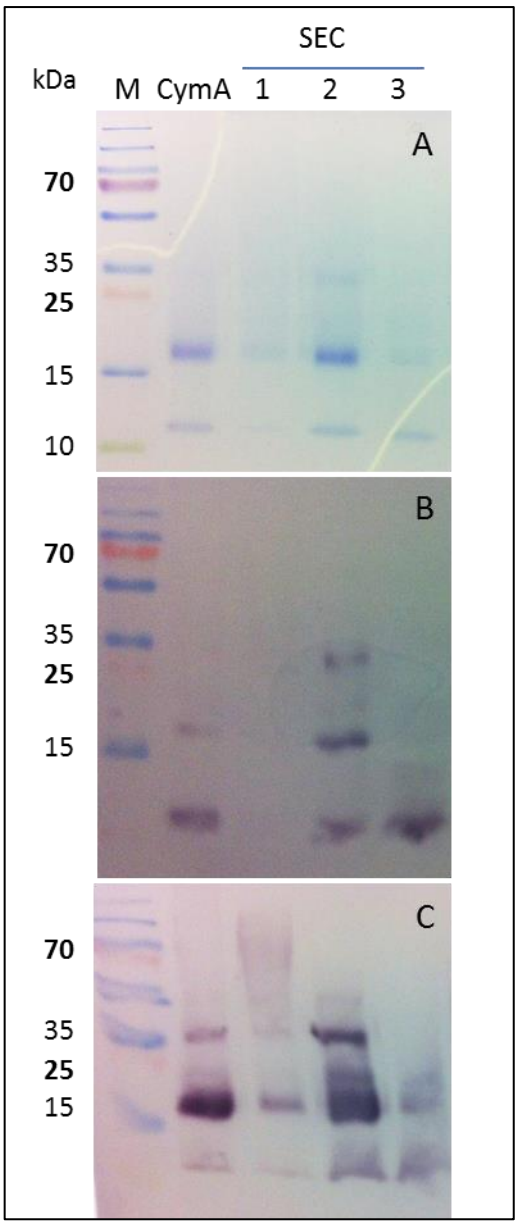

Figure 29: Electrophoretic analysis of peak fractions from size exclusion chromatography of purified recombinant CymA with subsequent immunodetection of the three prominent bands with monoclonal antibodies against both CymA-specific and poly-His epitopes. A: 15% SDS-PAGE stained with Coomassie stain. B: Western blot with α-poly-His mAb. C: Western blot with α-CymA mAb. M: molecular mass protein markers, CymA: purified recombinant CymA sample that was loaded onto the column, 1-3 S: peak fractions from size exclusion chromatography as shown in figure 9.

Modulation of the rate of protein expression with a decreased concentration of L-arabinose from 1 mM to 0.5 mM to support the correct folding of the recombinant protein during overexpression, along with EDTA-containing protease inhibitors during cell disruption to avoid proteolytic degradation from native proteases, significantly reduced the 11 kDa band (**figure 30**).

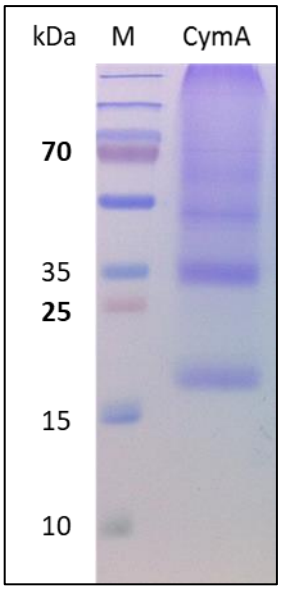

Figure 30: Electrophoretic profile of purified recombinant CymA by single step immobilised-Ni^{2+} affinity chromatography performed with ÄKTA pure 25. 15% SDS-PAGE stained with Coomassie stain. M: molecular mass protein markers. EDTA-containing protease inhibitors along with a decreased concentration of 0.5 mM L-arabinose eliminates low molecular mass truncations that were observed in earlier preparations.

3.2.4 Biochemical and electrochemical characterisation of purified CymA†

Purified recombinant CymA was analysed spectrophotometrically and the obtained UV-visible (λ = 250 nm – 800 nm) absorbance spectra of oxidised and reduced CymA are shown in **figure 31**. The spectrum of the oxidised CymA resolved a broad shoulder between 500 nm and 600 nm and a peak at 407 nm that corresponds to the Soret γ-band of light absorption by the haems. The spectrum of reduced CymA showed the resolution of the Soret α- and β-bands at 551 nm and 522 nm respectively, while the Soret γ-band shifted to 418 nm. The purity ratio of A_{407}/ A_{280} was 3.7. The recorded spectra showed characteristic features for c-type cytochromes and were in agreement with published spectra for CymA (1).

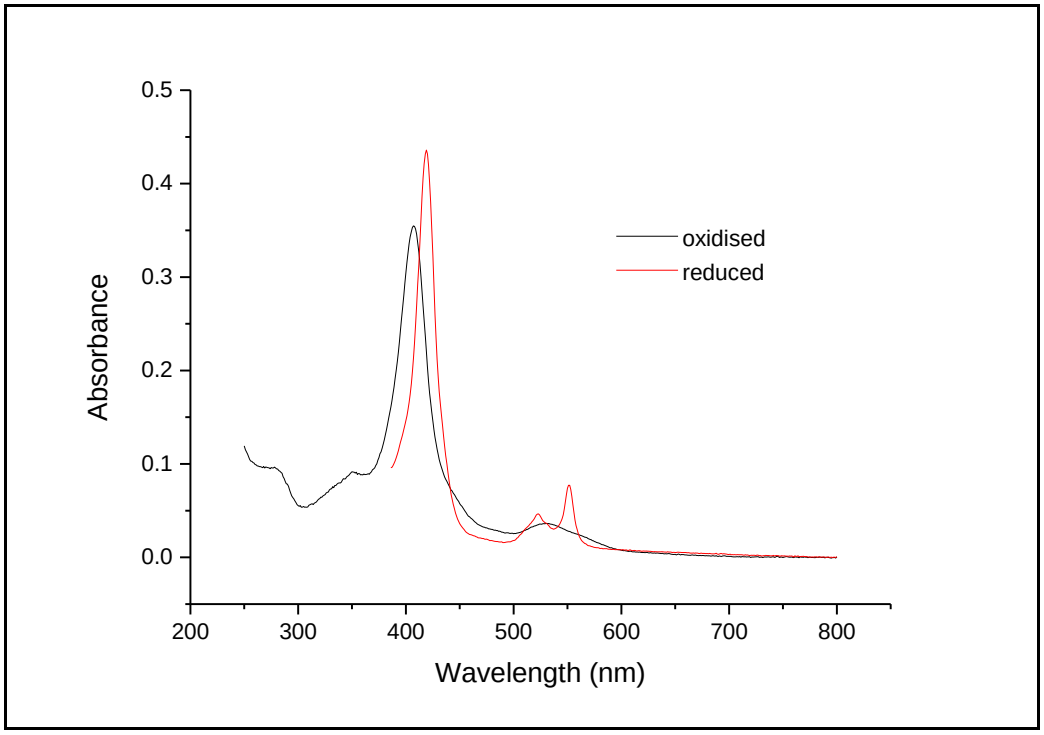

Figure 31: UV-visible absorbance spectra of oxidised and reduced purified recombinant CymA. Measurements were conducted at ambient conditions in 20 mM HEPES pH 7.5 and 150 mM NaCl. The spectra are baseline corrected. The spectrum of fully reduced CymA was obtained by addition of excess of dithionite.

CymA catalyses the reduction of menaquinone at the inner membrane of *S. oneidensis* MR-1 in order to support the anaerobic respiratory pathways by allowing electron flow during the oxidation of organic compounds in maintaining the proton gradient for ATP synthesis. The catalytic activity of CymA has been well characterized in vitro by protein film electrochemistry on modified gold electrodes (39). Thus, protein film electrochemistry was employed in order to assess whether the purified recombinant CymA maintained activity. To this end, ultra-flat gold electrodes were modified with a self-assembled monolayer of 8-amino-1-octanethiol and 8-mercapto-1-octanol at a ratio of 1:10 respectively in order to promote the electrostatic adsorption of CymA, forming a protein film onto the electrode. The electrode was poised by cycling the applied potential between -0.3 V and +0.3 V that resolved non-turnover signals of CymA (**figure 32**). That is the reductive and oxidative peaks as CymA is being reduced and oxidized. Upon addition of menaquinone-containing liposomes, the substrate for CymA, a catalytic reductive wave was observed (**figure 33**) with the same magnitude as

previously described (39). Thus, the purified recombinant CymA is catalytically active.

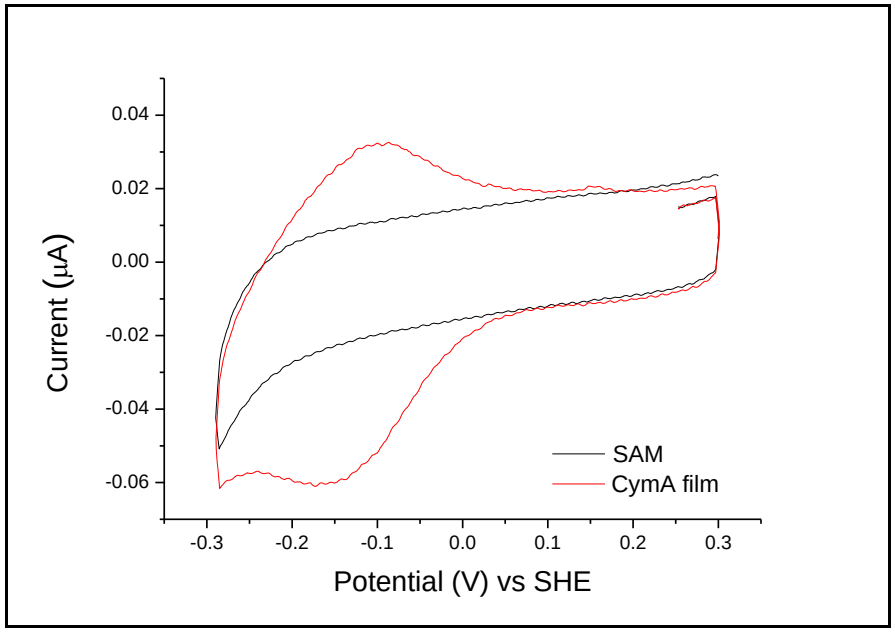

Figure 32: Cyclic voltammetry of CymA protein film resolving non-turnover signals. SAM: 1:10 NH^{3+}/OH^{-} thiol self-assembled monolayer. CymA film: adsorbed CymA protein film after removing excess of CymA by three buffer washes. The measurements were performed under a nitrogen atmosphere (0_2 ≤ 0.1 ppm) at ambient conditions and at a scan rate of 10 mV s^{-1}. The buffer composition was 20 mM MOPS pH 7.4 and 30 mM Na_2SO_4.

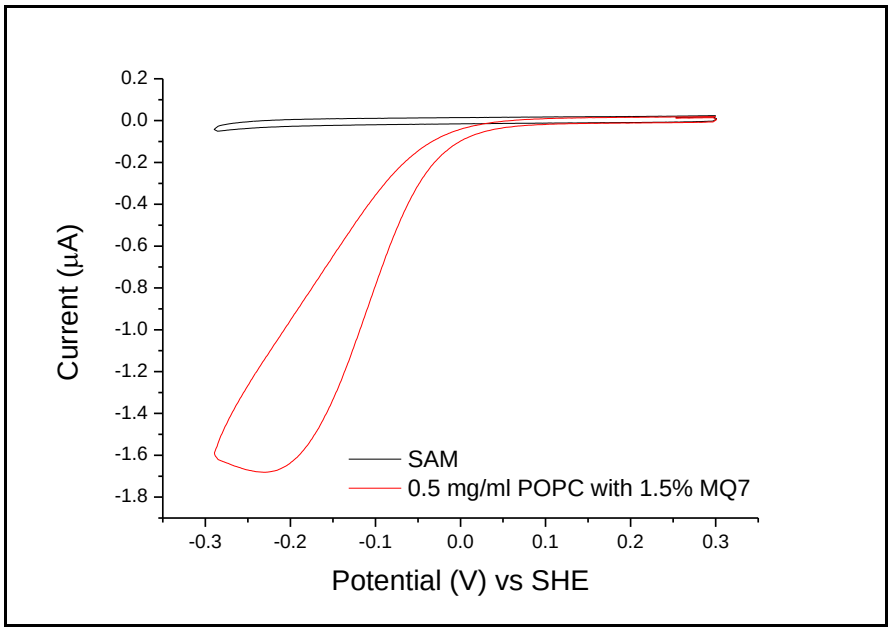

Figure 33: Cyclic voltammetry of CymA protein film resolving catalytic reductive signal on addition of menaquinone (MQ7)- containing POPC-liposomes. SAM: 1:10 NH^{3+}/OH^{-} thiol self-assembled monolayer. The measurements were performed under a nitrogen atmosphere (0_2 ≤ 0.1 ppm) at ambient conditions and at a scan rate of 10 mV s^{-1}. The buffer composition was 20 mM MOPS pH 7.4 and 30 mM Na_2SO_4.

3.3 Conclusions

The expression of multihaem cytochromes is particularly challenging for a number of reasons: (a) haem incorporation is ATP-dependent that increase the energetic requirements of the organism during overexpression; (b) these proteins are usually involved in respiratory pathways, which their overexpression can interfere with the normal metabolic functions; and (c) some of those enzymes, like CymA, are transmembrane proteins, which the inherent issues of overexpressing and purifying membrane proteins in general add to the overall challenges.

Current methodologies in circumventing some of those challenges involve the homologous expression of the target proteins. As such, *S. oneidensis* had been employed to homologously overexpress CymA with a modified pBAD/TOPO expression system under the tight regulation of the arabinose promoter. Here, further improvements on this system were presented with a resulting purification approach that is reproducible, while eliminating tag interference issues that may result from the presence of purification tags on the C-terminus of the protein. From the characterization of this new protein construct, the properties of CymA were not altered, while the purity and yield were significantly increased to > 90% and 2 mg per litre of culture respectively. Specifically, higher molecular mass contaminants that were previously seen (1) were eliminated. It must be noted that the yield was not previously reported (1). Moreover, CymA appears catalytically active under previously established electrochemical methods. However, it must be noted that the observed catalytic behaviour of CymA by protein film electrochemistry shows a reversal on the catalytic bias. That is, under the current understanding, CymA *in vivo* is responsible for the oxidation of the quinone pool, while the reduction of menaquinone is what was observed here. This is in complete agreement with the published literature (39), though, it is currently unknown whether this may imply the involvement of a yet undiscovered regulatory mechanism, or that the observed *in vitro* behaviour of CymA is an artefact.

Chapter 4 – Heterologous Expression in *Escherichia coli* and Purification of Recombinant *Shewanella oneidensis* MR-1 $CymA_{sol}$: Paving the Road Towards the Structural Determination of CymA

4.1 Introduction

The transmembrane quinol dehydrogenase CymA is a key component of the anaerobic respiratory system of *S. oneidensis*, which exhibits unique and versatile metabolic abilities. CymA belongs to the NapC/NirT family of quinol dehydrogenases, whose members are ubiquitous in anaerobic organisms. However, quinol dehydrogenases are usually part of larger multiprotein membrane complexes, which is in contrast to CymA that no co-purification of any of its partner proteins has been seen during its purification (1, 35). Moreover, sequence analysis of its closest homologues with bioinformatics suggests that CymA is evolutionary distinct (**figure 34**) and limited conservation with the closest homologues of CymA, except the highly conserved CXXCH motifs of the four haems (**figure 35**).

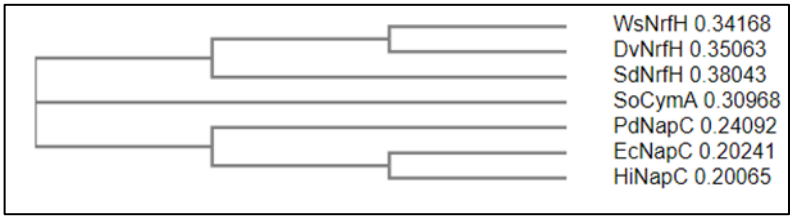

Figure 34: Phylogenetic tree of CymA and its closest homologues. WsNrfH: *Wolinella succinogenes* NrfH, DvNrfH: *Desulfovibrio vulgaris* NrfH, SdNrfH: *Sulfurospirillum deleyianum* NrfH, SoCymA: *Shewanella oneidensis* CymA, PdNapC: *Paracoccus denitrificans* NapC, EcNapC: *Escherichia coli* NapC, HiNapC: *Haemophilous influenza* NapC. The tree was generated with Multiple Sequence Comparison by Log-Expectation by EMBL-EBI.

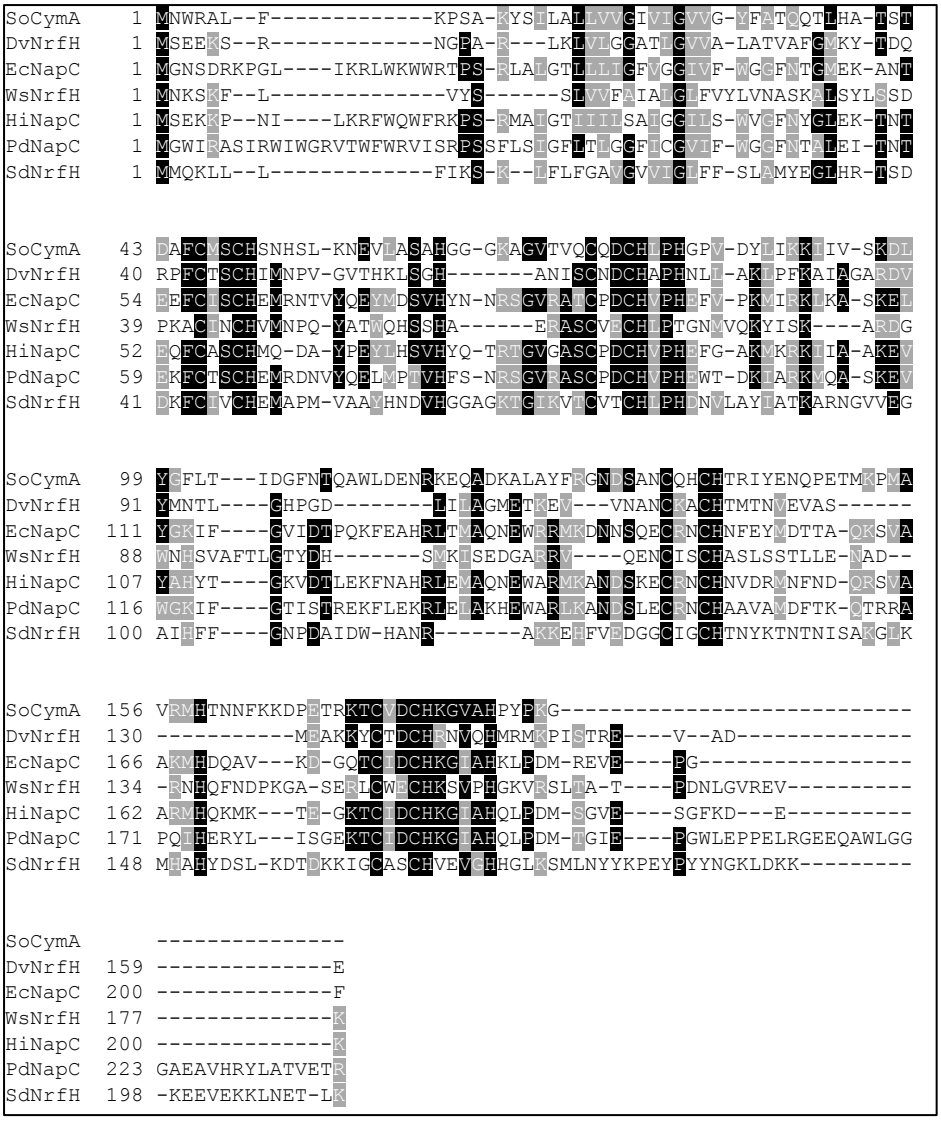

Figure 35: Multisequence alignment of CymA with its closest homologues. Limited conservation is observed across the protein other than the highly conserved CXXCH motifs of the four haems along with key residues that are involved in the co-ordination of the haems. SoCymA: *Shewanella oneidensis* CymA; EcNapC: *Escherichia coli* NapC; DvNrfH: *Desulfovibrio desulfuricans* NrfH; WsNrfH: *Wolinella succinogenes* NrfH; HiNapC: *Haemophilus influenza* NapC; PdNapC: *Paracoccus denitrificans* NapC; and SdNrfH: *Sulfurospirillum deleyianum* NrfH. The multisequence alignment was performed with T-Coffee (100, 101).

The closest homologue of CymA is NrfH with ~60% homology. NrfH of *Desulfovibrio vulgaris*, though, is part of a stable $NrfH_2A_4$ complex. As such, homology modelling of CymA based on NrfH reveals limiting information about the structural characteristics of CymA (**figure 36**). The model shows an N-terminal transmembrane α-helix and a second membrane-associated α-helix that closely resemble those of NrfH, not much else, however, is revealed from the model. Moreover, NrfH only exists as part of a strong multiprotein complex

with NrfA, from which it is hypothesised that structurally NrfH and CymA should have significant differences in their globular domains in order for the latter to be able to interact with a great number of different proteins.

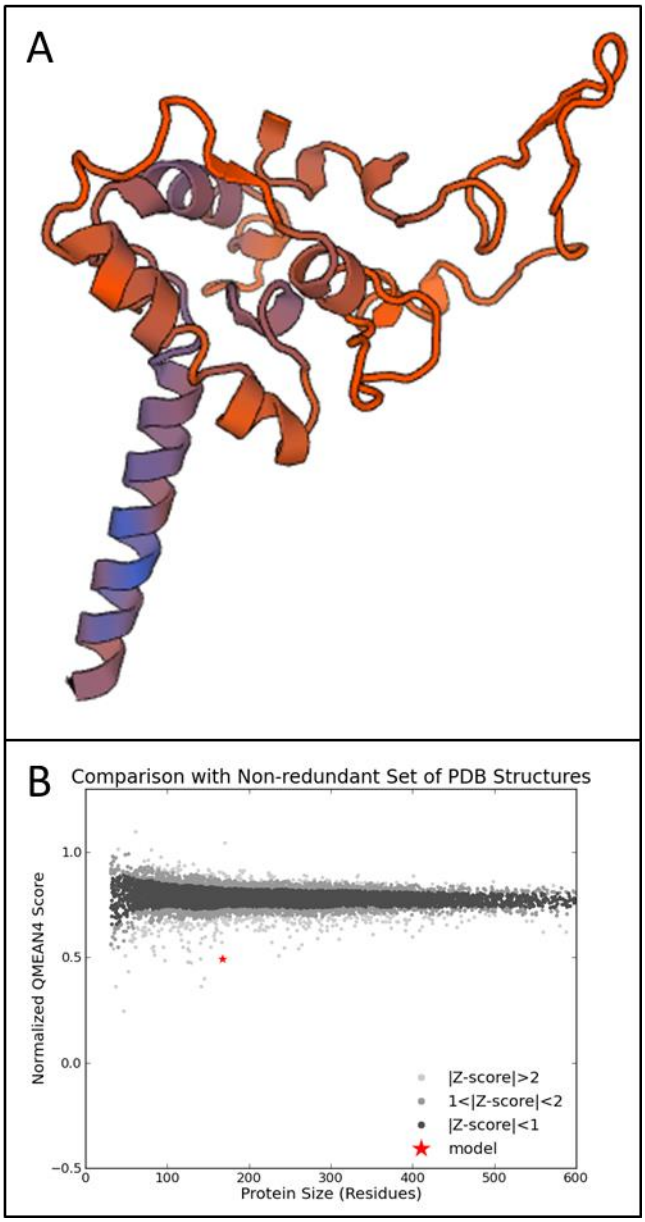

Figure 36: Structural homology model of CymA. A homology model was built using, as a template, the resolved crystal structure of NrfH (PDB: 2VR0), which was identified as the one with the closest homology to CymA by SWISS-MODEL (102, 103). A: structure of the CymA model. B: Quality comparison graph. The global model quality estimate score was 0.48, which is indicative of a low quality model (the closest to 1 the score is, the more reliable the model is).

Although a larger number of *S. oneidensis* proteins that comprise its anaerobic respiratory system had their crystal structures resolved, the crystal structure

of CymA remains elusive. This has been mainly due to limitations in producing sufficient quantities of the protein in a high quality monodisperse solution in order to enable crystallographic studies. However, a high-throughput system for the expression and purification of multi-haem cytochromes from *S. oneidensis* has been developed for their heterologous expression in *E. coli* (89). The pMKL1 plasmid from this system was explored in this chapter for the production of $CymA_{sol.}$ The pMKL1 plasmid encodes for a 6xHis-MBP-$CymA_{sol}$ construct with an engineered TEV proteolytic site at the end of MBP for the removal of the tags. $CymA_{sol}$ refers to a truncated soluble version of CymA, without the first 31 amino acids that comprise the majority of the transmembrane α-helix, but leaving intact the quinone binding site.

This chapter presents the first reported crystallisation attempt in the quest of elucidating the crystal structure of CymA. Firstly, the production of high quality recombinant $CymA_{sol}$ was presented, along with its characterization. Finally, the preliminary results of seven different crystallisation screens are presented, paving the way for the structural determination of CymA.

4.2 Results

4.2.1 Expression and purification of $CymA_{sol}$

E. coli BL21 cells were co-transformed with pMKL1 and pEC86, which were grown in TB medium in order to support higher cell mass during large-scale expression cultures. The cells were grown to mid-exponential phase (OD_{600} ~ 0.7) under microaerobic conditions at 30 °C with orbital shaking at 200 rpm, before they were induced with 50 µM IPTG. Normally, in an *E. coli* protein expression system, the ratio of the culture volume to the volume capacity of a flask is 1:5. However, this ratio was reduced to 1:2, which along with a decrease of the agitation speed, resulted in microanaerobic conditions in order to promote the incorporation of the four c-type haems. Moreover, the lower temperature, from the ideal for *E. coli* (37 °C), was employed for slowing protein overexpression and, by extension, promote correct protein folding.

Initially, the full $CymA_{sol}$ construct carrying a 6xHis-tag and MBP was purified from the isolated soluble periplasmic fraction of overexpressing cells by immobilised-Ni^{2+} affinity chromatography. The electrophoretic purification profile is shown in **figure 37**, which shows two prominent bands at around 65 kDa and around 40 kDa that both stain with an anti-His antibody on Western blot. These two bands are present in the load and in the eluates but not in the flowthrough or the wash samples. Thus, the purification was efficient with no loss in the form of unbound material. The full construct has an approximately theoretical molecular mass of 64 kDa, while a truncated version lacking the $CymA_{sol}$ has a theoretical molecular mass of 43 kDa (MBP of 42 kDa plus 6xHis of 1kDa). Thus, it was concluded that the two prominent bands from the purification are of the construct with and without $CymA_{sol}$ (denoted as whole and truncated respectively in **figure 37**). Such truncation was observed before when MBP is employed as an aid in expressing difficult proteins or increasing the solubility of the target protein (104).

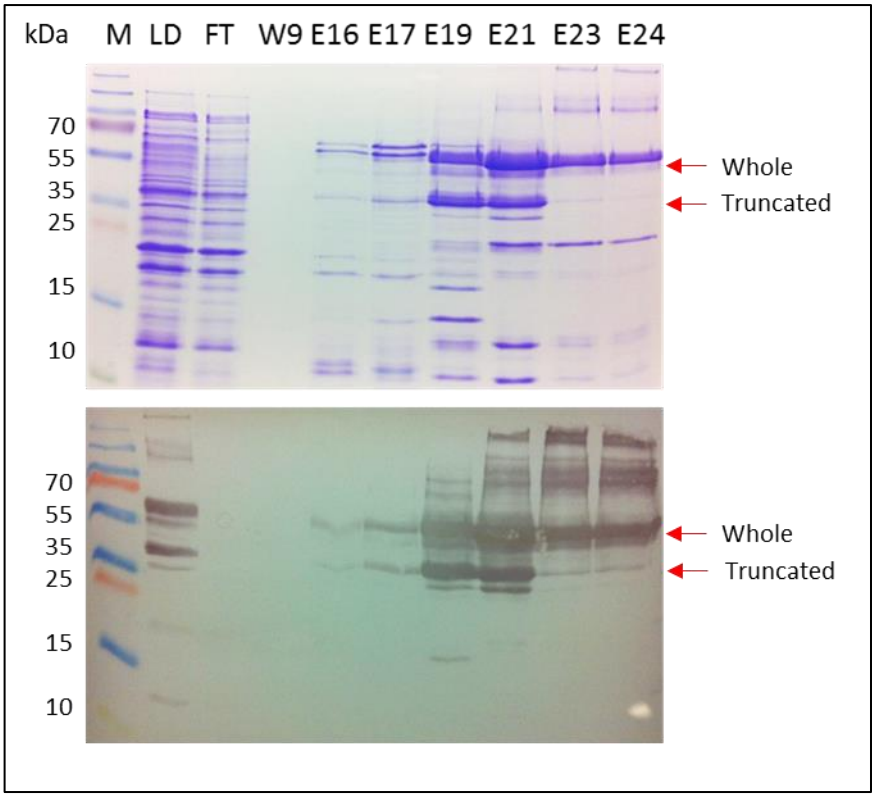

Figure 37: Immobilised-Ni^{2+} affinity electrophoretic purification profile from the periplasmic fraction of *E. coli* BL21 pMKL1/pEC86 cells overexpressing 6xHisMBPCymA_{sol} construct. 15% SDS-PAGE stained with Coomassie stain (top gel) or Western blot with anti-His antibody (bottom gel). M: molecular mass protein markers; LD: column load; FT: flow-through during binding; W9: 5 mM binding buffer wash; E16, E17, E19, E21, E23, and E24 eluates upon application of imidazole.

Subsequently, the eluates containing the protein of interest were pooled and subjected to proteolytic reaction mediated by TEV protease overnight at 4 °C for the removal of the tags. It was empirically observed that the cleavage reaction was not very efficient and TEV protease was required ideally at a ratio of 1:2 of total protein (mg) to TEV protease (mg). The mixture was then subjected to a reverse immobilised-Ni^{2+} affinity chromatography, where only $CymA_{sol}$ without tags came through the flowthrough. Typical yields from 1L of culture were 32 mg of total purified proteins (quantified by µBCA), from which 256 µg of $CymA_{sol}$ (quantified spectrophotometrically) were purified. It must be noted that care should be taken during the reverse affinity chromatographic step as to use excess of IMAC resin or columns in order to allow for the vast amount of TEV protease and non-cleaved/ contaminating material to bind.

The purified $CymA_{sol}$ was further polished by a S75 size exclusion chromatographic step (**figure 38**) in order to ensure high quality monodispersed material for crystallographic studies. The final purified $CymA_{sol}$ resulted in a >90% purity, determined by SDS-PAGE and shown in **figure 39**.

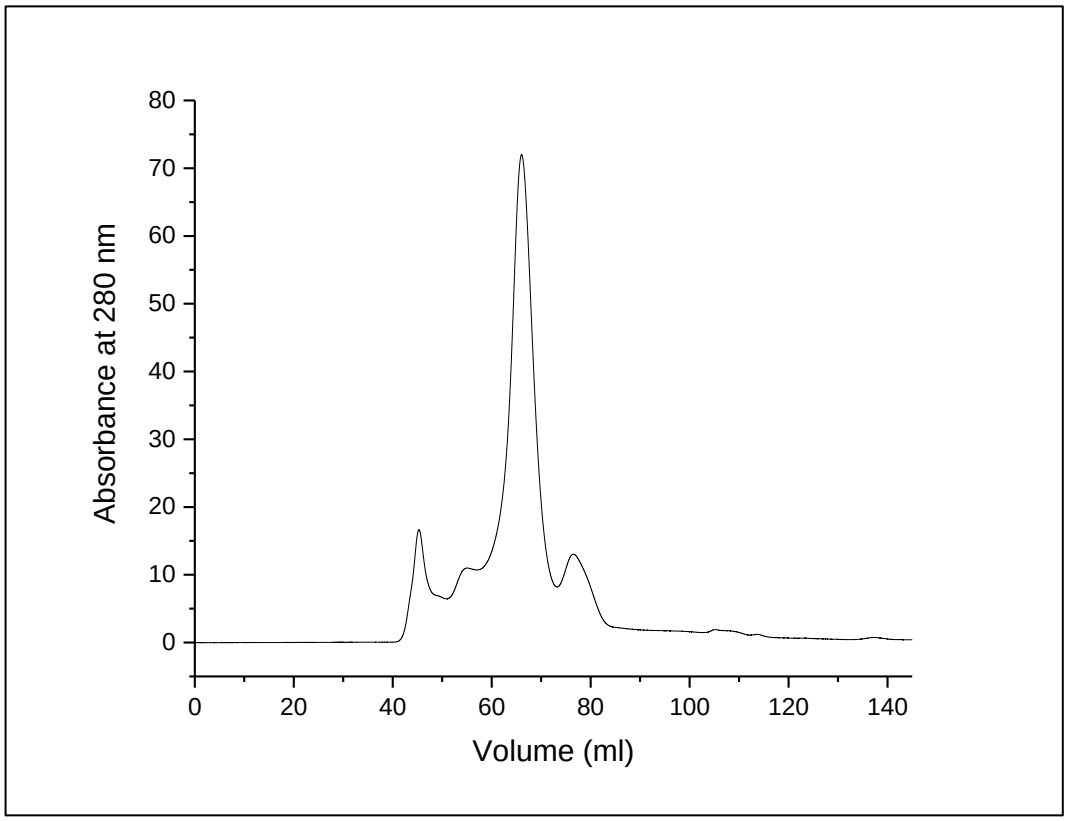

Figure 38: Size exclusion chromatographic profile of purified $CymA_{sol}$ with HiLoad 16/600 Superdex 75 prep-grade column. The void volume (V_o) is 45 ml. The chromatography was performed with ÄKTA pure 25 at 4 °C with a flow rate of 0.5 ml min^{-1}. The buffer composition was 20 mM HEPES pH 7.5, 150 mM NaCl.

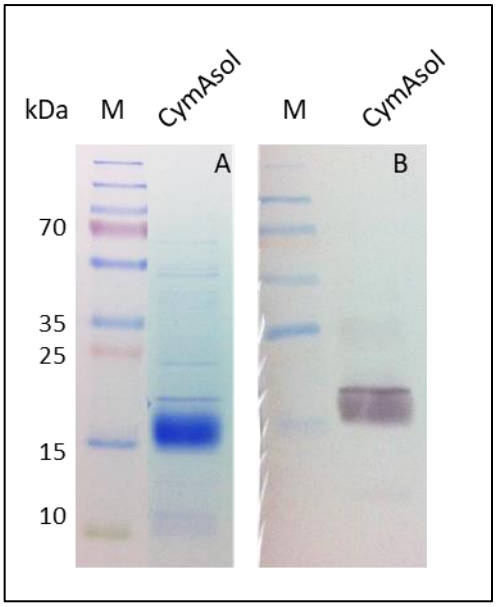

Figure 39: Electrophoretic profile of purified recombinant $CymA_{sol}$ after size exclusion chromatography. 15% SDS-PAGE stained with Coomassie stain (A), and Western blot with anti-CymA antibody (B). M: molecular mass protein markers.

4.2.2 Biochemical and electrochemical characterization of purified $CymA_{sol}$

Purified recombinant $CymA_{sol}$ was analysed spectrophotometrically and the obtained UV-visible (λ = 250 nm – 800 nm) absorbance spectra of oxidised and reduced $CymA_{sol}$ are shown in **figure 40**. The spectrum of the oxidised $CymA_{sol}$ resolved a broad shoulder between 500 nm and 600 nm and a peak at 407 nm that corresponds to the Soret γ-band of light absorption by the haems. The spectrum of reduced $CymA_{sol}$ showed the resolution of the Soret α- and β- bands at 551 nm and 522 nm respectively, while the Soret γ-band shifted to 418 nm. The purity ratio of A407/ A280 was 5.4.

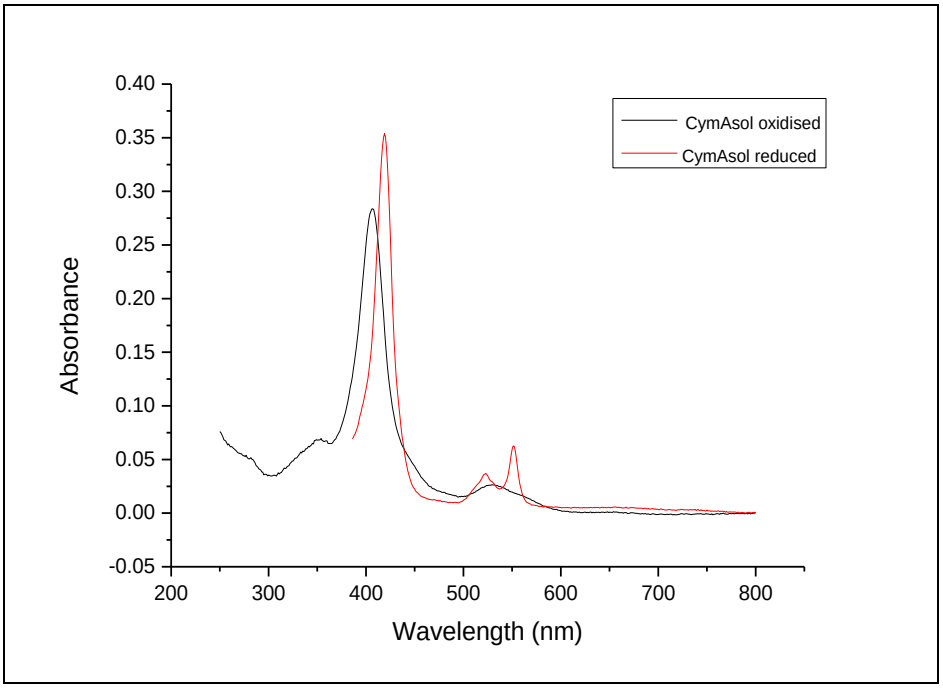

Figure 40: UV-visible absorbance spectra of oxidised and reduced purified recombinant $CymA_{sol}$. Measurements were conducted at ambient conditions in 20 mM HEPES pH 7.5 and 150 mM NaCl. The spectra are baseline corrected. The spectrum of fully reduced $CymA_{sol}$ (red line) was obtained by addition of excess of dithionite.

Protein film electrochemistry was employed to characterise the electrical properties of $CymA_{sol}$, as well as assay whether it is catalytically active in a similar manner as described for CymA† in chapter 3. Upon protein adsorption, non-turnover signals were observed (**figure 41**), which are in agreement with those for CymA. Subsequently, upon addition of menaquinone-loaded liposomes a catalytic reductive wave was observed (**figure 42**) with a slightly greater in magnitude signal than it had been observed for CymA. This can be explained by the truncation of most of the highly hydrophobic transmembrane α-helix, which could potentially allow for a quicker dissociation from the liposomes. Thus, the purified $CymA_{sol}$ is catalytically active, with its electrical properties unaltered.

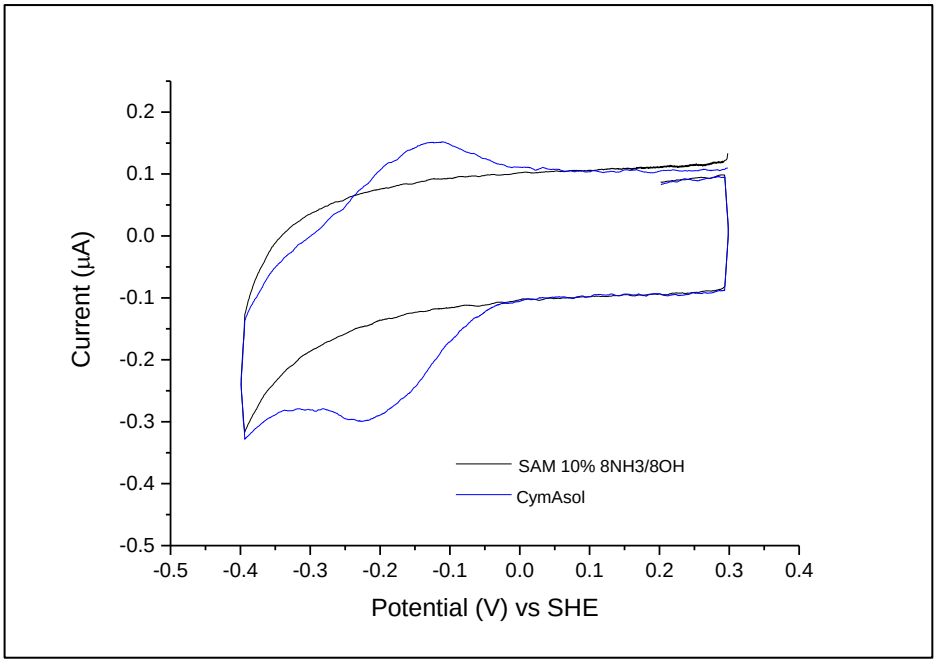

Figure 41: Cyclic voltammetry of $CymA_{sol}$ protein film resolving non-turnover signals. SAM: 1:10 NH^{3+}/OH^- thiol self-assembled monolayer. $CymA_{sol}$ film: adsorbed $CymA_{sol}$ protein film after removing excess of $CymA_{sol}$ by three buffer washes. The measurements were performed under a nitrogen atmosphere (0_2 ≤ 0.1 ppm) at ambient conditions and at a scan rate of 10 mV s^{-1}. The buffer composition was 20 mM MOPS pH 7.4 and 30 mM Na_2SO_4.

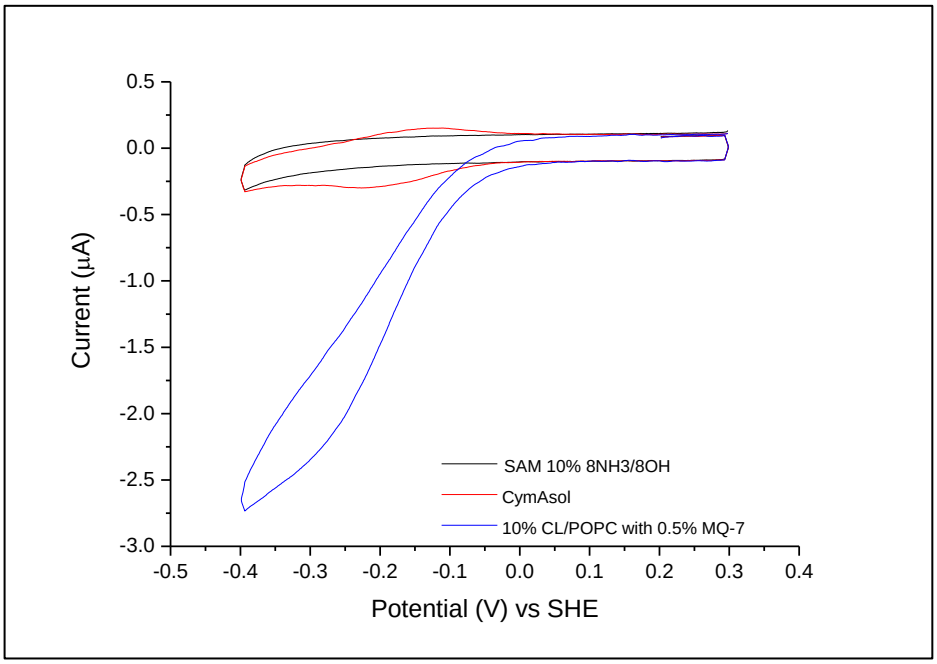

Figure 42: Cyclic voltammetry of $CymA_{sol}$ protein film resolving catalytic reductive signal on addition of menaquinone (MQ7)- containing POPC-liposomes. SAM: 1:10 NH^{3+}/OH^- thiol self-assembled monolayer. The measurements were performed under a nitrogen atmosphere (0_2 ≤ 0.1 ppm) at ambient conditions and at a scan rate of 10 mV s^{-1}. The buffer composition was 20 mM MOPS pH 7.4 and 30 mM Na_2SO_4.

4.2.3 Protein crystallisation: preliminary results

Although the production of $CymA_{sol}$ was challenging with low output yield, sufficient material was produced and used to set up crystallisation trays at 1 mg ml^{-1} protein concentration. This was possible because of, firstly, technological advances in liquid handling technologies that are able to accurately handle liquid volumes at the nL level. Secondly, a 10-fold lower protein concentration was used than what one would normally use for crystallisation. This was based on the hypothesis, that was partially in agreement with empirical observation during the purification, of a decreased solubility of $CymA_{sol}$ that were based on its partial truncation of the transmembrane α-helix and the intact second membrane-associated N-terminal α-helix.

As this was the first attempt to crystallise CymA of any form, initially four commercially available screens were employed, which contain a wide range of conditions for globular proteins: JCSG Core I, II, III, and IV Suites. Subsequent screens were set up with a screen that assays various conditions of PEG polymer as the precipitating agent (PACT Suite), as well as two screens that are specifically designed for membrane proteins (MemGold2™ and Morpheus®). A three-drop 96-well plate setup was employed, where drop 1, 2, and 3 were at 1:1, 1:2, and 2:1 protein to crystallization solution ratio respectively with incubation at room temperature and monitoring over 34 days.

The drops were imaged at specified intervals during this period of time with optical imaging, along with UV-TPEF and SHG imaging. UV-TREF allows UV imaging of excited amino acids with aromatic residues (such as tryptophan) while minimising protein damage that can be used to identify protein crystals from salt crystals. SHG imaging allows the identification of chiral crystals that appear white against a black background and it is particularly useful in identifying microcrystals that would have otherwise been missed when for example heavy protein precipitation is seen.

Figure 43 shows representative examples of the different drops that were observed during this screening. Those varied from clear drops, where the protein is in solution (**panel A figure 43**) to protein precipitation of various degrees and morphologies (**panels B-F figure 43**).

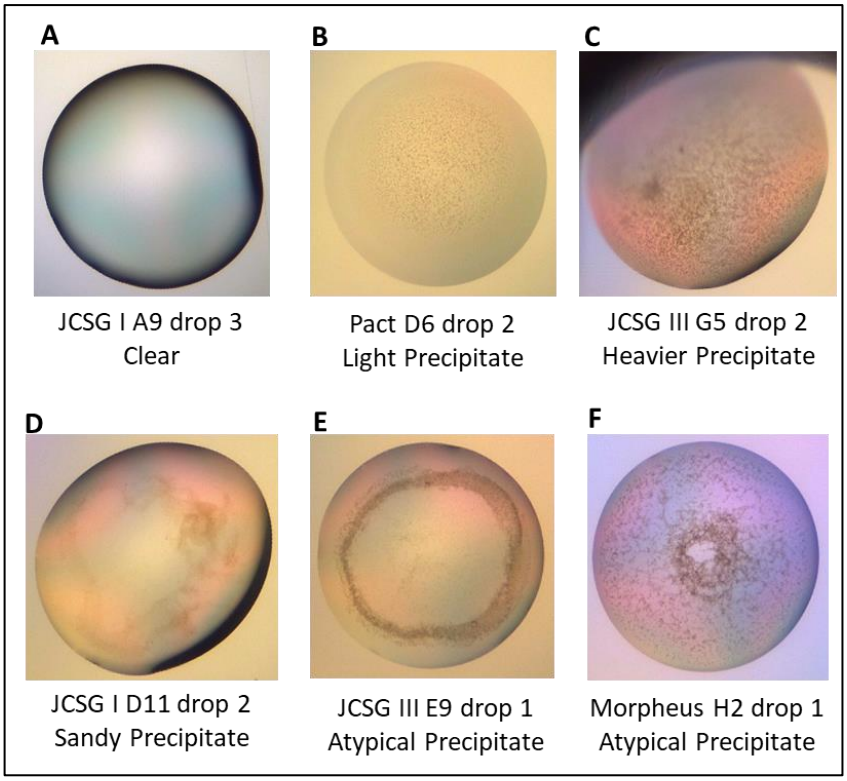

Figure 43: Representative images of the different types of drops that were observed during crystallization screening of $CymA_{sol}$.

The lower protein concentration that was employed was of initial concern in analysing the results of those trials. In order to gain a better understanding of the effect of this, all the drops of all the trials were analysed at the end of the incubation period. The drops were categorised into three groups: clear drops (C) as seen in **panel A of figure 43**, drops with precipitation (P) as seen in **panels B to F of figure 43**, and of blanks (where no drop was dispensed during the automatic liquid handling procedure). The results are summarised in **table 3**. The high accuracy and efficiency of the automatic liquid handling machine produced minimal blank wells with no drops (0-1% of the total drops per screen). The JCSG I, II, III, and IV screens had a ratio closer to 1:1 between clear drops and drops with protein precipitation, while the membrane protein-specific screens had a shifted ratio closer to 1:4. However, almost all of the drops (98%) in the Pact screen had protein precipitation of varying levels.

Table 3: Summary of the crystallisation results for $CymA_{sol}$. The counts of each drop per screen are shown, which were categorized as clear drops (C), drops with precipitation (P), and blanks (B) where no drops were dispensed by error. The total counts were converted into % total drops per screen.

Screen	JCSG I			JCSG II			JCSG III		
	C	P	B	C	P	B	C	P	B
Drop 1	45	50	1	31	64	1	43	53	0
Drop 2	18	78	0	28	66	2	28	66	2
Drop 3	40	55	1	49	47	0	54	42	0
Total	103	183	2	108	177	3	125	161	2
% Total	36%	64%	1%	38%	61%	1%	43%	56%	1%

Screen	JCSG IV			Pact			MemGold2		
	C	P	B	C	P	B	C	P	B
Drop 1	51	45	0	1	95	0	18	78	0
Drop 2	43	53	0	2	94	0	24	72	0
Drop 3	51	44	1	2	94	0	22	74	0
Total	145	142	1	5	283	0	64	224	0
% Total	50%	49%	0%	2%	98%	0%	22%	78%	0%

Screen	Morpheous		
	C	P	B
Drop 1	11	85	0
Drop 2	17	79	0
Drop 3	12	84	0
Total	40	248	0
% Total	14%	86%	0%

The rationale of this analysis stems from the principles of protein crystallisation during which both the protein and the precipitant concentration are important in having the protein arriving into the nucleation zone in order to promote its crystallisation. Undersaturated, seen as clear drops, and supersaturated material, seen as drops with heavy precipitation, sit at the two extremes of the precipitation spectrum and far from the nucleation zone (**figure 44**). As such, screens where the majority of the drops are clear or highly saturated would indicate that a change in the initial protein concentration is required before assaying the crystallisation conditions themselves or addressing protein regions with high disorder. Empirically a ratio of 1:1 or slightly shifted ratio towards precipitation of the number of drops within a particular screen is recognized as an acceptable ratio for crystallisation screening. Thus, although $CymA_{sol}$ was at 1 mg ml^{-1}, acceptable ratios of clear drops to drops with precipitation were observed for most of the screens, yielding a degree of confidence during these screens.

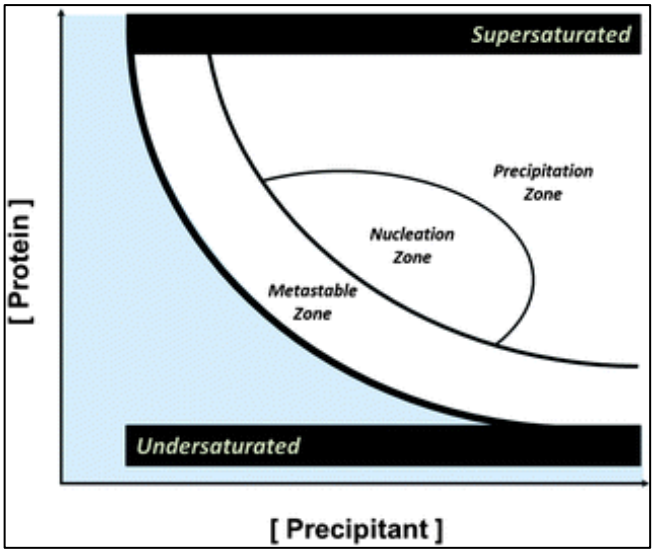

Figure 44: A schematic diagram of the different zones of protein state as a function of protein concentration versus precipitant concentration. In the undersaturated zone the protein is soluble and in solution, while at the other extreme in the supersaturated zone/ precipitation zone, most of the protein has precipitated out of solution. In the metastable zone, the protein may exhibit atypical precipitation to some degree, while in the nucleation zone, the protein if possible will start packing in a crystal lattice. The figure was reproduced with modifications from (105).

Overall, no crystals were obtained from those experiments. More specifically, no chiral crystals were observed with SHG imaging in any drop from any screen. However, some protein precipitation in patterns with observed "growth" was observed in some drops (**figure 45**) that showed UV absorption with UV-TREF imaging. Although they did not yield a crystal, those conditions (**table 4**) and/ or expansion around those conditions in future trials may prove fruitful.

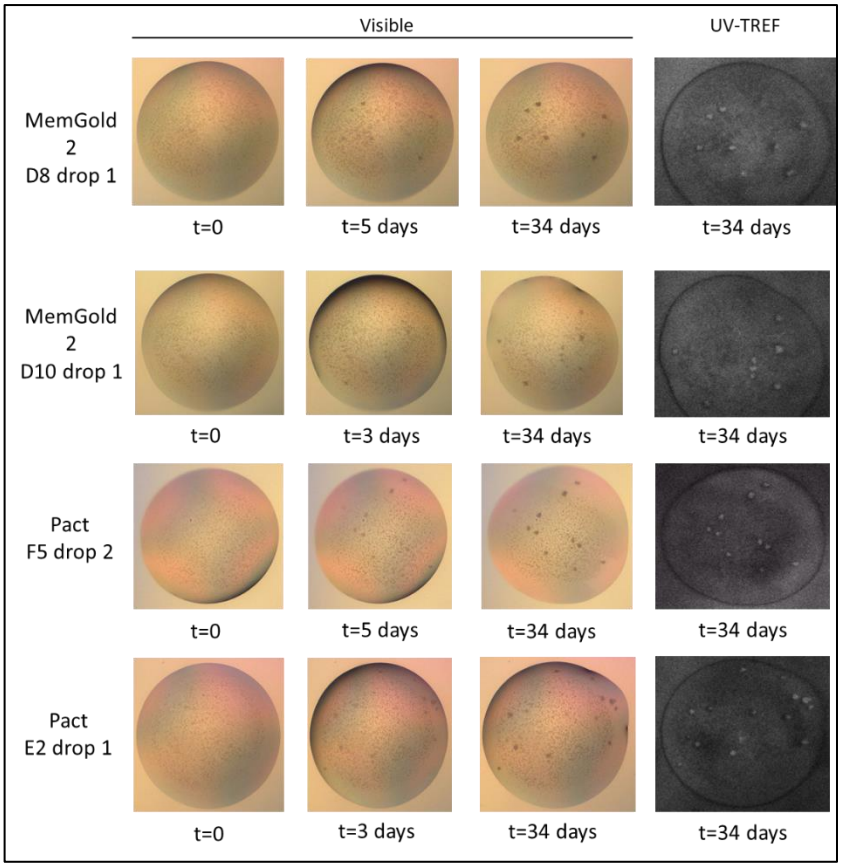

Figure 45: Drops with protein precipitation in patterns with positive UV-TREF imaging from the crystallisation screening of $CymA_{sol}$. The drops with atypical/ in pattern precipitation that grew overtime. Snapshots at time zero and at day 3 and day 34 were shown, along with the UV-TREF imaging at day 34.

Table 4: Composition of the crystallisation solutions. The solution composition and the protein to solution ratio of the drops from figure 41 that showed protein precipitation in patterns with positive UV-TREF imaging.

Screen	Position	Composition	protein to solution ratio
MemGold2	D8	0.2 M Magnesium formate dihydrate 0.5 M Tris pH 8.0 19% w/v PEG 3350	1:1
MemGold2	D10	0.2 M Ammonium nitrate 0.05 M HEPES pH 7.0 20% w/v PEG 3350	1:1
PACT Suite	F5	0.2 M Sodium nitrate 0.1 M bis-Tris propane pH 6.5 20% w/v PEG 3350	1:2
PACT Suite	E2	0.2 M Sodium fluoride 20% w/v PEG 3350	1:1

4.3 Conclusions

CymA is a distinct member of the NapC/NirT family of quinol dehydrogenases as in contrast to the majority of the members of this family CymA is not part of a multiprotein membrane complex. This does not come as a surprise, though, when the fact that it is able to interact with a number of different periplasmic proteins is taken into account. One can assume that the globular domain of CymA must be significantly structurally different. Thus, the elucidation of its crystal structure is hoped to shed some light into its mechanistic details of CymA, but it has been challenging due to the limitations in producing sufficient amounts of pure protein in a homogenous solution. Here, the first attempt to crystallise a soluble truncated version of CymA was presented, where 2,016 different conditions were assayed. The preliminary results of this crystallisation screening, although they have not been very fruitful, they have indicated a few conditions that could be of interest in the future. Notably, the same precipitant, 19-20% w/v PEG 3350, was found in all of the promising drops that showed atypical protein precipitation, along with 0.2 M of salt. Thus, it is likely that further screening closely around 20% w/v PEG 3350 may uncover the conditions necessary for crystallising CymA.

As part of this work, the heterologous expression and purification of this soluble truncated version of CymA was also presented. Although $CymA_{sol}$ has been used in previous studies (39, 88), it lacked a purification protocol and its purification has not been presented before, while its characterisation has been limited. The final output yield (~0.3 mg of untagged $CymA_{sol}$ per litre of culture) has been limited both in comparison with soluble proteins in general (tens to hundreds of mg per litter of culture) and even to CymA (~2 mg per litre of culture). The limitation lies on the TEV protease cleavage reaction. However, this could be overcome by a linker between the MBP and the proteolytic site in order to address occlusion of the site by the MBP tag. Also, a different protease that has improved activity in comparison to TEV (such as the HRV3C) could be tried. Lastly, an on-the-column proteolytic cleavage could also potentially be tested for improving the final output yield.

The crystallisation screening of soluble proteins is straight-forward, where the target protein is mixed with the different crystallisation solutions that screen

different conditions (at varying ratios), and dispensed in drops. In contrast, membrane proteins are more challenging to crystallise and it usually involves a pre-screening of different detergents and/or lipid mixtures. Because of this and of time constrains $CymA_{sol}$ was selected as a target. Nonetheless, purified CymA described herein could potentially yield a crystal, since it can be obtained at higher quantities.

Approaches involving the co-crystallisation of CymA or $CymA_{sol}$ with antibodies (106, 107) may help address flexible regions of increased disorder. Lastly, besides the standard approach of generating different constructs with varied truncations of CymA, an MBP fusion with the target protein has great potential for proteins that are resistant to crystallisation (108).

Chapter 5 – The evaluation of CymA: FccA interaction points to a weak transient nature of interaction

5.1 Introduction

The anaerobic respiratory system of *S. oneidensis* is comprised of a great number of different terminal reductases, as well as electron mediating proteins. This allows a metabolic versatility that is unique to *Shewanella* species by the utilisation of different anaerobic pathways based on the availability of terminal electron acceptors in the environment. CymA is a central pillar of the exhibited versatility by acting as an electron distribution hub from the inner membrane quinone pool, where it is located, to a plethora of periplasmic proteins. The promiscuity of CymA maintains the electron flow and, by extension, contributes to the maintenance of the proton gradient for ATP synthesis. As such, the interactome of CymA has been of particular research interest in advancing our understanding with respect to the mechanistic details that allow specific protein-protein interactions to take place for the large number of its identified partners, and the factors that regulate those.

Protein – protein interactions in nature are divided into permanent and transient ones with K_D in the nano- and micromolar range respectively. Transient protein complexes are further subdivided into weak and strong; a strong transient protein complex describes a protein complex that is strongly bound only when it is triggered by, for instance, the binding of its substrate. Overall, features, such as residue conservation (109, 110), the lever of surface planarity (111), and the level of disorder (flexible regions) (112) distinctly define the protein – protein interfaces from the rest of the protein. Specifically, since transiently interacting proteins need to remain soluble when they are dissociated, they are often comprised of a mixture of polar and non-polar residues that are solvent exposed (113). In contrast, strongly interacting proteins that form permanent protein complexes have very hydrophobic residues on their interface (113). Moreover, the interface of permanent protein complexes are larger than weak transient complexes and do not involve electrostatic interactions to the extend that the proteins that interact transiently do (114). It must be noted, though, that sometimes a protein may exhibit

features from both groups (permanent complexes and weak transient complexes) and can, thus, be difficult to categorise it based on those parameters alone.

The periplasmic fumarate reductase FccA of *S. oneidensis* is necessary for the terminal reduction of fumarate to succinate via CymA. However, the nature of FccA: CymA interaction has recently come under intense debate due to contradicting evidence of two published research articles (87, 88). On the one hand, CymA and FccA in purified form were studied by NMR *in vitro* in solution. From these studies, their K_D was determined at ~0.4 mM (87), which since $K_D = K_{off} / K_{on}$, this high K_D implies that CymA and FccA interact transiently through weak interactions (high K_{off}). However, it must be noted that those experiments were conducted in the absence of DDM detergent, which was used for the purification of CymA. Thus, DDM detergent was introduced into the experiment during protein titration and its contribution, or lack of, to the observations or to the determined K_D has not been shown.

On the other hand, purified CymA, $CymA_{sol}$, and FccA were studied by cyclic voltammetry, an electrochemical method, and by QCM-D monitoring (88). In both of those approaches, a lipid bilayer membrane system with reconstituted CymA was employed in order to mimic the native environment of CymA. For cyclic voltammetry, the lipid bilayer membrane, which contained menaquinone in order to support catalysis, was tethered to the surface of the electrode by cholesterol tethers, while for QCM-D the lipid bilayer membrane was solid supported on the surface of the quartz crystal. Regarding $CymA_{sol}$, the same lipid bilayer membrane systems were employed, but with $CymA_{sol}$ adsorbed on the surface of the membrane. Reductive catalytic waves were obtained by cyclic voltammetry when FccA with fumarate were introduced. However, the onset of the catalytic wave did not coincide with the onset of the non-turnover reductive menaquinone signal. In order to address this, the competitive inhibitor of CymA, HQNO, was employed, which diminished the observed catalytic signal. However, HQNO was dissolved in DMSO, which is detrimental to protein stability (115, 116). The lack of a control experiment with only DMSO and the fact that competitive inhibition was not observed raise questions around this line of experimentation. The QCM-D binding studies showed binding of FccA in the presence of fumarate to the CymA-

reconstituted lipid bilayer membrane, which was retained during a subsequent washing step. The quantification of the bound FccA (as seen as mass deposition) could not be explained stoichiometrically (88). Thus, the authors argued in support of the formation of a long-lived stable complex between CymA and FccA (88). Those binding studies, though, are limited in scope without investigating the binding kinetics that could have also served as a way of explaining the deposited mass (the observed binding event). Overall, their proposed model of interaction comes in direct contradiction to the previously described NMR studies.

Having designed a new CymA construct with no C-terminal tags that could interfere in protein-protein interactions experiments, and developed a reproducible purification strategy, this controversy surrounding the nature of FccA: CymA interaction was investigated. The initial aim was to employ the same systems of the second paper described above in further probing those observations with the ultimate goal to map any contributing factors that may regulate a potential FccA: CymA complex formation. As such, this chapter begins with the purification and characterization of native FccA from *S. oneidensis*, in order to validate the quality and activity of all the purified proteins that were used. The ability of those two proteins to interact was then validated in vitro by a biochemical spectroscopic assay. Subsequently, cyclic voltammetry and QCM-D were employed, which did not show any catalytic or binding events that could be attributed to FccA. Moreover, the systems themselves were further investigated providing explanations of the obtained data, before validating their conclusions by isothermal titration calorimetry.

5.2 Results

5.2.1 Expression, purification, and characterisation of native FccA

S. oneidensis MR-1 was grown in 5L Duran bottles anaerobically in LB medium that was supplemented with fumarate, which promoted the expression of FccA. The way this was achieved was by incubating fully filled 5L Duran bottles at 30 °C with no agitation for 24 h. Although this was not resulted in a strictly anoxic environment, it takes advantage of the metabolic versatility of *S. oneidensis*, along with the limited oxygen diffusion. The cells, therefore, start growing by using the readily available dissolved oxygen in the medium first until the level of which significantly drops. At that point, the cells switch to using fumarate as the terminal electron acceptor in order to promote their growth, since fumarate is at much higher levels than the limited dissolved oxygen and by extension promotes the survival of the organism.

Native FccA was then purified from the isolated soluble periplasmic fraction of the harvested cells. Initially, the periplasmic proteins were fractionated by IEC (**figure 46**). FccA was eluted at around 120 mM NaCl, which was identified by SDS-PAGE from the molecular mass, along with confirmation from haem staining of the gel (**figure 47**).

The pooled fractions from the IEC were subjected to 50% ammonium sulphate fractionation to reduce the contaminating proteins, before it was polished with a S200 size exclusion chromatographic step (**figure 48**). The final purified native FccA was of >95% purity, determined by SDS-PAGE. The electrophoretic profile of FccA post high-salt fractionation and of the final FccA are shown in **figure 49**.

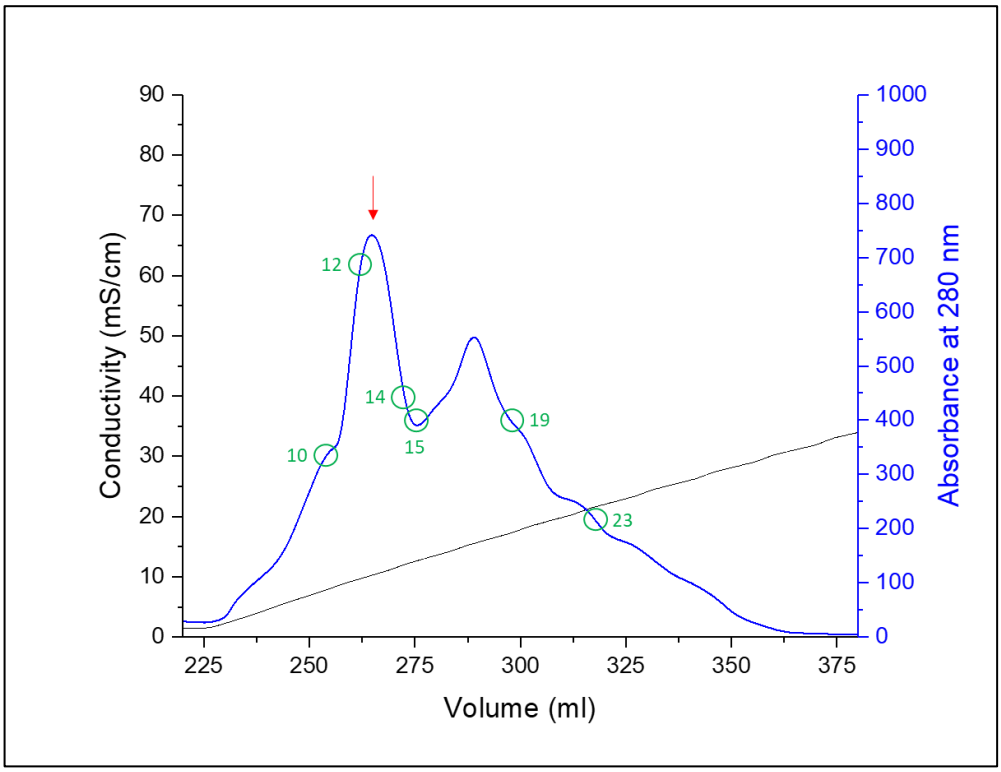

Figure 46: Ion exchange chromatographic purification profile of the elution over a gradient of NaCl from the periplasmic fraction of *S.oneidensis* MR-1 grown anaerobically with fumarate for FccA purification. The chromatography was performed with ÄKTA pure 25 at 4 °C with a flow rate of 1 ml min^{-1} in 20 mM Tris-HCl pH 8.0 with a gradient of NaCl concentration. The red arrow indicates the point of FccA elution and the green numbered circles indicate the fractions that were analysed by SDS-PAGE (**figure 46**).

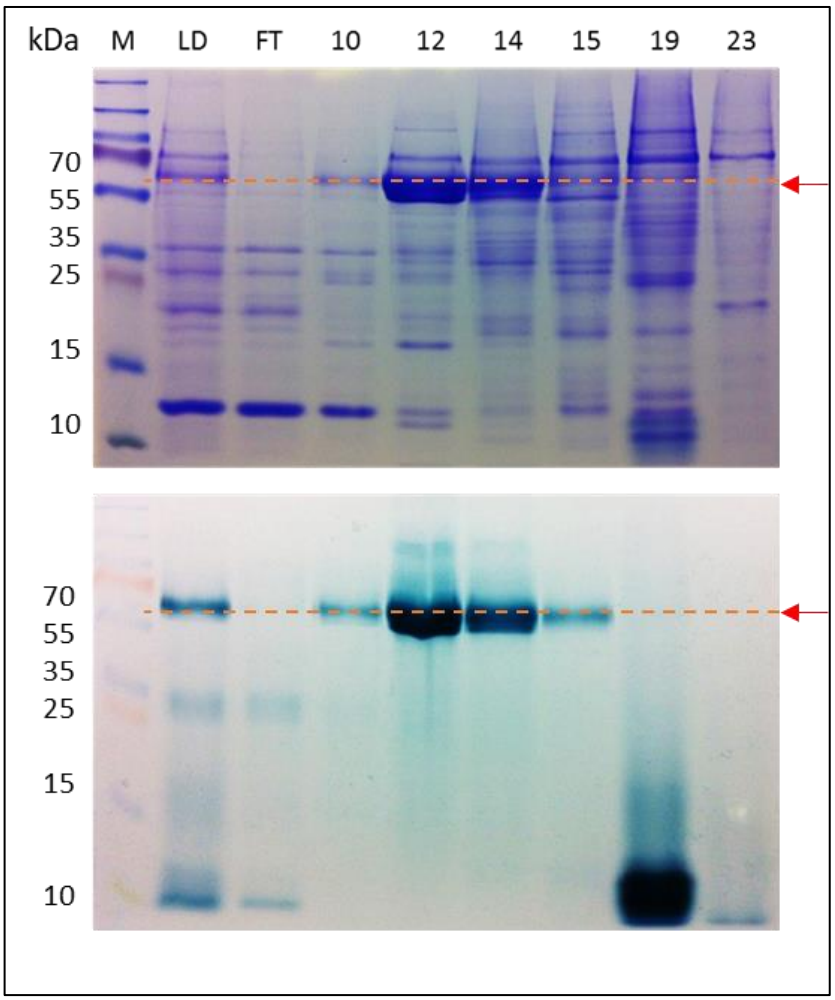

Figure 47 Ion exchange electrophoretic purification profile from the periplasmic fraction of *S. oneidensis* MR-1 grown anaerobically with fumarate for FccA purification. 15% SDS-PAGE stained with Coomassie stain (top gel) or c-type haem staining (bottom gel). M: molecular mass protein markers; LD: column load; FT: flow-through during column loading; 10, 12, 14, 15, 19, 23 eluting fractions corresponding to the chromatographic profile in figure 45.

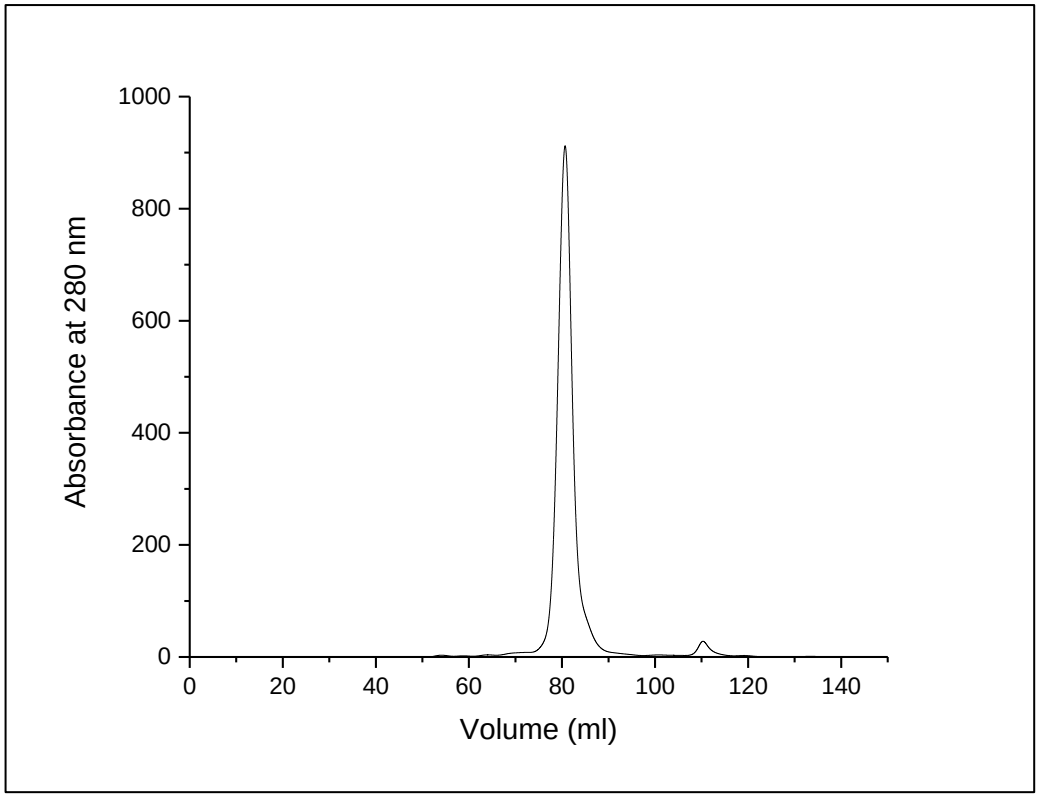

Figure 48: Size exclusion chromatographic profile of FccA with HiLoad 16/600 Superdex 200 prep-grade column. The void volume (V_o) is 45 ml. The chromatography was performed with ÄKTA pure 25 at 4 °C with a flow rate of 0.5 ml min^{-1}. The buffer composition was 20 mM HEPES pH 7.5, 150 mM NaCl.

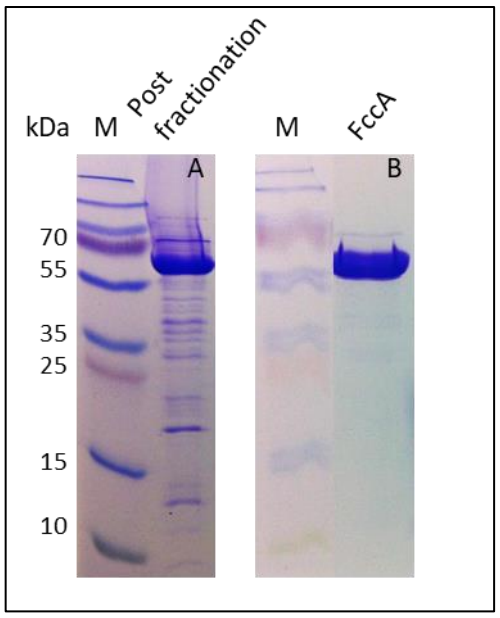

Figure 49: Electrophoretic profile of FccA after fractionation (A) and after size exclusion chromatography (B). 15% SDS-PAGE stained with Coomassie stain. M: molecular mass markers.

Purified native FccA was analysed spectrophotometrically and the obtained UV-visible (λ = 250 nm – 700 nm) absorbance spectra of oxidised and reduced FccA are shown in **figure 50**. The spectrum of the oxidised FccA resolved a broad shoulder between 500 nm and 600 nm and a peak at 409 nm that corresponds to the Soret γ-band of light absorption by the haems. The spectrum of reduced FccA showed the resolution of the Soret α- and β- bands at 551 nm and 523 nm respectively, while the Soret γ-band shifted to 420 nm.

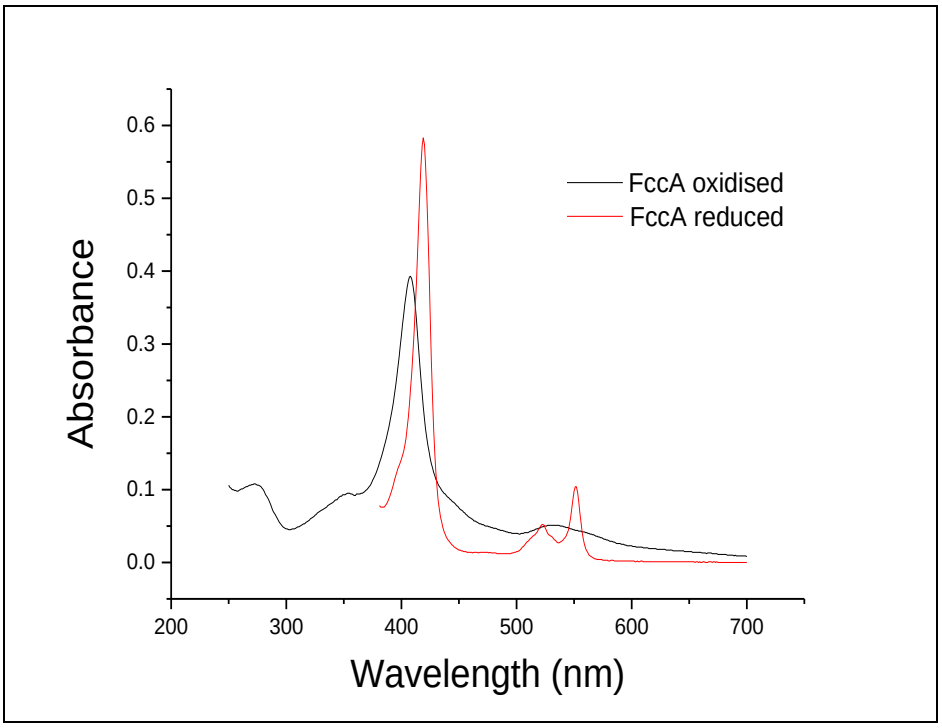

Figure 50: UV-visible absorbance spectra of oxidised and reduced purified native FccA. Measurements were conducted at ambient conditions in 20 mM HEPES pH 7.5 and 150 mM NaCl. The spectra are baseline corrected. The spectrum of fully reduced FccA was obtained by addition of excess of dithionite.

Protein film electrochemistry was employed to assess the electrical properties of purified native FccA, as well as to validate its catalytic activity with electrochemical methods. The non-turnover signals and subsequent reductive catalytic wave of significant magnitude upon addition of 1 mM fumarate in solution are shown in **figure 51**. Thus, native FccA was highly pure and catalytically active.

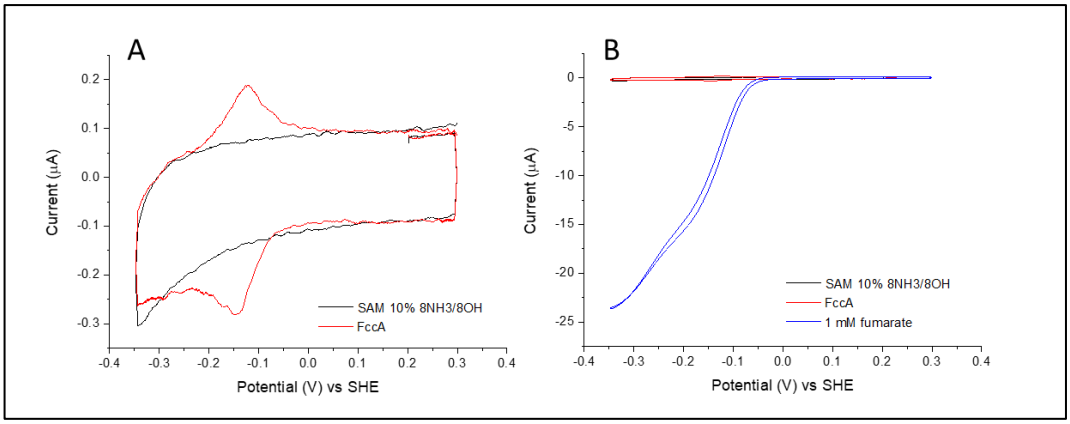

Figure 51: Cyclic voltammetry of FccA protein film resolving (A) non-turnover and (B) turnover signals upon addition of 1 mM fumarate in solution. SAM: 1:10 NH^{3+}/OH^{-} thiol self-assembled monolayer. FccA film: adsorbed $CymA_{sol}$ protein film after removing excess of $CymA_{sol}$ by three buffer washes. The measurements were performed under a nitrogen atmosphere ($0_2 \leq 0.1$ ppm) at ambient conditions and at a scan rate of 10 mV s^{-1}. The buffer composition was 20 mM MOPS pH 7.4 and 30 mM Na_2SO_4.

5.2.2 CymA† and FccA are able to interact *in vitro*

The initial question was whether CymA† and FccA were able to interact with each other. In order to address this, a biochemical assay was employed which couples the oxidation of NADH to menadione reduction by the diaphorase from *Clostridium kluyveri* to the sequential reduction of CymA, FccA, and ultimately fumarate to succinate (schematically depicted in **figure 52**). In this spectrophometrically based assay the amount of NADH was monitored at 340 nm over time. The assay was performed under anoxic conditions in the presence of DDM at room temperature. The assay buffer was 20 mM Hepes pH 7, 0.5 mM EDTA, 0.05% DDM. CymA† and FccA were at a final concentration of 1 µM, fumarate at 1 mM, NADH at 100 µM, menadione at ~10 µM (a more polar analogue of menaquinone), and diaphorase was in excess at 3 µM.

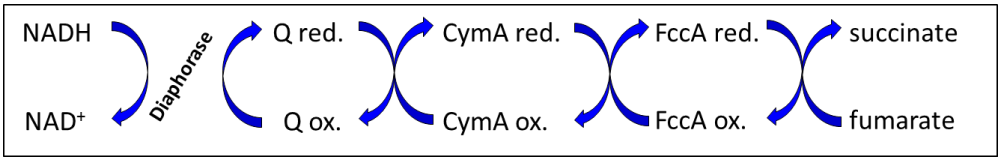

Figure 52: Diagram of the diaphorase assay. The sequential reduction (flow of electrons) is shown of the individual components that comprise this assay. Diaphorase initiates the reaction by oxidizing NADH and reducing menadione (Q), which in turn reduces CymA, and then FccA via CymA, which catalyses the terminal reduction of fumarate to succinate.

A steady drop in absorbance at 340 nm upon addition of diaphorase, which initiates the reaction by the coupled NADH oxidation and menadione reduction, was observed with an initial rate of 3.3 (±0.3, n=3) µM NADH oxidised min^{-1} (a represenative trace is shown in **panel B figure 53**). As a control, CymA† was eliminated and no change in the absorbance at 340 nm was observed (represenative trace is shown in **panel A figure 53**). Furthermore, in order to verify the necessity of CymA† in the observed change of measured signal, a further experiment was conducted, where the CymA† was added last (representative trace is shown in **panel C figure 53**). This addition of CymA† re-established a change overtime of NADH oxidation. Thus, CymA† is able to interact *in vitro* under those conditions with FccA and it is necessary for the sequential FccA-specific reduction of fumarate.

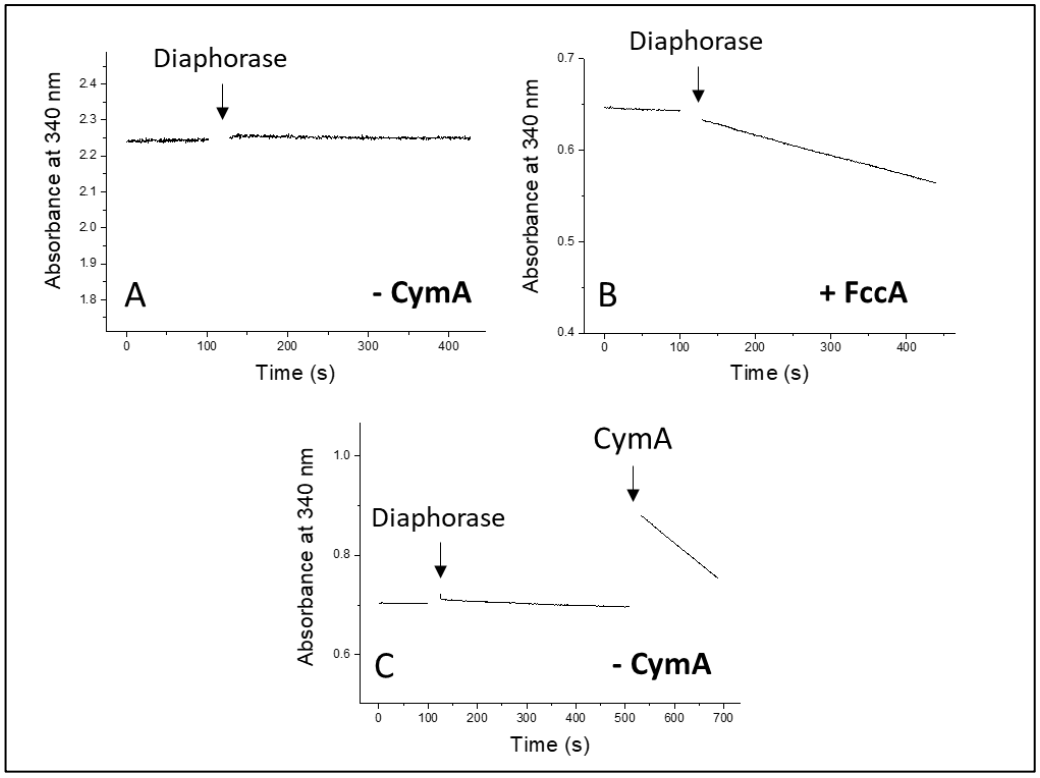

Figure 53: Diaphorase assay traces (absorbance at 340 nm overtime), where CymA is necessary and required for the specific reduction of FccA via CymA. The assay consisted of 1 µM FccA and CymA, 100 µM NADH, 3 µM diaphorase, 10 µM menadione, and 1 mM fumarate. The assay buffer was 20 mM HEPES pH 7.0, 0.5 mM EDTA, 0.05% w/v DDM. The assay was performed under anoxic conditions at room temperature.

5.2.3 Binding of FccA to a CymA†-ssBLM system is not observed during QCM-D measurements

Having established that CymA and FccA are able to interact *in vitro*, the surface sensitive technique of QCM-D was employed in order to investigate further the nature of their interaction. That is, it is employed as a mass sensor that is able to monitor in real time without the need of labelling the association and dissociation of molecules on its surface with a reported sensitive of 0.5 ng cm^{-2}. QCM-D is comprised of a quartz crystal sandwiched between two electrodes, whose surface can be coated with various materials to suit a wide range of applications. The quartz crystal, upon application of an alternating current, oscillates at its resonance frequency. When the application of the current is stopped, the oscillation decays exponentially while any changes in its resonance frequency and in its energy dissipation (the loss of energy per period from the total energy of the system) are displayed. Mass

measurements can then be made by using the Sauerbrey equation that links the change in frequency (Δf) to the change in mass (Δm): $\Delta f = - C_f \cdot \Delta m$, where C_f is the sensitivity factor of the crystal that is used. Change in the dissociation (ΔD) is linked with the softness of the material/solution on the surface of the crystal.

In the experiments described in this thesis a silicon oxide quartz crystal is used in order to promote the rupture of liposomes or proteoliposomes of CymA and the spontaneous assembly of a solid-supported lipid bilayer. As such, CymA in an artificial lipid bilayer environment that mimics its native environment can be used to investigate the association of FccA, when FccA is in a continuous slow flow in a buffer solution over the bilayer. All the measurements were conducted at room temperature.

CymA†-proteoliposomes of 10% w/w CL/POPC were employed since that lipid mixture was previously used in obtaining what was reported as FccA binding, although the authors could not ascribe the binding stoichiometry from mass calculations (88). Thus, initially, this replication attempt of those data would have served as the basis for further characterizing the FccA binding to CymA and later be extended to investigate unpublished observations of the necessity of fumarate in promoting FccA: CymA binding. However, extensive experimentation with this system by QCM-D monitoring, did not produce any evidence of FccA association that would have been observed as a shift in Δf (representative trace is shown in **figure 54**). Same traces of no FccA association were obtained in the presence or absence of fumarate, when FccA concentration was doubled, and when FccA was incubated in situ (by stopping the continuous flow of solution). Taking into account that (1) a stoichiometry could not be ascribed, and (2) the lack of kinetic information of the association and dissociation events, the published traces of FccA binding could be explained as a non-specific binding event. This non-specific binding could further be explained by either a contaminating protein in the FccA production, where the non-specific binding of the contaminant to the lipids most likely mediated electrostatically. Or of the formation of a non-uniform solid supported lipid bilayer that would have been resulted in areas of solvent exposed silicon oxide crystal surface, where FccA would bind to the surface non-specifically.

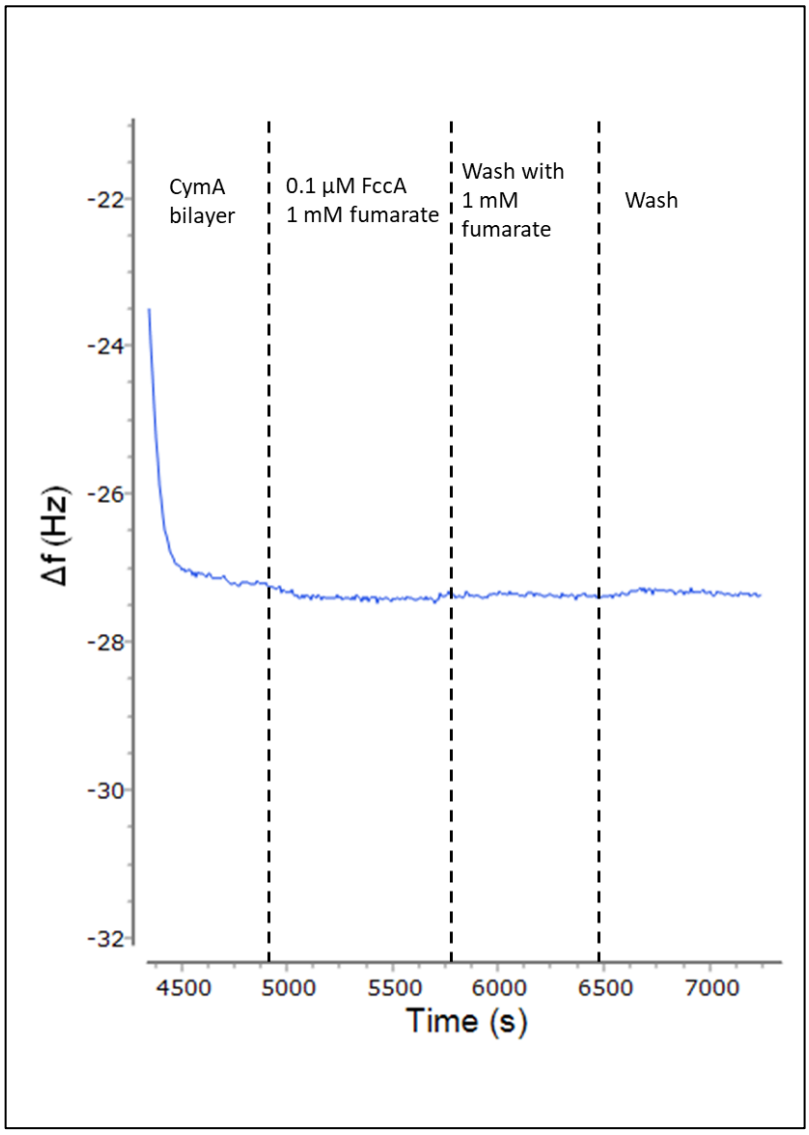

Figure 54: QCM-D binding experiment with CymA 10% w/w CL/POPC solid supported lipid bilayer membrane and FccA in solution in the presence of 1 mM fumarate, where no association of FccA is observed. The experiment was conducted at room temperature. The wash buffer composition was 20 mM MOPS pH 7.4 and 30 mM Na_2SO_4.

5.2.4 Electrochemical investigations in a tBLM system and with FccA does not resolve catalytic activity

A tethered bilayer lipid membrane (tBLM) system was used in order to electrochemically investigate the CymA:FccA interaction. A tBLM system employs thiol-terminated cholesterol tethers in a mixture of thiols to modify the surface of a gold electrode. Liposomes are then incubated *in situ* in the

presence of calcium chloride, where spontaneously ruptured and formed a suspended bilayer lipid membrane. Calcium chloride is usually required when charged lipids are used, where it screens their surface charge and by extension promotes their aggregation onto the surface of the modified electrode. The percentage of the cholesterol tethers on the surface is also important in allowing sufficient space between the electrode and the lipid bilayer membrane in order to accommodate the liposome-reconstituted membrane proteins.

CymA was reconstituted in liposomes containing menaquinone-7 (MQ7), its substrate. The tBLM is electrochemically linked to the MQ7 in the bilayer, where under non-turnover conditions the oxidation and the reduction of MQ7 is observed as the voltage is cycled through the varying potentials. Previously reported data showed a reductive wave of the MQ7 reduction using the same system upon addition of FccA in the presence of fumarate (88). Generally, during catalysis, the oxidation peak of MQ7 disappears, as all MQ7 molecules are oxidised by CymA and the reduction peak of MQ7 appears as a catalytic wave. That is, as the electrode reduces MQ7 it is concurrently being oxidised by CymA. Thus, it provides indirectly evidence of the terminal fumarate reduction by FccA via CymA. All of the electrochemical investigations reported in this thesis were conducted at room temperature under anoxic conditions (in a N_2 atmosphere inside a glovebox).

10% w/w CL/POPC CymA†-tBLM and FccA

Initially, CymA† was reconstituted in 10% w/w CL/POPC and used to form a tBLM on the surface of a modified electrode in a replication attempt of the previously reported data under the published conditions (88). This would have formed the basis for further probing the system in gaining a more detailed understanding of the nature of CymA: FccA interactions during catalysis. However, upon extensive investigation (a representative trace is shown in **figure 55**) no evidence of catalytic activity was observed. The amount of CymA was doubled during reconstitution in order to address potential limitations in the available CymA with the correct orientation on the tBLM, as well as lowering the pH to 6 in order to further resemble the pH at the periplasmic space of *S. oneidensis*, although the later can very slightly in

nature. In order to understand this controversy in obtained data from the published data the system was further explored.

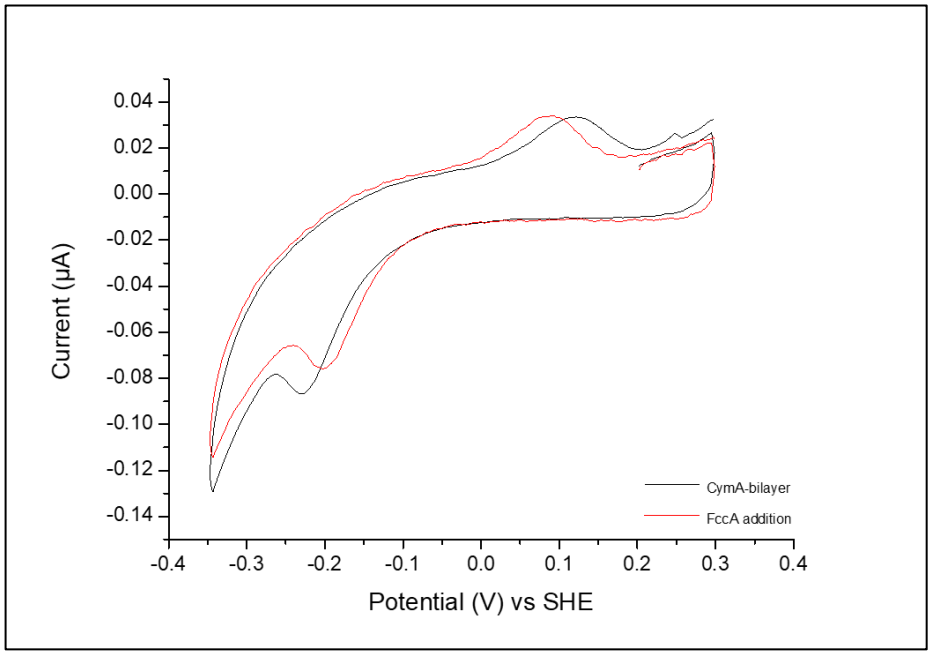

Figure 55: Representative trace of cyclic voltammetry of CymA 10% CL/POPC tBLM and addition of 1 μM FccA in the presence of 1 mM fumarate, where no catalysis is observed. SAM: 6-mercaptohexanol/ EO_3C. The measurements were performed under a nitrogen atmosphere ($0_2 \leq 0.1$ ppm) at ambient conditions and at a scan rate of 10 mV s^{-1}. The buffer composition was 20 mM MOPS pH 7.4 and 30 mM Na_2SO_4.

E. coli polar lipids CymA†-tBLM and FccA

E. coli polar lipids were employed to replace the CL/POPC under the rationale that the former would resemble more the native lipid composition of *S. oneidensis* in case protein: lipid interactions may be a contributing factor in vivo. The increased amount of CymA reconstituted was maintained, and both pH 7.4 and pH 6 were tested along with increasing concentration of FccA. However, none of which provided any evidence of catalysis either (representative traces are shown in **panel A figure 56**). The rate of the cycling voltage was also lowered to 1 mV/s in order to allow more time at any given potential in order to address the possibility of a slow reaction. No evidence of catalysis was obtained either (representative trace is shown in **panel B figure 56**). Considering that neither QCM-D nor electrochemical methods provided evidence of interaction between CymA and FccA, a new hypothesis was

formed, which was based on an impure FccA sample. Should an impure FccA sample was used previously (88), then a missing protein that would have been unknowingly present in that sample may be part of the fumarate reduction anaerobic pathway.

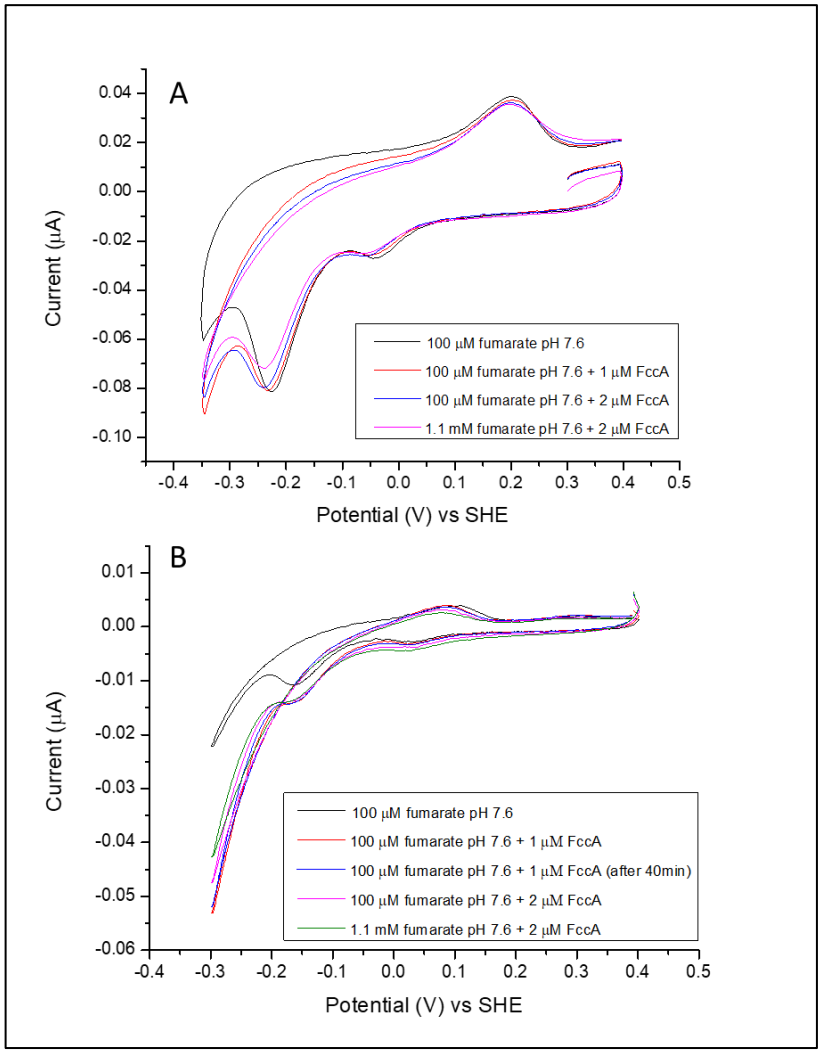

Figure 56: Representative trace of cyclic voltammetry of CymA *E. coli* polar lipids tBLM and addition of FccA in the presence of 1 mM fumarate, where no catalysis is observed. SAM: 6-mercaptohexanol/ EO_3C. The measurements were performed under a nitrogen atmosphere ($0_2 \leq 0.1$ ppm) at ambient conditions and at a scan rate of (A) 10 mV s^{-1}, and (B) 1 mV s^{-1}. The buffer composition was 20 mM MOPS pH 7.4 and 30 mM Na_2SO_4. The coloured lines in the key indicate the final solution concentrations of fumarate and FccA. The same CymA-containing tBLM was used for each set of measurements.

E.coli polar lipids CymA†-tBLM and periplasmic proteins from S. oneidensis

In testing the new hypothesis of a missing component from the FccA-specific fumarate reduction via CymA, the periplasmic proteins of anaerobically grown *S. oneidensis* MR-1 with fumarate (as described for FccA purification) was isolated. The electrophoretic profile is shown in **figure 57**, where FccA is estimated to be 20-30% present of the total proteins (**panel A figure 57**). Moreover, fumarate reductase activity of the isolated periplasmic proteins was verified by methyl-viologen assay (raw data are presented in **panel B figure 57**). Having established that both FccA was present and that the sample exhibited fumarate reductase activity, it was used in a tBLM system of reconstituted CymA in *E. coli* polar lipids at ~1 mg ml^{-1}. However, those conditions also did not provide any evidence of catalysis. A representative trace is shown in **figure 58**, where only a minor shift in the redox peaks of MQ7 is observed. This shift is due to a pH difference between the buffer and the sample which alters the redox potentials of MQ7. Thus, an investigation was prompted into the system that could explain both the previously obtained traces that had been interpreted as catalysis (88), and the lack of evidence for catalysis under a great number of different conditions that were presented here.

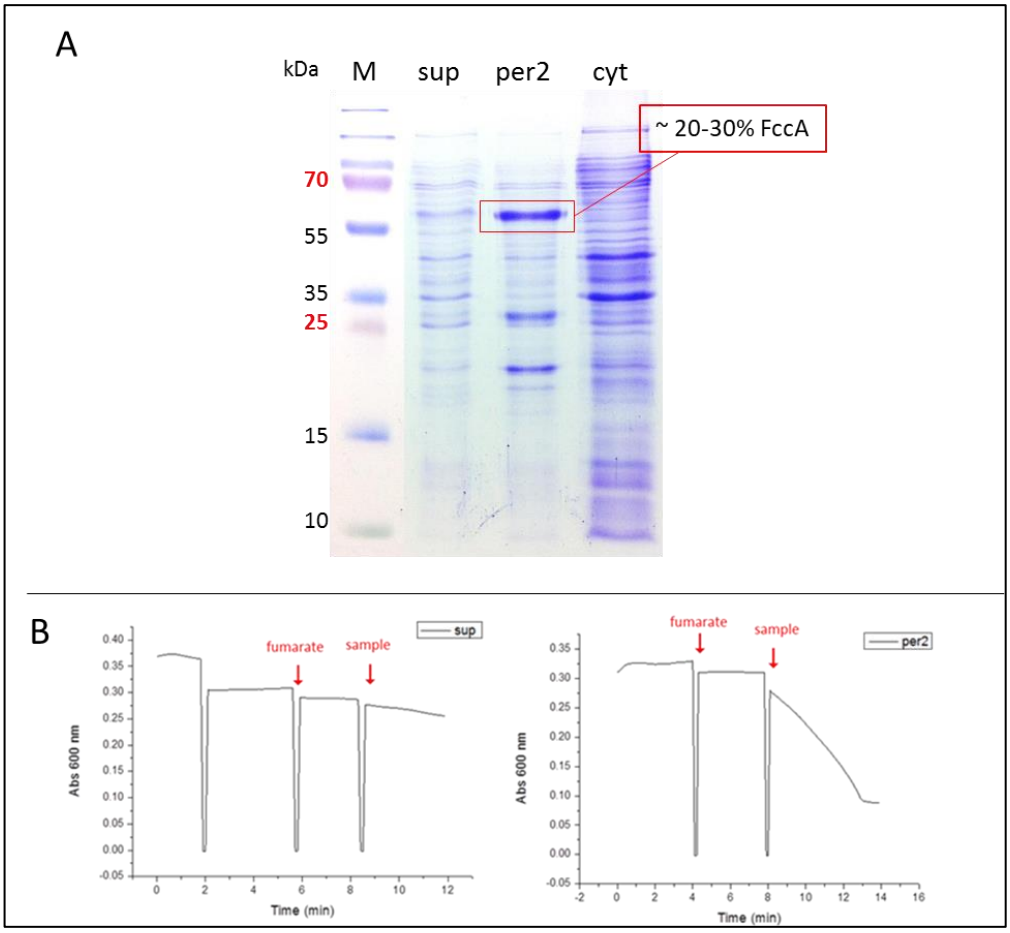

Figure 57: Isolation of periplasmic globular proteins from anaerobically grown *S. oneidensis* MR-1 in the presence of fumarate with fumarate reductase activity. A. Coomassie-stained SDS-PAGE of the fraction 1 (sup) and 2 (per2) of the soluble components of the periplasm, as well as the cytoplasmic fraction (cyt). The FccA was visually estimated from this gel to be between 20-30%. **B.** Methyl-viologen assay for fumarate reductase activity of the two fractions. The second fraction (per2) was used in electrochemical experiments.

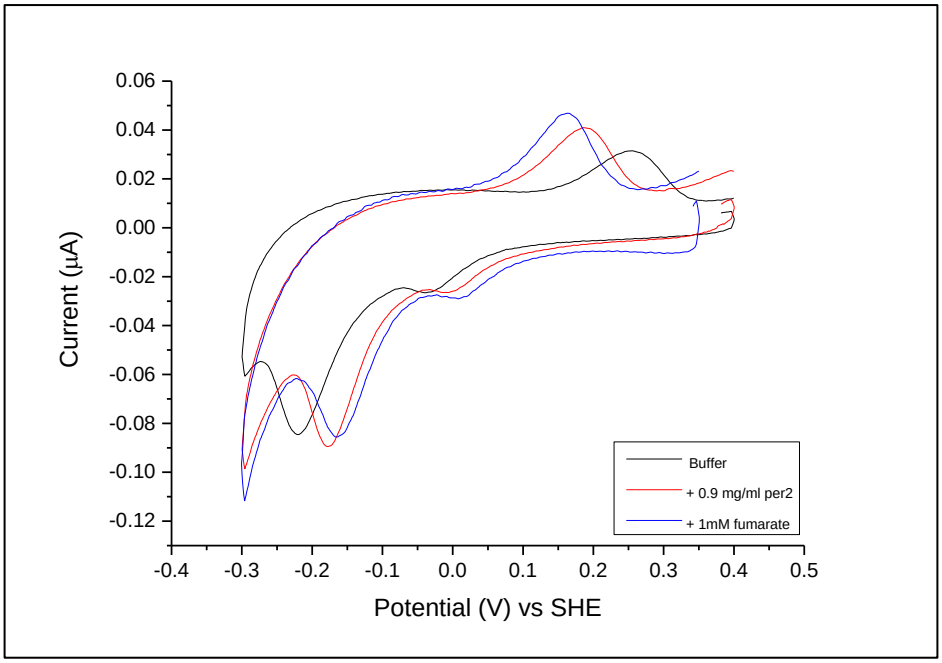

Figure 58: Representative trace of cyclic voltammetry of CymA *E. coli* polar lipids tBLM and addition of periplasmic proteins from *S. oneidensis* MR-1 anaerobically grown with fumarate, where no catalysis is observed. SAM: 6-mercaptohexanol/ EO_3C. The measurements were performed under a nitrogen atmosphere (0_2 ≤ 0.1 ppm) at ambient conditions and at a scan rate of 10 mV s^{-1}. The buffer composition was 20 mM MOPS pH 7.4 and 30 mM Na_2SO_4.

5.2.5 The effect of oxygen in a CymA†-tBLM system during electrochemical investigations

The investigation of the system was further guided by a closer inspection of the published data (88), where the onset of the reported catalysis (~ 0 V) did not coincide with the onset of MQ7 reduction. This is important as it would imply that electrons do not flow through MQ7, but it is a different redox reaction that is occurring on the electrode. This resulted in investigating the effect of dissolved oxygen in a CymA†-tBLM. More specifically, two questions have arisen: (1) what would the impact of dissolved oxygen be? And (2) whether oxygen could accumulate in the electrochemical cell during cyclic voltammetry?

When dissolved oxygen was introduced at 27 µM concentration, a reductive catalytic wave was observed of significant magnitude and with an onset at around ~ 0 V (**panel A figure 59**). Moreover, the oxidation peak of MQ7 disappeared, in effect replicating the published data (88) (**panel A figure 59**). The magnitude of the reductive catalytic current was increased when the

concentration of dissolved oxygen increased, and persisted when cyclic voltammetric measurements were taken after 15 min and 30 min (**panel B figure 59**). Nonetheless, it is more likely that other factors, along with oxygen, may have contributed in obtaining the published data than oxygen alone. However, this explains to a degree the controversy.

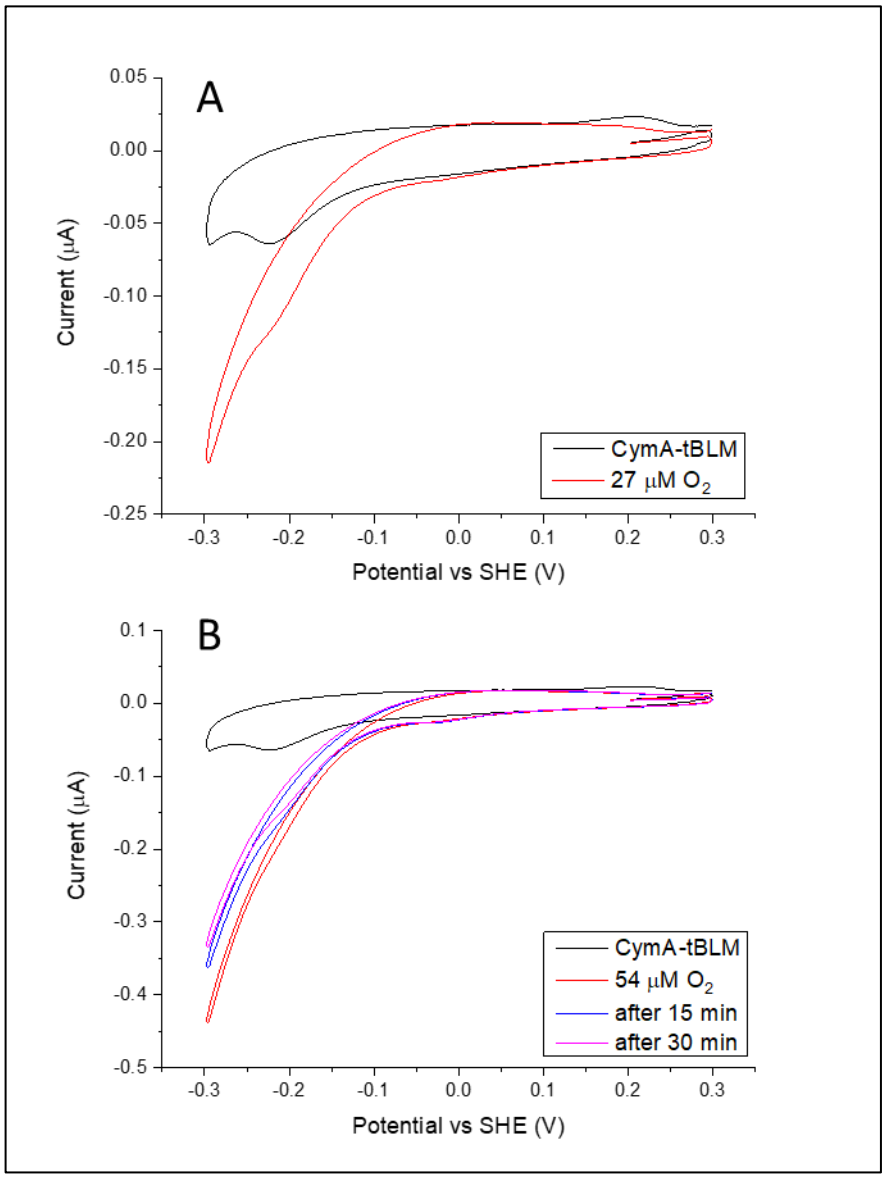

Figure 59: Cyclic voltammetry of CymA *E. coli* polar lipids tBLM and addition of small volumes of air-equilibrated buffer, where (A) a reductive wave is observed that (B) persists overtime. SAM: 6-mercaptohexanol/ EO_3C. The measurements were performed under a nitrogen atmosphere ($0_2 \leq 0.1$ ppm) at ambient conditions and at a scan rate of 10 mV s^{-1}. The buffer composition was 20 mM MOPS pH 7.4 and 30 mM Na_2SO_4. Red lines: air-equilibrated buffer was added to the shown final concentration of dissolved oxygen. Blue and magenta lines are the measurements after 15 min and 30 min respectively inside the glovebox (N_2 atmosphere) without changing the solution.

5.2.6 The influence of bilayer membrane surface charge in the adsorption of $CymA_{sol}$

$CymA_{sol}$ was previously used both in investigations of the FccA: CymA interaction both by electrochemical methods and by QCM-D measurements (88), which could not be replicated under the published conditions. As such, an investigation into that system was necessary in understanding this controversy. This investigation was guided by observations during $CymA_{sol}$ production, where, as mentioned before, the whole or truncated construct (6xHisMBPCymA_{sol} or 6xHisMBP respectively) could escape in the flowthrough, along with the untagged $CymA_{sol}$, during reverse affinity chromatography after the TEV proteolytic cleavage reaction. Hence, the whole construct was purified at around 90% purity (**figure 60**).

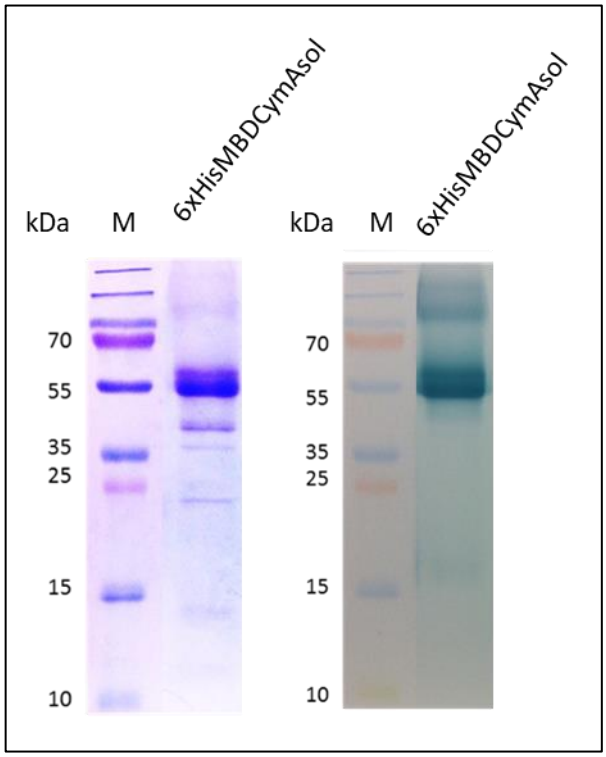

Figure 60: Electrophoretic profile of purified 6xHisMBPCymAsol whole construct. 15% SDS-PAGE stained with Coomassie stain (left gel) and c-type haem staining (right). M: molecular mass protein markers.

The rationale was to investigate the electrostatic non-specific binding of either pure $CymA_{sol}$ or of the whole construct (and by the process of elimination the 6xHisMBP component of the construct) on three different lipid bilayers: POPC that is neutral at physiological pH, mixture with DOTAP that is positively charged at physiological pH, or mixture with CL that is negatively charged at physiological pH. Strong binding of the whole construct was observed to negatively charged lipid bilayer by QCM-D (**panel B figure 61**) and not to either neutral or to a positively charged one (**panels A and C figure 61**).

On the other hand, pure $CymA_{sol}$ binding was observed to a positively charged lipid bilayer (**panel F figure 61**) and not to either a neutral or to a negatively charged one (**panels D and E figure 61**). Incidentally, the conditions that have been previously used in the published data (88) were of those where binding of the whole construct is observed and not of pure $CymA_{sol}$.

Thus, any electrochemical or binding data that had been previously obtained with $CymA_{sol}$ could not be attributed to $CymA_{sol}$. That is, the whole construct and more specifically the presence of the 42 kDa MBP occludes the binding site of $CymA_{sol}$ rendering it catalytically inactive. Moreover, the evidence presented here can also provide some explanation of the non-specific nature of binding that was previously observed during QCM-D measurements.

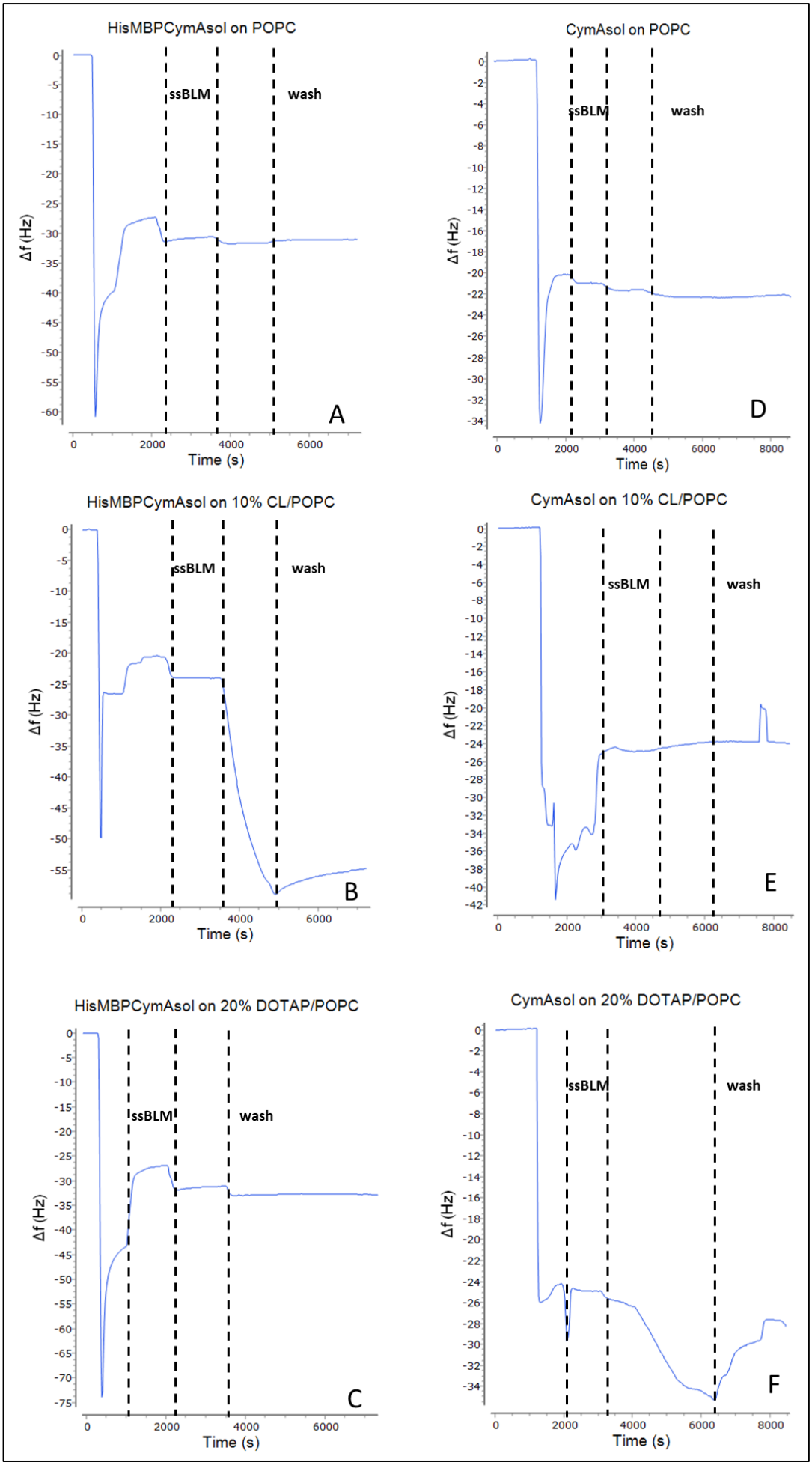
HisMBPCymAsol on POPC
ssBLM
wash
Δf (Hz)
Time (s)
A
CymAsol on POPC
ssBLM
wash
Δf (Hz)
Time (s)
D
HisMBPCymAsol on 10% CL/POPC
ssBLM
wash
Δf (Hz)
Time (s)
B
CymAsol on 10% CL/POPC
ssBLM
wash
Δf (Hz)
Time (s)
E
HisMBPCymAsol on 20% DOTAP/POPC
ssBLM
wash
Δf (Hz)
Time (s)
C
CymAsol on 20% DOTAP/POPC
ssBLM
wash
Δf (Hz)
Time (s)
F

Figure 61: QCM-D binding experiments of HisMBPCymA_{sol} (A-C) or pure untagged CymA_{sol} (D-F) on lipid bilayer membranes with different net surface charges, where the whole construct only binds to negatively charged membrane while pure untagged CymA_{sol} only binds to positively charged membrane. Introduction of the proteins occurs at the markers segment after the ssBLM segment. QCM-D experiments were conducted at room temperature. The buffer composition was 20 mM MOPS pH 7.4 and 30 mM Na_2SO_4, which was also used for the wash step.

5.2.7 Probing CymA_{sol}: FccA interaction by ITC

Having arrived to the understanding that the previously published evidence that argued the formation of a stable complex of CymA: FccA (88) may to an extend have stemmed from a misinterpretation of the obtained data, as well as in order to verify that the evidence presented in this thesis, the CymA:FccA interaction was probed by ITC.

ITC is able to directly monitor the changes in temperature of a stirring solution as another is titrated, whose energy is also quantified from the power that is required to maintain the cell at the baseline temperature. As such, it is employed to determine the thermodynamic parameters of interactions in solution. Also, any results that show that no interactions are taking place in solution can be trusted more than of other techniques that indirectly probe interactions of biomolecules. This was the reason of employing this technique in case CymA and FccA associate very weakly, most likely due to a transient nature of interaction, which would have been implied from the very high reported K_D of ~0.4 mM for these proteins.

CymA_{sol} was chosen over CymA, since the latter would require the presence of DDM detergent. DDM molecules could exchange within the formed micelles and, therefore, give false signals. CymA_{sol} was in the cell at 10 μM and FccA at 100 μM (**panel C figure 62**) and 390 μM (**panel D figure 62**) was titrated. Control titrations of buffer to buffer and of buffer to CymA_{sol} are shown in **panels A and B respectively of figure 62**. No interactions were observed by ITC during those conditions. Usually, a good quality (i.e. sufficient points before and after binding saturation of available binding sites) binding curve is obtained with the titrant at concentration 10-fold higher than the K_D, it can be concluded that the K_D of CymA:FccA interaction must be >3.9 μM, which is in agreement with the reported K_D of 0.4 mM. It should be noted that some

changes in power was seen when FccA at 390 µM was titrated (**panel D figure 62**). This is most likely due to the very high viscosity of FccA at that concentration, which is also the limitation in obtaining a binding curve by ITC should the K_D be as high as previously reported.

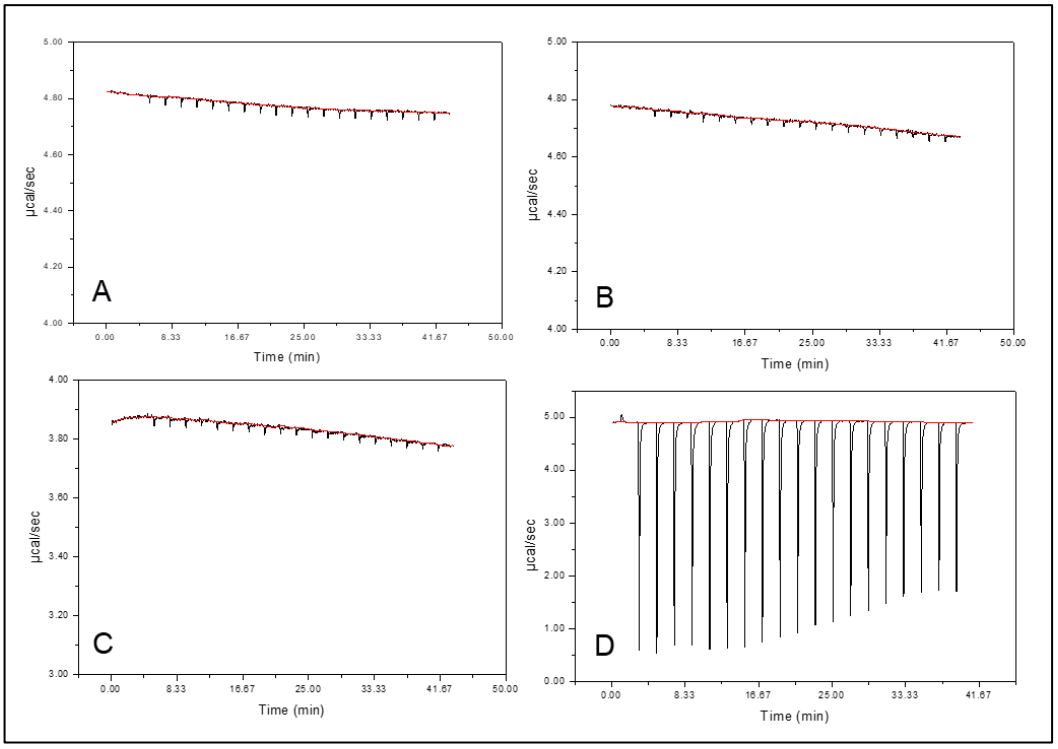

Figure 62: Isothermal titration profiles with 10 µM $CymA_{sol}$ in the cell and FccA as titrant. A: control titration of buffer to buffer in order to assess for buffer mismatch. B: control titration of buffer to $CymA_{sol}$. C: FccA titration at 100 µM. D: FccA titration at 390 µM. The titrations were conducted at room temperature. The cell temperature was maintained at 25 °C.

5.3 Conclusions

The nature of the FccA: CymA interaction was the focus of this chapter. Initially, the ability of these two proteins to interact in vitro was demonstrated with the diaphorase assay where an initial rate of 3.3 (±0.3, n=3) μM NADH oxidised min^{-1}, which although it seems as a particularly slow reaction, it was slightly higher than what has been reported before (1). This is most likely attributed to the presence of detergent, the use of a menaquinone analogue, and /or a combination of those factors, without excluding other possibilities that may exist and result in lowering the apparent rate of the reaction. Nonentheless, the purified proteins used throughout in this thesis were able to specifically interact in vitro.

However, the replication of previously published data, which were linked with the presence of a stable long-lived complex between CymA and FccA were not replicated, both under the previously published conditions and under several other conditions. Although it appears that these two proteins do not form a stable complex, its presence under perhaps certain regulatory elements cannot be ruled out completely at the present time. However, from multisequence allignment and the resulting structural model of CymA that were presented in chapter 4, the CymA surface of the globular domain is not strongly hydrophobic, which further supports that CymA and FccA interact through weak transient interactions. Moreover, the negatively charged proprionate groups of the four haems provide a negatively charged surface that CymA may employ in interacting with its binding partners transiently, instead of through hydrophobic interactions that are normally found in permanent protein complexes.

It must also be noted that the tBLM system that was used for the electrochemical measurements, it was limited in the amount of CymA present in the formed lipid bilayer membrane. This was addressed here by increasing significantly the amount of CymA during reconstitution. The number of accessible for interactions CymA molecules in the tBLM more generally limits this approach as the orientation of CymA during the tBLM formation is random. A way to address this could be by directly tethering CymA on the surface through its N-terminal tags that would significatly increase the electrode

coverage of CymA in a favouring orientation and reconstituting it into a lipid bilayer membrane *in situ*. This approach, among other similar ones, have been used successfully before and have been recently reviewed elsewhere (117).

New evidence were presented from direct investigations into the employed systems that provided a coherent explanation and attributing the signals to technical faults that led the authors to misinterpret the obtained data. More specifically, catalytic reductive waves were shown to be due to the presense of dissolved oxygen. This was further supported by QCM-D bindings studies of the whole and truncated forms of $CymA_{sol}$, where under the published conditions (10% CL/POPC), only the whole catalytically inactive form, carrying 6xHisMBP tags, could bind.

Chapter 6 – Discussion and Future Directions

Although *S. oneidensis* is a particularly challenging organism to work with, its unique metabolic profile has given it a model organism status for microbial electrochemistry. However, the current approaches for the overexpression and production of purified proteins are diverse and protein-specific. Moreover, the transformation of *S. oneidensis* presents yet another challenge, as foreign plasmids can only be electroporated into the organism with very low transformation efficiency. By further improving the current expression vector, an improved approach was presented here for the production of one of the most challenging membrane proteins, CymA. However, in moving forward, the underlying difficulties in genetically modifying *S. oneidensis,* emphasises the need for the development of a new strain that could be used specifically for the production of homologous proteins, but also for metalloproteins in general. Similar genomic changes to address proteolytic degradation, but also to facilitate the homologous and heterologous expression of a target protein has already been achieved for *E. coli*. Moreover, the technological advances that the field of molecular biology has seen, including the more recently CRISPR/Cas9 system, makes the manipulation of genomes much easier than it has been in the past. Thus, the development of an expression strain of *S. oneidensis* will ease the production of metalloproteins, opening up the field to more researchers as well.

Developments on the front of CymA crystallisation and by extension the resolution of its crystal structure have also been reported as part of this work. Although its limited success in obtaining a crystal, several approaches are now more easier to take with the use of tools presented here in terms of gene cloning and purification of CymA protein constructs. Thus, the next steps could involve, but are not limited to, both the crystallisation screening of the full length CymA, and the production of several truncated constructs for eliminating highly flexible regions.

The main contributions of this thesis arrive from partly resolving the debate of CymA: FccA interaction. Also, since our current understanding of the anaerobic respiratory system of *S. oneidensis* involves the interaction of a number of different proteins with CymA under dynamic redox environments,

where this organism is found, the formation of stable complexes seems unlikely. That is, such complexes will compromise the survival of the organism under those dynamic environments by restricting access to CymA molecules for one partner protein when the former is complexed with a different partner protein with a low k_{off}. Taking into account, now, that these two proteins most likely interact transiently, new approaches can be employed in conclusively proving this, as well as further characterising those interactions. Two methods are of particular interest for future studies, without excluding others. First, further NMR studies for the validation of the previously obtained data, especially in the presence of detergent, as well extending basic NMR studies to include paramagnetic probes as a signal boost. Second, taking advantage of the ease of purification of the new CymA construct reported herein, a Foster resonance energy transfer (FRET) based experiments can be designed with fluorescence probes tagged to both proteins at different locations in mapping their interactions. However, it must be noted that care should be taken to address the intrinsic fluorescence of the haems of both CymA and FccA and the FAD of FccA.

Lastly, the applications of this work are primarily to the fields of biotechnology and electrosynthesis. For example, *S. oneidensis* remarkable ability of extracellular metal reduction has already found interest for its use for bioremediation for the removal of pollutants from water. Strong pollutants, such as U and Cr, would primarily exist in the soluble forms of U(VI) and Cr(VI) in a contaminated area, which, through reduction by *S. oneidensis*, can be converted to the insoluble oxide-state that is less toxic. Such change of physical state of the pollutants will greatly aid their removal and, hence, the final de-contamination of water. Such bioremediation strategies can be enhanced through the reconstitution of the desired molecular pathways in *E. coli*, or the transformation of *S. oneidensis* strains, by fine-tuning their metabolism for a certain bioremediation application, so the environmental and human hazard are minimised. Lastly, molecular understanding of the flow of electrons during bacterial respiration, and especially, extracellular bacterial respiration, can be exploited for nanoscale biosensor applications. That is, when a target molecule binds to a genetically engineered protein, a cascade of electron relay would be initiated transferring electrons along a modified

protein-wire to an electrode (instead of the native solid oxides found in the environment), where the signal can be amplified and translated. It is, hence, reasonable to envisage that when such applications are commercialised, they will help the society.

List of References

1. Marritt, S.J., Lowe, T.G., Bye, J., McMillan, D.G.G., Shi, L., Fredrickson, J., Zachara, J., Richardson, D.J., Cheesman, M.R., Jeuken, L.J.C. and Butt, J.N. A functional description of CymA, an electron-transfer hub supporting anaerobic respiratory flexibility in *Shewanella*. *Biochemical Journal.* 2012, **444**, pp.465-474.
2. Dietrich, L.E.P., Tice, M.M. and Newman, D.K. The co-evolution of life and Earth. *Current Biology.* 2006, **16**(11), pp.R395-R400.
3. Schopf, J. and Packer, B. Early Archean (3.3-billion to 3.5-billion-year-old) microfossils from Warrawoona Group, Australia. *Science.* 1987, **237**(4810), pp.70-73.
4. Schopf, J.W., Kudryavtsev, A.B., Agresti, D.G., Wdowiak, T.J. and Czaja, A.D. Laser–Raman imagery of Earth's earliest fossils. *Nature.* 2002, **416**(6876), pp.73-76.
5. Lyons, T.W., Reinhard, C.T. and Planavsky, N.J. The rise of oxygen in Earth's early ocean and atmosphere. *Nature.* 2014, **506**(7488), pp.307-315.
6. Catling, D.C. and Claire, M.W. How Earth's atmosphere evolved to an oxic state: A status report. *Earth and Planetary Science Letters.* 2005, **237**(1-2), pp.1-20.
7. Vargas, M., Kashefi, K., Blunt-Harris, E.L. and Lovley, D.R. Microbiological evidence for Fe (III) reduction on early Earth. *Nature.* 1998, **395**(6697), pp.65-67.
8. Seckbach, J. Origins: Genesis, Evolution and Diversity of Life. *Springer,* 2006.
9. Myers, C. and Nealson, K.H. Bacterial manganese reduction and growth with manganese oxide as the sole electron acceptor. *Science.* 1988, **240**(4857), pp.1319-1321.
10. Lovley, D.R., Stolz, J.F., Nord, G.L. and Phillips, E.J. Anaerobic production of magnetite by a dissimilatory iron-reducing microorganism. *Nature.* 1987, **330**(6145), pp.252-254.
11. Park, H.S., Kim, B.H., Kim, H.S., Kim, H.J., Kim, G.T., Kim, M., Chang, I.S., Park, Y.K. and Chang, H.I. A Novel Electrochemically Active and Fe(III)-reducing Bacterium Phylogenetically Related to *Clostridium*

butyricum Isolated from a Microbial Fuel Cell. *Anaerobe.* 2001, **7**(6), pp.297-306.

12. Pham, C.A., Jung, S.J., Phung, N.T., Lee, J., Chang, I.S., Kim, B.H., Yi, H. and Chun, J. A novel electrochemically active and Fe (III)-reducing bacterium phylogenetically related to *Aeromonas hydrophila*, isolated from a microbial fuel cell. *Fems Microbiology Letters.* 2003, **223**(1), pp.129-134.
13. Finneran, K.T., Johnsen, C.V. and Lovley, D.R. *Rhodoferax ferrireducens sp.* nov., a psychrotolerant, facultatively anaerobic bacterium that oxidizes acetate with the reduction of Fe (III). *International Journal of Systematic and Evolutionary Microbiology.* 2003, **53**(3), pp.669-673.
14. Holmes, D.E., Bond, D.R. and Lovley, D.R. Electron transfer by *Desulfobulbus propionicus* to Fe (III) and graphite electrodes. *Applied and Environmental Microbiology.* 2004, **70**(2), pp.1234-1237.
15. Weber, K.A., Achenbach, L.A. and Coates, J.D. Microorganisms pumping iron: anaerobic microbial iron oxidation and reduction. *Nature Reviews Microbiology.* 2006, **4**(10), pp.752-764.
16. Debby, H. and Hammer, B.W. Bacteriology Of Butter-Bacteriological Studies On Surface Taint Butter. 1931.
17. Khashe, S. and Janda, J.M. Biochemical and Pathogenic Properties of *Shewanella alga* and *Shewanella putrefaciens*. *Journal of clinical microbiology.* 1998, **36**(3), pp.783-787.
18. Kozińska, A. and Pekala, A. First isolation of *Shewanella putrifaciens* from freshwater fish-a potential new pathogen of fish. *Bull. Eur. Ass. Fish Pathol.* 2004, **24**(4), p.189.
19. Shewan, J.M., Hobbs, G. and Hodgkiss, W. A Determinative Scheme for the Identification of Certain Genera of Gram-Negative Bacteria, with Special Reference to the *Pseudomonadaceae*. *Journal of Applied Bacteriology.* 1960, **23**(3), pp.379-390.
20. Lee, J., Gibson, D. and Shewan, J.M. A numerical taxonomic study of some *Pseudomonas*-like marine bacteria. *Journal of General Microbiology.* 1977, **98**(2), pp.439-451.

21. Macdonell, M.T. and Colwell, R.R. Phylogeny of the Vibrionaceae, and Recommendation for 2 New Genera, *Listonella* and *Shewanella*. *Systematic and Applied Microbiology.* 1985, **6**(2), pp.171-182.

22. Venkateswaran, K., Moser, D.P., Dollhopf, M.E., Lies, D.P., Saffarini, D.A., MacGregor, B.J., Ringelberg, D.B., White, D.C., Nishijima, M. and Sano, H. Polyphasic taxonomy of the genus *Shewanella* and description of *Shewanella oneidensis sp*. nov. *Int J Syst Bacteriol.* 1999, **49**(2), pp.705-724.

23. Beliaev, A.S., Klingeman, D.M., Klappenbach, J., Wu, L., Romine, M.F., Tiedje, J.M., Nealson, K.H., Fredrickson, J.K. and Zhou, J. Global transcriptome analysis of *Shewanella oneidensis* MR-1 exposed to different terminal electron acceptors. *Journal of Bacteriology.* 2005, **187**(20), pp.7138-7145.

24. Nealson, K.H. and Saffarini, D. Iron and manganese in anaerobic respiration: environmental significance, physiology, and regulation. *Annual Reviews in Microbiology.* 1994, **48**(1), pp.311-343.

25. Liu, C., Gorby, Y.A., Zachara, J.M., Fredrickson, J.K. and Brown, C.F. Reduction kinetics of Fe (III), Co (III), U (VI), Cr (VI), and Tc (VII) in cultures of dissimilatory metal-reducing bacteria. *Biotechnology and Bioengineering.* 2002, **80**(6), pp.637-649.

26. Bencheikh-Latmani, R., Williams, S.M., Haucke, L., Criddle, C.S., Wu, L., Zhou, J. and Tebo, B.M. Global transcriptional profiling of *Shewanella oneidensis* MR-1 during Cr (VI) and U (VI) reduction. *Applied and Environmental Microbiology.* 2005, **71**(11), pp.7453-7460.

27. Myers, C., Carstens, B., Antholine, W. and Myers, J. Chromium (VI) reductase activity is associated with the cytoplasmic membrane of anaerobically grown Shewanella putrefaciens MR-1. *Journal of Applied Microbiology.* 2000, **88**(1), pp.98-106.

28. Scott, J.H. and Nealson, K.H. A biochemical study of the intermediary carbon metabolism of *Shewanella putrefaciens*. *Journal of Bacteriology.* 1994, **176**(11), pp.3408-3411.

29. Myers, C.R. and Myers, J.M. Cloning and sequence of cymA a gene encoding a tetraheme cytochrome c required for reduction of iron(III),

fumarate, and nitrate by Shewanella putrefaciens MR-1. *Journal of Bacteriology.* 1997, **179**(4), pp.1143-1152.

30. Rodrigues, M.L., Oliveira, T.F., Pereira, I.A. and Archer, M. X-ray structure of the membrane-bound cytochrome c quinol dehydrogenase NrfH reveals novel haem coordination. *Embo j.* 2006, **25**(24), pp.5951-5960.
31. Kern, M., Einsle, O. and Simon, J. Variants of the tetrahaem cytochrome c quinol dehydrogenase NrfH characterize the menaquinol-binding site, the haem c-binding motifs and the transmembrane segment. *Biochem. J.* 2008, **414**, pp.73-79.
32. Cartron, M., Roldan, M., Ferguson, S., Berks, B. and Richardson, D. Identification of two domains and distal histidine ligands to the four haems in the bacterial c-type cytochrome NapC; the prototype connector between quinol/quinone and periplasmic oxido-reductases. *Biochem. J.* 2002, **368**, pp.425-432.
33. Schwalb, C., Chapman, S.K. and Reid, G.A. The tetraheme cytochrome CymA is required for anaerobic respiration with dimethyl sulfoxide and nitrite in Shewanella oneidensis. *Biochemistry.* 2003, **42**(31), pp.9491-9497.
34. Rodrigues, M.L., Scott, K.A., Sansom, M.S., Pereira, I.A. and Archer, M. Quinol Oxidation by c-Type Cytochromes: Structural Characterization of the Menaquinol Binding Site of NrfHA. *Journal of Molecular Biology.* 2008, **381**(2), pp.341-350.
35. Field, S.J., Dobbin, P.S., Cheesman, M.R., Watmough, N.J., Thomson, A.J. and Richardson, D.J. Purification and magneto-optical spectroscopic characterization of cytoplasmic membrane and outer membrane multiheme c-type cytochromes from *Shewanella frigidimarina* NCIMB400. *Journal of Biological Chemistry.* 2000, **275**(12), pp.8515-8522.
36. Myers, C.R. and Myers, J.M. Role of menaquinone in the reduction of fumarate, nitrate, iron(III) and manganese(IV) by *Shewanella putrefaciens* MR-1. *Fems Microbiology Letters.* 1993, **114**(2), pp.215-222.

37. Myers, J.M. and Myers, C.R. Role of the tetraheme cytochrome CymA in anaerobic electron transport in cells of *Shewanella putrefaciens* MR-1 with normal levels of menaquinone. *Journal of Bacteriology.* 2000, **182**(1), pp.67-75.

38. Nishijima, M., Araki-Sakai, M. and Sano, H. Identification of isoprenoid quinones by frit-FAB liquid chromatography–mass spectrometry for the chemotaxonomy of microorganisms. *Journal of microbiological methods.* 1997, **28**(2), pp.113-122.

39. McMillan, D.G.G., Marritt, S.J., Butt, J.N. and Jeuken, L.J.C. Menaquinone-7 Is Specific Cofactor in Tetraheme Quinol Dehydrogenase CymA. *Journal of Biological Chemistry.* 2012, **287**(17), pp.14215-14225.

40. Todorovic, S., Rodrigues, M.L., Matos, D. and Pereira, I.s.A. Redox Properties of Lysine-and Methionine-Coordinated Hemes Ensure Downhill Electron Transfer in NrfH2A4 Nitrite Reductase. *The Journal of Physical Chemistry B.* 2012, **116**(19), pp.5637-5643.

41. Arnoux, P., Sabaty, M., Alric, J., Frangioni, B., Guigliarelli, B., Adriano, J.-M. and Pignol, D. Structural and redox plasticity in the heterodimeric periplasmic nitrate reductase. *Nature Structural & Molecular Biology.* 2003, **10**(11), pp.928-934.

42. Brigé, A., Leys, D., Meyer, T.E., Cusanovich, M.A. and Van Beeumen, J.J. The 1.25 Å resolution structure of the diheme NapB subunit of soluble nitrate reductase reveals a novel cytochrome c fold with a stacked heme arrangement. *Biochemistry.* 2002, **41**(15), pp.4827-4836.

43. Gao, H., Yang, Z.K., Barua, S., Reed, S.B., Romine, M.F., Nealson, K.H., Fredrickson, J.K., Tiedje, J.M. and Zhou, J. Reduction of nitrate in *Shewanella oneidensis* depends on atypical NAP and NRF systems with NapB as a preferred electron transport protein from CymA to NapA. *Isme Journal.* 2009, **3**(8), pp.966-976.

44. Kern, M., Volz, J. and Simon, J. The oxidative and nitrosative stress defence network of Wolinella succinogenes: cytochrome c nitrite reductase mediates the stress response to nitrite, nitric oxide,

hydroxylamine and hydrogen peroxide. *Environmental Microbiology.* 2011, **13**(9), pp.2478-2494.

45. Poock, S.R., Leach, E.R., Moir, J.W., Cole, J.A. and Richardson, D.J. Respiratory detoxification of nitric oxide by the cytochromec nitrite reductase of *Escherichia coli*. *Journal of Biological Chemistry.* 2002, **277**(26), pp.23664-23669.
46. Rodrigues, M.L., Oliveira, T.F., Pereira, I.A. and Archer, M. X-ray structure of the membrane-bound cytochrome c quinol dehydrogenase NrfH reveals novel haem coordination. *Embo j.* 2006, **25**(24), pp.5951-5960.
47. Cunha, C.A., Macieira, S., Dias, J.M., Almeida, G., Gonçalves, L.L., Costa, C., Lampreia, J., Huber, R., Moura, J.J. and Moura, I. Cytochrome c Nitrite Reductase from *Desulfovibrio desulfuricans* ATCC 27774 The relevance of the two calcium sites in the structure of the catalytic subunit NrfA. *Journal of Biological Chemistry.* 2003, **278**(19), pp.17455-17465.
48. Lukat, P., Rudolf, M., Stach, P., Messerschmidt, A., Kroneck, P.M.H., Simon, J. and Einsle, O. Binding and reduction of sulfite by cytochrome c nitrite reductase. *Biochemistry.* 2008, **47**(7), pp.2080-2086.
49. Kemp, G., Clarke, T., Marritt, S., Lockwood, C., Poock, S., Hemmings, A., Richardson, D., Cheesman, M. and Butt, J. Kinetic and thermodynamic resolution of the interactions between sulfite and the pentahaem cytochrome NrfA from *Escherichia coli*. *Biochem. J.* 2010, **431**, pp.73-80.
50. Youngblut, M., Judd, E.T., Srajer, V., Sayyed, B., Goelzer, T., Elliott, S.J., Schmidt, M. and Pacheco, A.A. Laue crystal structure of *Shewanella oneidensis* cytochrome c nitrite reductase from a high-yield expression system. *Journal of Biological Inorganic Chemistry.* 2012, **17**(4), pp.647-662.
51. Judd, E.T., Youngblut, M., Pacheco, A.A. and Elliott, S.J. Direct electrochemistry of *Shewanella oneidensis* cytochrome c nitrite reductase: evidence of interactions across the dimeric interface. *Biochemistry.* 2012, **51**(51), pp.10175-10185.

52. Angove, H.C., Cole, J.A., Richardson, D.J. and Butt, J.N. Protein film voltammetry reveals distinctive fingerprints of nitrite and hydroxylamine reduction by a cytochrome c nitrite reductase. *Journal of Biological Chemistry.* 2002, **277**(26), pp.23374-23381.

53. Bollag, J.-M. and Henninger, N.M. Effects of nitrite toxicity on soil bacteria under aerobic and anaerobic conditions. *Soil Biology and Biochemistry.* 1978, **10**(5), pp.377-381.

54. Barrett, E. and Kwan, H. Bacterial reduction of trimethylamine oxide. *Annual Reviews in Microbiology.* 1985, **39**(1), pp.131-149.

55. Dos Santos, J.-P., Iobbi-Nivol, C., Couillault, C., Giordano, G. and Méjean, V. Molecular analysis of the trimethylamine N-oxide (TMAO) reductase respiratory system from a *Shewanella species*. *Journal of Molecular Biology.* 1998, **284**(2), pp.421-433.

56. Czjzek, M., Dos Santos, J.-P., Pommier, J., Giordano, G., Méjean, V. and Haser, R. Crystal structure of oxidized trimethylamine N-oxide reductase from *Shewanella massilia* at 2.5 å resolution. *Journal of Molecular Biology.* 1998, **284**(2), pp.435-447.

57. Morris, C.J., Black, A., Pealing, S.L., Manson, F., Chapman, S.K., Reid, G., Gibson, D.M. and Ward, F.B. Purification and properties of a novel cytochrome: flavocytochrome c from *Shewanella putrefaciens*. *Biochem. J.* 1994, **302**, pp.587-593.

58. Leys, D., Tsapin, A.S., Nealson, K.H., Meyer, T.E., Cusanovich, M.A. and Van Beeumen, J.J. Structure and mechanism of the flavocytochrome c fumarate reductase of *Shewanella putrefaciens* MR-1. *Nature Structural & Molecular Biology.* 1999, **6**(12), pp.1113-1117.

59. Taylor, P., Pealing, S.L., Reid, G.A., Chapman, S.K. and Walkinshaw, M.D. Structural and mechanistic mapping of a unique fumarate reductase. *Nature Structural & Molecular Biology.* 1999, **6**(12), pp.1108-1112.

60. Schwalb, C., Chapman, S.K. and Reid, G.A. The membrane-bound tetrahaem c-type cytochrome CymA interacts directly with the soluble fumarate reductase in *Shewanella*. *Biochemical Society Transactions.* 2002, **30**, pp.658-662.

61. Schuetz, B., Schicklberger, M., Kuermann, J., Spormann, A.M. and Gescher, J. Periplasmic Electron Transfer via the c-Type Cytochromes MtrA and FccA of *Shewanella oneidensis* MR-1. *Applied and Environmental Microbiology.* 2009, **75**(24), pp.7789-7796.

62. Beliaev, A.S., Thompson, D.K., Khare, T., Lim, H., Brandt, C.C., Li, G., Murray, A.E., Heidelberg, J.F., Giometti, C.S., Yates, J., III, Nealson, K.H., Tiedje, J.M. and Zhou, J. Gene and protein expression profiles of *Shewanella oneidensis* during anaerobic growth with different electron acceptors. *OMICS A Journal of Integrative Biology.* 2002, **6**(1), pp.39-60.

63. Ross, D.E., Ruebush, S.S., Brantley, S.L., Hartshorne, R.S., Clarke, T.A., Richardson, D.J. and Tien, M. Characterization of protein-protein interactions involved in iron reduction by *Shewanella oneidensis* MR-1. *Applied and Environmental Microbiology.* 2007, **73**(18), pp.5797-5808.

64. Fonseca, B.M., Paquete, C.M., Neto, S.E., Pacheco, I., Soares, C.M. and Louro, R.O. Mind the gap: cytochrome interactions reveal electron pathways across the periplasm of *Shewanella oneidensis* MR-1. *Biochemical Journal.* 2013, **449**, pp.101-108.

65. Gordon, E.H., Pike, A.D., Hill, A.E., Cuthbertson, P.M., Chapman, S.K. and Reid, G.A. Identification and characterization of a novel cytochrome c(3) from *Shewanella frigidimarina* that is involved in Fe(III) respiration. *Biochem J.* 2000, **349**(Pt 1), pp.153-158.

66. Coursolle, D. and Gralnick, J.A. Modularity of the Mtr respiratory pathway of *Shewanella oneidensis* strain MR-1. *Molecular Microbiology.* 2010, **77**(4), pp.995-1008.

67. Leys, D., Meyer, T.E., Tsapin, A.S., Nealson, K.H., Cusanovich, M.A. and Van Beeumen, J.J. Crystal structures at atomic resolution reveal the novel concept of "electron-harvesting" as a role for the small tetraheme cytochrome c. *Journal of Biological Chemistry.* 2002, **277**(38), pp.35703-35711.

68. Rosenbaum, M., Frawley, E.R., Lee, R.E., Angenent, L.T. and Kranz, R.G. Recombinant Engineering of *Shewanella oneidensis* MR-1 c-type

Cytochromes in Escherichia coli. *Abstracts of the General Meeting of the American Society for Microbiology.* 2008, **108**, pp.621-621.

69. Coursolle, D. and Gralnick, J.A. Reconstruction of Extracellular Respiratory Pathways for Iron(III) Reduction in *Shewanella Oneidensis* Strain MR-1. *Frontiers in microbiology.* 2012, **3**, pp.56-56.
70. Pitts, K.E., Dobbin, P.S., Reyes-Ramirez, F., Thomson, A.J., Richardson, D.J. and Seward, H.E. Characterization of the *Shewanella oneidensis* MR-1 decaheme cytochrome MtrA. *Journal of Biological Chemistry.* 2003, **278**(30), pp.27758-27765.
71. Hartshorne, R.S., Reardon, C.L., Ross, D., Nuester, J., Clarke, T.A., Gates, A.J., Mills, P.C., Fredrickson, J.K., Zachara, J.M., Shi, L., Beliaev, A.S., Marshall, M.J., Tien, M., Brantley, S., Butt, J.N. and Richardson, D.J. Characterization of an electron conduit between bacteria and the extracellular environment. *Proceedings of the National Academy of Sciences.* 2009.
72. Firer-Sherwood, M.A., Ando, N., Drennan, C.L. and Elliott, S.J. Solution-based structural analysis of the decaheme cytochrome, MtrA, by small-angle X-ray scattering and analytical ultracentrifugation. *The Journal of Physical Chemistry B.* 2011, **115**(38), pp.11208-11214.
73. Vollmer, W. and Seligman, S.J. Architecture of peptidoglycan: more data and more models. *Trends in microbiology.* 2010, **18**(2), pp.59-66.
74. Matias, V.R., Al-Amoudi, A., Dubochet, J. and Beveridge, T.J. Cryo-transmission electron microscopy of frozen-hydrated sections of Escherichia coli and Pseudomonas aeruginosa. *Journal of Bacteriology.* 2003, **185**(20), pp.6112-6118.
75. Beliaev, A.S. and Saffarini, D.A. *Shewanella putrefaciens* mtrB encodes an outer membrane protein required for Fe(III) and Mn(IV) reduction. *Journal of Bacteriology.* 1998, **180**(23), pp.6292-6297.
76. Baslé, A., Rummel, G., Storici, P., Rosenbusch, J.P. and Schirmer, T. Crystal Structure of Osmoporin OmpC from *E. coli* at 2.0 Å. *Journal of Molecular Biology.* 2006, **362**(5), pp.933-942.
77. Shi, L., Deng, S., Marshall, M.J., Wang, Z.M., Kennedy, D.W., Dohnalkova, A.C., Mottaz, H.M., Hill, E.A., Gorby, Y.A., Beliaev, A.S., Richardson, D.J., Zachara, J.M. and Fredrickson, J.K. Direct

involvement of type II secretion system in extracellular translocation of *Shewanella oneidensis* outer membrane cytochromes MtrC and OmcA. *Journal of Bacteriology.* 2008, **190**(15), pp.5512-5516.

78. Clarke, T.A., Edwards, M.J., Gates, A.J., Hall, A., White, G.F., Bradley, J., Reardon, C.L., Shi, L., Beliaev, A.S. and Marshall, M.J. Structure of a bacterial cell surface decaheme electron conduit. *Proceedings of the National Academy of Sciences.* 2011, **108**(23), pp.9384-9389.
79. Edwards, M., Fredrickson, J., Zachara, J., Richardson, D. and Clarke, T. Analysis of structural MtrC models based on homology with the crystal structure of MtrF. *Biochemical Society Transactions.* 2012, **40**(6), pp.1181-1185.
80. Shi, L., Chen, B., Wang, Z., Elias, D.A., Mayer, M.U., Gorby, Y.A., Ni, S., Lower, B.H., Kennedy, D.W. and Wunschel, D.S. Isolation of a high-affinity functional protein complex between OmcA and MtrC: two outer membrane decaheme c-type cytochromes of *Shewanella oneidensis* MR-1. *Journal of Bacteriology.* 2006, **188**(13), pp.4705-4714.
81. Lower, B.H., Shi, L., Yongsunthon, R., Droubay, T.C., McCready, D.E. and Lower, S.K. Specific bonds between an iron oxide surface and outer membrane cytochromes MtrC and OmcA from *Shewanella oneidensis* MR-1. *Journal of Bacteriology.* 2007, **189**(13), pp.4944-4952.
82. Edwards, M.J., Baiden, N.A., Johs, A., Tomanicek, S.J., Liang, L., Shi, L., Fredrickson, J.K., Zachara, J.M., Gates, A.J. and Butt, J.N. The X-ray crystal structure of *Shewanella oneidensis* OmcA reveals new insight at the microbe–mineral interface. *Febs Letters.* 2014, **588**(10), pp.1886-1890.
83. Stanley, N.R., Sargent, F., Buchanan, G., Shi, J.R., Stewart, V., Palmer, T. and Berks, B.C. Behaviour of topological marker proteins targeted to the Tat protein transport pathway. *Molecular Microbiology.* 2002, **43**(4), pp.1005-1021.
84. McEWAN, A.G., Ferguson, S. and Jackson, J.B. Purification and properties of dimethyl sulphoxide reductase from Rhodobacter capsulatus. A periplasmic molybdoenzyme. *Biochemical Journal.* 1991, **274**(Pt 1), p.305.

85. Gralnick, J.A., Vali, H., Lies, D.P. and Newman, D.K. Extracellular respiration of dimethyl sulfoxide by *Shewanella oneidensis* strain MR-1. *Proceedings of the National Academy of Sciences of the United States of America.* 2006, **103**(12), pp.4669-4674.

86. Bewley, K.D., Firer-Sherwood, M.A., Mock, J.Y., Ando, N., Drennan, C.L. and Elliott, S.J. Mind the gap: diversity and reactivity relationships among multihaem cytochromes of the MtrA/DmsE family. 2012.

87. Fonseca, B.M., Paquete, C.M., Neto, S.E., Pacheco, I., Soares, C.M. and Louro, R.O. Mind the gap: cytochrome interactions reveal electron pathways across the periplasm of *Shewanella oneidensis* MR-1. *Biochem J.* 2013, **449**(1), pp.101-108.

88. McMillan, D.G.G., Marritt, S.J., Firer-Sherwood, M.A., Shi, L., Richardson, D.J., Evans, S.D., Elliott, S.J., Butt, J.N. and Jeuken, L.J.C. Protein-Protein Interaction Regulates the Direction of Catalysis and Electron Transfer in a Redox Enzyme Complex. *Journal of the American Chemical Society.* 2013, **135**(28), pp.10550-10556.

89. Londer, Y.Y., Giuliani, S.E., Peppler, T. and Collart, F.R. Addressing *Shewanella oneidensis* "cytochromome": The first step towards high-throughput expression of cytochromes c. *Protein Expression and Purification.* 2008, **62**(1), pp.128-137.

90. Dobbin, P., Butt, J., Powell, A., Reid, G. and Richardson, D. Characterization of a flavocytochrome that is induced during the anaerobic respiration of Fe3+ by *Shewanella frigidimarina* NCIMB400. *Biochem. J.* 1999, **342**, pp.439-448.

91. Myers, C.R. and Myers, J.M. Replication of plasmids with the p15A origin in *Shewanella putrefaciens* MR-1. *Letters in Applied Microbiology.* 1997, **24**(3), pp.221-225.

92. Meyer, T. and Lamberts, B. Use of coomassie brilliant blue R250 for the electrophoresis of microgram quantities of parotid saliva proteins on acrylamide-gel strips. *Biochimica et Biophysica Acta (BBA)-General Subjects.* 1965, **107**(1), pp.144-145.

93. Thomas, P.E., Ryan, D. and Levin, W. An improved staining procedure for the detection of the peroxidase activity of cytochrome P-450 on

sodium dodecyl sulfate polyacrylamide gels. *Analytical biochemistry.* 1976, **75**(1), pp.168-176.

94. Carter, K. and Gennis, R.B. Reconstitution of the Ubiquinone-dependent pyruvate oxidase system of *Escherichia coli* with the cytochrome o terminal oxidase complex. *J Biol Chem.* 1985, **260**(20), pp.10986-10990.
95. Jeuken, L.J., Connell, S.D., Henderson, P.J., Gennis, R.B., Evans, S.D. and Bushby, R.J. Redox enzymes in tethered membranes. *Journal of the American Chemical Society.* 2006, **128**(5), pp.1711-1716.
96. Boden, N., Bushby, R.J., Clarkson, S., Evans, S.D., Knowles, P.F. and Marsh, A. The design and synthesis of simple molecular tethers for binding biomembranes to a gold surface. *Tetrahedron.* 1997, **53**(31), pp.10939-10952.
97. Jeuken, L.J.C., Daskalakis, N.N., Han, X.J., Sheikh, K., Erbe, A., Bushby, R.J. and Evans, S.D. Phase separation in mixed self-assembled monolayers and its effect on biomimetic membranes. *Sensors and Actuators B-Chemical.* 2007, **124**(2), pp.501-509.
98. Cho, N.J., Frank, C.W., Kasemo, B. and Hook, F. Quartz crystal microbalance with dissipation monitoring of supported lipid bilayers on various substrates. *Nat Protoc.* 2010, **5**(6), pp.1096-1106.
99. Shi, L., Lin, J.T., Markillie, L.M., Squier, T.C. and Hooker, B.S. Overexpression of multi-heme C-type cytochromes. *Biotechniques.* 2005, **38**(2), pp.297-299.
100. Di Tommaso, P., Moretti, S., Xenarios, I., Orobitg, M., Montanyola, A., Chang, J.M., Taly, J.F. and Notredame, C. T-Coffee: a web server for the multiple sequence alignment of protein and RNA sequences using structural information and homology extension. *Nucleic Acids Res.* 2011, **39**(Web Server issue), pp.W13-17.
101. Notredame, C., Higgins, D.G. and Heringa, J. T-Coffee: A novel method for fast and accurate multiple sequence alignment. *J Mol Biol.* 2000, **302**(1), pp.205-217.

102. Arnold, K., Bordoli, L., Kopp, J. and Schwede, T. The SWISS-MODEL workspace: a web-based environment for protein structure homology modelling. *Bioinformatics.* 2006, **22**(2), pp.195-201.

103. Biasini, M., Bienert, S., Waterhouse, A., Arnold, K., Studer, G., Schmidt, T., Kiefer, F., Gallo Cassarino, T., Bertoni, M., Bordoli, L. and Schwede, T. SWISS-MODEL: modelling protein tertiary and quaternary structure using evolutionary information. *Nucleic Acids Res.* 2014, **42**(Web Server issue), pp.W252-258.

104. Hewitt, S.N., Choi, R., Kelley, A., Crowther, G.J., Napuli, A.J. and Van Voorhis, W.C. Expression of proteins in *Escherichia coli* as fusions with maltose-binding protein to rescue non-expressed targets in a high-throughput protein-expression and purification pipeline. *Acta Crystallographica Section F: Structural Biology and Crystallization Communications.* 2011, **67**(Pt 9), pp.1006-1009.

105. Kertis, F., Khurshid, S., Okman, O., Kysar, J.W., Govada, L., Chayen, N. and Erlebacher, J. Heterogeneous nucleation of protein crystals using nanoporous gold nucleants. *Journal of Materials Chemistry.* 2012, **22**(41), pp.21928-21934.

106. Griffin, L. and Lawson, A. Antibody fragments as tools in crystallography. *Clinical and Experimental Immunology.* 2011, **165**(3), pp.285-291.

107. Lim, H.-H., Fang, Y. and Williams, C. High-Efficiency Screening of Monoclonal Antibodies for Membrane Protein Crystallography. *Plos One.* 2011, **6**(9), p.e24653.

108. Clifton, M.C., Dranow, D.M., Leed, A., Fulroth, B., Fairman, J.W., Abendroth, J., Atkins, K.A., Wallace, E., Fan, D., Xu, G., Ni, Z.J., Daniels, D., Van Drie, J., Wei, G., Burgin, A.B., Golub, T.R., Hubbard, B.K. and Serrano-Wu, M.H. A Maltose-Binding Protein Fusion Construct Yields a Robust Crystallography Platform for MCL1. *Plos One.* 2015, **10**(4), p.e0125010.

109. Mintseris, J. and Weng, Z. Structure, function, and evolution of transient and obligate protein-protein interactions. *Proc Natl Acad Sci U S A.* 2005, **102**(31), pp.10930-10935.

110. Choi, Y.S., Yang, J.S., Choi, Y., Ryu, S.H. and Kim, S. Evolutionary conservation in multiple faces of protein interaction. *Proteins.* 2009, **77**(1), pp.14-25.

111. Jones, S. and Thornton, J.M. Principles of protein-protein interactions. *Proc Natl Acad Sci U S A.* 1996, **93**(1), pp.13-20.

112. Jones, S. and Thornton, J.M. Protein-protein interactions: a review of protein dimer structures. *Prog Biophys Mol Biol.* 1995, **63**(1), pp.31-65.

113. Tsai, C.J., Lin, S.L., Wolfson, H.J. and Nussinov, R. Studies of protein-protein interfaces: a statistical analysis of the hydrophobic effect. *Protein Sci.* 1997, **6**(1), pp.53-64.

114. Block, P., Paern, J., Hüllermeier, E., Sanschagrin, P., Sotriffer, C.A. and Klebe, G. Physicochemical descriptors to discriminate protein–protein interactions in permanent and transient complexes selected by means of machine learning algorithms. *Proteins: Structure, Function, and Bioinformatics.* 2006, **65**(3), pp.607-622.

115. Tjernberg, A., Markova, N., Griffiths, W.J. and Hallen, D. DMSO-related effects in protein characterization. *J Biomol Screen.* 2006, **11**(2), pp.131-137.

116. Arakawa, T., Kita, Y. and Timasheff, S.N. Protein precipitation and denaturation by dimethyl sulfoxide. *Biophys Chem.* 2007, **131**(1-3), pp.62-70.

117. Laftsoglou, T. and Jeuken, L.J.C. Supramolecular electrode assemblies for bioelectrochemistry. *Chemical Communications (Cambridge, England).* 2017, **53**(27), pp.3801-3809.

Appendix A
List of vendors

[Purity or grade] as provided by the vendor.

- **Melford**

Yeast extract, tryptone, EDTA (disodium salt) dihydrate, sodium dodecyl sulfate micro-pellets, ammonium sulfate, urea [>99%], sodium acetate anhydrous [>99%], L(+) arabinose [>99%], glycine [>99.5%], Tris [molecular biology grade >99.9%], potassium phosphate monobasic [>98%], kanamycin monosulfate, TEMED, ammonium persulfate, 40% w/v acrylamide, 2% w/v bis-acrylamide, albumin bovine fraction V (BSA) [>98%], carbenicillin disodium, n-octyl-β-D-glycoside.

- **Fisher**

Sodium chloride, glycerol [molecular biology grade], methanol [analytical grade], isopropanol [analytical grade], calcium chloride dihydrate, hydrogen peroxide >30% w/v, Triton X-100 [electrophoresis grade].

- **Sigma-Aldrich**

D-sorbitol, fumaric acid disodium salt, copper (II) sulfate pentahydrate, HEPES [≥99.5%], MOPS [≥99.5%], fumaric acid for cell culture, sodium sulfate [>99%], ethanol [≥99.8%], sodium dithionite [≥82%], brilliant blue R250 coomassie, sodium-DL-lactate 60% w/v solution, tetramethylbenzidine dihydrochloride hydrate, lysozyme from chicken egg white [≥90%], DL-dithiothreitol, tris(2-carboxyethyl) phosphine hydrochloride [≥98%], dimethyl-sulfoxide [≥99.5%], TWEEN20, acetic acid [99-100%].

- **OXOID**

Agar bacteriological (Agar No. 1).

- **Thermo Scientific**

BCA protein assay reagent A.

- **VMR chemicals**

Dipotassium hydrogen phosphate, chloroform [HPLC grade].

- **ACROS organics**

Imidazole [99%], methyl viologen hydrate [98%], 2-mercaptoethanol [99%], magnesium chloride [pure].

- **Scientific Laboratory Supplies**

Bromophenol blue.

- **Alfa Aesor**

Chloramphenicol [99+%].

- **Anatrace**

Anapoe-X-100 (10% w/v Triton X-100) [membrane grade], n-dodecyl-β-D-maltopyranoside.

- **Generon**

Page ruler plus pre-stained protein ladder (10-250 kDa) (cat. No.: 26619), InstantBlue protein stain (cat. No.: ISB1L), isopropyl-β-D-thiogalactopyranoside,

Appendix B
Sequences of the Recombinant CymA

1. *8xHisHRVCymA construct*

CCATGGCAAAACATCATCACCATCACCATCACCATCTGGAAGTTCTGTTCCAG
GGTCCGAACTGGCGTGCTTTATTCAAACCATCTGCTAAATACTCTATCTTAGCT
TTATTAGTTGTTGGTATCGTTATCGGTGTTGTTGGTTACTTCGCTACTCAACAA
ACTTTACACGCTACTTCTACTGATGCTTTCTGTATGTCTTGTCACTCTAACCACT
CTTTAAAAAACGAAGTTTTAGCTTCTGCTCACGGTGGTGGTAAAGCTGGTGTTA
CTGTTCAATGTCAAGATTGTCACTTACCACACGGTCCAGTTGATTACTTAATCA
AAAAAATCATCGTTTCTAAAGATTTATACGGTTTCTTAACTATCGATGGTTTCAA
CACTCAAGCGTGGTTAGATGAAAACCGTAAAGAACAAGCTGATAAAGCTCTCG
CTTACTTCCGTGGTAACGATTCTGCTAACTGTCAACACTGTCACACTCGTATCT
ACGAAAACCAACCAGAAACTATGAAACCAATGGCTGTTCGTATGCACACTAAC
AACTTCAAAAAAGATCCAGAAACTCGTAAAACTTGTGTTGATTGTCACAAAGGT
GTTGCTCACCCATACCCAAAAGGTTAAAAGCTT

Key: Restriction sites are underlined (NcoI at the beginning of the construct, and HindIII at the end of the construct); start and stop codons are highlighted in green and red respectively; 8xHis-tag is highlighted in purple; and the HRV 3C proteolytic site is highlighted in light blue.

2. *Protein alignment of the translated construct and the wt CymA from S. oneidensis.*

```
SoCymA             1 ------------------MNWRALFKPSAKYSILALLVVGIVIGVVGYFA     32
                                       .||||||||||||||||||||||||||||||||
8xisHRVCymA        1 MAKHHHHHHHHLEVLFQGPNWRALFKPSAKYSILALLVVGIVIGVVGYFA     50

SoCymA            33 TQQTLHATSTDAFCMSCHSNHSLKNEVLASAHGGGKAGVTVQCQDCHLPH     82
                     ||||||||||||||||||||||||||||||||||||||||||||||||||
8xisHRVCymA       51 TQQTLHATSTDAFCMSCHSNHSLKNEVLASAHGGGKAGVTVQCQDCHLPH    100

SoCymA            83 GPVDYLIKKIIVSKDLYGFLTIDGFNTQAWLDENRKEQADKALAYFRGND    132
                     ||||||||||||||||||||||||||||||||||||||||||||||||||
8xisHRVCymA      101 GPVDYLIKKIIVSKDLYGFLTIDGFNTQAWLDENRKEQADKALAYFRGND    150

SoCymA           133 SANCQHCHTRIYENQPETMKPMAVRMHTNNFKKDPETRKTCVDCHKGVAH    182
                     ||||||||||||||||||||||||||||||||||||||||||||||||||
8xisHRVCymA      151 SANCQHCHTRIYENQPETMKPMAVRMHTNNFKKDPETRKTCVDCHKGVAH    200

SoCymA           183 PYPKG    187
                     |||||
8xisHRVCymA      201 PYPKG    205
```

3. *Cloning confirmation by Sanger sequencing; Sanger sequencing results aligned to the synthesized gene sequence by GenScript.*

```
                ....|....| ....|....| ....|....| ....|....| ....|....|
                         10         20         30         40         50
CL2_F_PBAD      NNNNNNNNNN NNNNNNNNNN NNNNNNNNNN NNCTCTCTAC TGTTTCTCCN
GenScript       ---------- ---------- ---------- ---------- ----------

                ....|....| ....|....| ....|....| ....|....| ....|....|
                         60         70         80         90        100
CL2_F_PBAD      TNCCCGTTTT TTTGGGCNNG AANNNNNNNN NNNNNNCTTT AANAAGGAGA
GenScript       ---------- ---------- ---------- ---------- ----------

                ....|....| ....|....| ....|....| ....|....| ....|....|
                        110        120        130        140       150
CL2_F_PBAD      TATACATACC CATGGCAAAA CATCATCACC ATCACCATCA CCATCTGGAA
GenScript       ---------C CATGGCAAAA CATCATCACC ATCACCATCA CCATCTGGAA

                ....|....| ....|....| ....|....| ....|....| ....|....|
                        160        170        180        190       200
CL2_F_PBAD      GTTCTGTTCC AGGGTCCGAA CTGGCGTGCT TTATTCAAAC CATCTGCTAA
GenScript       GTTCTGTTCC AGGGTCCGAA CTGGCGTGCT TTATTCAAAC CATCTGCTAA

                ....|....| ....|....| ....|....| ....|....| ....|....|
                        210        220        230        240       250
CL2_F_PBAD      ATACTCTATC TTAGCTTTAT TAGTTGTTGG TATCGTTATC GGTGTTGTTG
GenScript       ATACTCTATC TTAGCTTTAT TAGTTGTTGG TATCGTTATC GGTGTTGTTG

                ....|....| ....|....| ....|....| ....|....| ....|....|
                        260        270        280        290       300
CL2_F_PBAD      GTTACTTCGC TACTCAACAA ACTTTACACG CTACTTCTAC TGATGCTTTC
GenScript       GTTACTTCGC TACTCAACAA ACTTTACACG CTACTTCTAC TGATGCTTTC

                ....|....| ....|....| ....|....| ....|....| ....|....|
                        310        320        330        340       350
CL2_F_PBAD      TGTATGTCTT GTCACTCTAA CCACTCTTTA AAAAACGAAG TTTTAGCTTC
GenScript       TGTATGTCTT GTCACTCTAA CCACTCTTTA AAAAACGAAG TTTTAGCTTC

                ....|....| ....|....| ....|....| ....|....| ....|....|
                        360        370        380        390       400
CL2_F_PBAD      TGCTCACGGT GGTGGTAAAG CTGGTGTTAC TGTTCAATGT CAAGATTGNN
GenScript       TGCTCACGGT GGTGGTAAAG CTGGTGTTAC TGTTCAATGT CAAGATTGTC

                ....|....| ....|....| ....|....| ....|....| ....|....|
                        410        420        430        440       450
CL2_F_PBAD      NNTTACCACA CGGTCCAGTT GATTACTTAA TCAAAAAAAT CATCGTTTCT
GenScript       ACTTACCACA CGGTCCAGTT GATTACTTAA TCAAAAAAAT CATCGTTTCT
```

```
                ....|....| ....|....| ....|....| ....|....| ....|....|
                       460        470        480        490        500
CL2_F_PBAD      AAAGATTTAT ACGGNTTCTT AACTATCGAT GGTTTCAACA CTCAAGCGTG
GenScript       AAAGATTTAT ACGGTTTCTT AACTATCGAT GGTTTCAACA CTCAAGCGTG

                ....|....| ....|....| ....|....| ....|....| ....|....|
                       510        520        530        540        550
CL2_F_PBAD      GTTAGATGAA AACCGTAAAG AACAAGCTGA TAAAGCTCTC GCTTACTTCC
GenScript       GTTAGATGAA AACCGTAAAG AACAAGCTGA TAAAGCTCTC GCTTACTTCC

                ....|....| ....|....| ....|....| ....|....| ....|....|
                       560        570        580        590        600
CL2_F_PBAD      GTGGTAACGA TTCTGNNNNN NGTCAACACT GTCACACTCG TATCTACNAA
GenScript       GTGGTAACGA TTCTGCTAAC TGTCAACACT GTCACACTCG TATCTACGAA

                ....|....| ....|....| ....|....| ....|....| ....|....|
                       610        620        630        640        650
CL2_F_PBAD      AACCAACCAN AAACTATGAA ACCAATGGCT GTTCNNNNGC ACACTAACNA
GenScript       AACCAACCAG AAACTATGAA ACCAATGGCT GTTCGTATGC ACACTAACAA

                ....|....| ....|....| ....|....| ....|....| ....|....|
                       660        670        680        690        700
CL2_F_PBAD      CTTCAAAAAA GATCCANAAA CTCGTAAAAC TTGTGTTGAT TGTCACAAAG
GenScript       CTTCAAAAAA GATCCAGAAA CTCGTAAAAC TTGTGTTGAT TGTCACAAAG

                ....|....| ....|....| ....|....| ....|....| ....|....|
                       710        720        730        740        750
CL2_F_PBAD      GTGTTGCTCA CCCATACCCA AAAGGTTAAA AGCTTGAAGG TAAGCCTATC
GenScript       GTGTTGCTCA CCCATACCCA AAAGGTTAAA AGCTT----- ----------

                ....|....| ....|....| ....|....| ....|....| ....|....|
                       760        770        780        790        800
CL2_F_PBAD      CCTAACCCTC TCCTCGGTCT CGANTCTACG CGTANCGGTC NNCNTCACCA
GenScript       ---------- ---------- ---------- ---------- ----------
```

Appendix C
Purification Profile of TEV protease

The electrophoretic profile of TEV protease is shown in **figure I** as a reference from the in house purification of it, which was used for the removal of purification 6xHisMBP tags of the whole $CymA_{sol}$ construct.

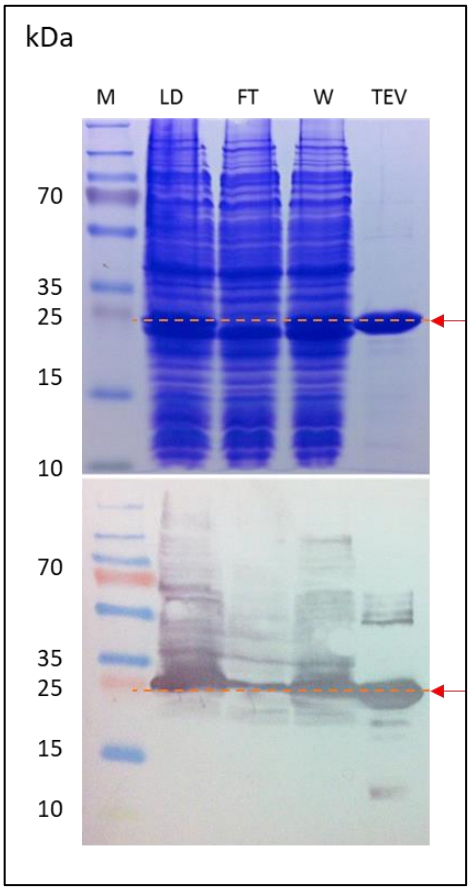

Figure I: The electrophoretic purification profile of TEV protease. 15% SDS-PAGE. M: molecular mass protein markers, LD: load, FT: flowthrough, W: wash, TEV: final purified TEV protease.